

DISSERTATION

THREE-DIMENSIONAL FINITE ELEMENT MODEL
TO PREDICT POLE STRENGTH

Submitted by

Nilson Franco

Department of Forest Sciences

In partial fulfillment of the requirements
for the Degree of Doctor of Philosophy
Colorado State University
Fort Collins, Colorado
Spring, 1992

TA
420
-F73
1992

COLORADO STATE UNIVERSITY

DECEMBER 10, 1991

WE HEREBY RECOMMEND THAT THE DISSERTATION PREPARED UNDER OUR SUPERVISION BY NILSON FRANCO ENTITLED THREE-DIMENSIONAL FINITE ELEMENT MODEL TO PREDICT POLE STRENGTH BE ACCEPTED AS FULFILLING IN PART REQUIREMENTS FOR THE DEGREE OF DOCTOR OF PHILOSOPHY

Committee on Graduate Work

J. Bodig

Craig E. Hunter

Martin E. Crivello

Patrick J. Vellicone

Roger M. Hoffer

Adviser
Department Head

COLORADO STATE UNIVERSITY LIBRARIES

ABSTRACT

THREE DIMENSIONAL FINITE ELEMENT MODEL TO PREDICT POLE STRENGTH

A three-dimensional finite element model was used to predict the strength and location of failure of nine wood transmission poles. The poles were made from three commonly-used species (western redcedar, Douglas-fir and southern pine) in North America. All poles were tested to failure as a cantilever beam with a concentrated load applied to the tip. The methodology involved was to select several eighteen inches long segments, located along the poles, which contained the most severe defects such as cluster of knots, spiral grain, including material inhomogeneity in the highly stressed region. Each segment was analyzed using the finite element technique with appropriate boundary conditions. Material properties for each segment were determined by measuring clear-wood elastic and strength parameters in bores taken from broken poles.

The information about knots and spiral grain, obtained by visual inspection of the pole surface, was used to identify the worst knot clusters and grain deviation in any segment. Knots were modeled in the finite element mesh and the localized grain deviation around the knots were determined through the use of the flow-grain analogy model. Finite

element computer analysis were performed through the use of the program GTSTRU DL. The model resulted in a total of 288 three-dimensional, isoparametric, linear strain, 20-node parallelepiped and 15-node wedge shaped elements.

For the nine poles studied, the results showed good agreement between predicted and experimental strength. The predicted values for strength differed from the actual ones with an average deviation of 7% (below the actual). Concerning failure location, in six of the poles, failure was verified in the same places as those predicted by the model. In the three other cases the failure with the maximum error of three feet, except for one pole where the deviation was twelve feet.

The study revealed that the three-dimensional finite element approach to model growth characteristics applied to the more critical segments along the pole length proved to be very useful tool for strength and failure location prediction of poles.

Nilson Franco
Department of Forest Sciences
Colorado State University
Fort Collins, CO 80523
Spring, 1992.

ACKNOWLEDGEMENTS

The author wishes to express his grateful appreciation to his Adviser Dr. Patrick J. Pellicane for his guidance, patience, friendship and care that he demonstrates during the author's study at CSU.

His sincerest appreciation is also extended to the members of his graduate committee: Dr. Jozsef Bodig, Dr. Marwin E. Criswell and Dr. Craig E. Shuler for their review of manuscripts and suggestions given.

Acknowledgement is given to the "Comissão de Aperfeiçoamento de Pessoal de Nível Superior (CAPES) who granted the author's scholarship to carry out this study.

Additional support for this project was obtained from the Engineering Data Management (EDM) and Electrical Power Research Institute (EPRI) which provided the opportunity to follow the Research Project (EPRI-RP 3078-01) allowing the author to use material and data. The above contributions are gratefully acknowledged. Appreciation is extended to the EDM's personnel for their support with data collection.

A personal note of thanks is given to Dr. Amantino Ramos de Freitas, Head of the Wood Division of the Instituto de Pesquisas Tecnológicas do Estado de São Paulo (IPT) for his enthusiasm and encouragement demonstrated to the author to

pursue this study, Mr. Luiz Tadashi Watai and Mr. Takashi Yojo for their assistance at IPT for fulfilling the author's obligations during his absence, and IPT's staff for their support.

Special gratitude is extended to his wife Maria Auxiliadora and his sons Daniel, Érico and Thiago for their love, affection, and companionship. They provided emotional support needed to conduct such an investigation, and who sacrificed many family activities throughout this project.

Lastly, but not the least, the author also thanks his fellows graduate students, friends, and faculty who made his stay at CSU and Fort Collins enjoyable and memorable one.

DEDICATION

To his parents Balbina and Orlando Silveira Franco for the many years of aid and encouragement, who provided the basic educational opportunities and unquestioning support throughout the author's life.

TABLE OF CONTENTS

<u>Chapter</u>	<u>Page</u>
1 INTRODUCTION	1
1.1 Background	1
1.2 Objective	3
1.3 Scope	4
2 REVIEW OF LITERATURE	6
2.1 General	6
2.2 Wood Characteristics and their effect on Pole Structures	9
2.2.1 Knots	10
2.2.2 Spiral Grain	12
2.2.3 Taper	15
2.2.4 Density and Specific Gravity	16
2.2.4.1 Influence of Position in the Tree on Density	19
2.2.4.2 Variation of Specific Gravity Throughout the Cross Section	21
2.2.4.3 Variation of Specific Gravity Within Species	21
2.3 Tests for Wood Characterization	24
2.3.1 Methods	24
2.3.2 Data Available from Wood Standard Methods	29
2.4 Tests for Pole Characterization	31
2.5 Strength Grading of Wood Poles	33
2.5.1 Classical Deterministic Method	34
2.5.2 Reliability Based Design	38
2.5.3 Simulation Procedures Combined with Non-Destructive Evaluation of Wood Poles	42
2.6 Previous Studies Related to Wood	45
2.7 Finite Element Approach for Orthotropic Problems	47
2.8 Constitutive Law in Orthotropic Elasticity	49
2.9 Elastic Parameters of Wood	53
3 MATHEMATICAL MODEL FOR WOOD POLES	56
3.1 General	56
3.2 3-D Model for Wood Poles with Natural Defects	58

3.2.1	Finite Element Model	58
3.2.2	Element Definition	59
3.2.3	Loading Representation	64
3.2.4	Knot Modeling	66
3.2.5	Grain Deviation Representation	68
3.2.6	3-D Segment Model	77
4	MATERIAL CHARACTERISTICS AND DATA COLLECTION ...	84
4.1	General	84
4.2	Geometry, Spiral Grain and Knot Measurements	86
4.2.1	Pole Profile	86
4.2.2	Spiral Grain	89
4.2.3	Knot Map	89
4.3	Mechanical Characteristics of Poles	91
4.3.1	Full Scale Testing of Poles	91
4.3.2	Small Clear Specimens for MOE and MOR Evaluation	94
4.3.2.1	Bending Tests	97
4.3.2.2	Longitudinal Modulus of Elasticity and Strength Values	101
4.3.2.3	Elastic Parameters of Wood	101
5	EXPERIMENTAL VERIFICATION OF THE MODEL	118
5.1	General	118
5.2	Results of Trial Analysis with Isotropic and Orthotropic Materials	121
5.3	Comparison of Previous Results with those Based on the Strength of Materials Theory .	124
5.3.1	Longitudinal Stresses on the Cross Section	128
5.3.2	Stresses along the Top Line of Segments	128
5.4	Finite Element Analysis on Selected Poles .	131
5.4.1	GTSTRUDL analysis	134
5.4.2	Criteria Used to Obtain the Maximum Stress at Pole Segments	135
5.5	Results of Finite Element Analysis for Western redcedar, Douglas-fir and Southern pine Characteristics	135
5.6	Prediction of the Strength of the Poles ...	136
5.7	Adjustments on Predicted Load	142
5.8	Prediction of Failure Location	146
5.9	Results from Full Scale Tests	146
6	DISCUSSION	148
6.1	General	148
6.2	Basic Material Properties	148
6.3	Grain Deviation	149
6.4	Prediction of Pole Strength and Failure Location	150

7	SUMMARY AND CONCLUSIONS	154
7.1	Summary	154
7.2	Conclusions	156
7.3	Future Research Needs	158
7.4	Limitations of the Model	158
	REFERENCES	160
	APPENDICES	167
A.	Matrix Transformation for 3-D Elements	168
B.	Program Stress	172
C.	Input File for the GTSTRUDL Program	175
D.	Examples of Records on Pole Data.....	177
	D-1 Example of Pole Profile Data File.....	178
	D-2 Example of Pole Spiral Grain Data File	179
	D-3 Example of Pole Knot Map Data File	180
	D-4 Example of Pole Data Form and Deflection Curves from Pole Test	183
	D-5 Example of Load-Deflection Curves from Bending Tests on Small-clear Specimens	186
E.	Program STIFMAT	188
F.	Example of Pole Segment Characteristics data Sheet	195
G.	Tables with the Results of the GTSTRUDL Finite Element Analysis for each Segment ...	198

CHAPTER 1

INTRODUCTION

1.1 BACKGROUND

Specifications for distribution, telephone and transmission poles are designed to assure that these structures present adequate performance and can resist the service loads imposed on them during their service life. Wood, as an engineering material, has long been studied with considerable emphasis on the physical and mechanical properties in order to provide data to support product standards (Brotero 1956; Wood and Markwardt 1965; deFreitas 1973, 1978; ABNT 1980; Goodman et al. 1981; Phillips et al 1985; Bodig et al. 1986; ANSI 1987). Investigations concerning growth characteristics of wood have also been conducted to verify their effects on structural members (Dabholkar 1980; Cramer 1981, 1984; Anthony 1986; Bodig 1986; Wang 1987; Cramer et al. 1989; Stahl et al. 1990). As a result, standard tables for poles sizes and classes have been developed to assure the safe load assignments and rational designs (ABNT 1973, 1984; ANSI 1987).

The traditional method of estimating wood pole properties follows the strength of materials procedures (Wood and Markwardt 1965; ABNT 1980; Goodman et al. 1981), and uses small, clear specimen test values for wood strength. This

approach is clearly approximate, since properties of small specimens rather than full size poles are studied.

The above procedure has been used for decades in many countries. Nevertheless, as more and more data from tests on full size pole members become available, a more refined and general direct statistical approach becomes feasible (Phillips et al. 1985; Bodig et al. 1986). Statistical analysis, coupled with reliability-based design, provides a means for a probabilistic approach. This approach leads to methods for strength prediction of entire pole populations in terms of reliability. Data for use in reliability-based design are provided in ANSI.05.01-87 Appendix C (ANSI 1987).

By using the simulation technique and pole test data from a small sample, a statistical approach can be employed to predict the strength of poles for an entire population (Goodman et al. 1981). This method has the advantage of low cost and reduced number of poles to be tested.

Strength prediction of wood members has been done using state-of-the-art analytic methods (Dabholkar 1980; Cramer 1981, 1984; Zandbergs 1985); statistical approaches (Goodman et al. 1981), and by empirical methods (Dashiel 1985). Dabholkar (1980) first modeled the grain pattern around a knot using the finite element method in analogy with the laminar flow (Flow-Grain analogy). With this model and the computer program SAP-IV, Dabholkar (1980) predicted the behavior of wood subjected to uniaxial tension. The contribution of knots

and associated cross-grain to the strength and stiffness behaviors were considered.

The study presented here encompasses the combined use of the finite element method and the flow grain analogy to model the geometry of poles and thus to develop a strength prediction model. Experimental results from actual tests of wood poles were used to verify the proposed prediction model.

The results obtained in this study and through other techniques are used to predict pole performance as an alternative to full-scale destructive pole tests. For species with general mechanical properties already determined, the small-clear specimens approach is considered less costly, and will be favored for future use if the basic clear properties can be combined with observed pole geometry in a reasonably accurate prediction model.

As the basic data used in this study were obtained from softwood species available in North America, if the model is to be used to predict the strength of hardwoods (including tropical hardwoods), which may present a different pattern for knot and spiral grain and sometimes interlocked grain, some modifications may be necessary to be introduced in the proposed model in order to account for these possible differences.

1.2 OBJECTIVE

The objective of this study is to develop a three-dimensional (3-D) finite element model capable of predicting

the location of the critical bending stresses, (consequently the maximum concentrated load possible to be applied at the tip) and the most likely failure location for wood poles loaded as cantilever beams.

The strength prediction model, which accounts for pole geometry and strength, was developed for a cylindrical segment of a pole and includes the effects of knots and spiral grain. The elastic parameter values utilized in the model were obtained from small clear specimens taken from poles previously tested to failure.

1.3 SCOPE

The scope of this research was to develop a model which has the ability to predict the strength and failure location for full-size wood poles. The method considers several short length pole segments, for which the precise location of interest in the pole was determined by applying the appropriate boundary conditions, knot occurrence detected by visual inspection, and spiral grain measurements on poles. The mathematical model was composed of 3-D finite elements defined by a mesh idealized over the segment. Matrix transformations on the finite element stiffness matrices were used to represent the cross grain and knot effects.

Some assumptions were necessary regarding the material (wood) and the geometry. The following basic assumptions were made:

a. pole sections of all samples can be considered green, and

- therefore the effect of checking or drying defects do not need to be included;
- b. the knots can be considered as holes, hence the effect of the knot itself was included as a void and through its localized cross grain in the tension or compression zones;
 - c. cross sections of poles can be treated as perfectly circular in shape;
 - d. a pole segment can be modeled as a cylinder, with its maximum diameter used as the diameter;
 - e. the wood behaves as a linear-elastic material under load;
 - f. the spiral grain can be considered uniform (constant) throughout the cross section represented by the measured grain angle on the pole surface.

The model was verified using destructive test load and geometry results from nine poles of three different species, Douglas-fir, western redcedar and southern pine. The test specimens were evaluated as part of a sponsored project by the Electrical Power Research Institute (EPRI) conducted by Engineering Data Management Inc. (EDM) at the Structures Laboratory of the Engineering Research Center at Colorado State University (CSU).

CHAPTER 2

REVIEW OF LITERATURE

2.1 GENERAL

Wood has many features which make it desirable and economical for structural uses in commercial and residential buildings, frames, piles and poles. Wood is a renewable material. The short growth period of certain exotic (non-native) species, such as eucalyptus in Brazil (Zobel 1988), in favorable regions makes it possible to provide, in a relatively short time, adequate quantities of required material through well conducted reforestation.

Wood requires an energy consumption for its processing which is low when compared to steel, aluminum, concrete and other materials.

Wood has high tensile strength-to-weight ratio (Kollman and Cote 1968). It has good workability and physical properties (Faherty and Williamson 1988) such as thermal, electrical at low moisture content, acoustical (ability to damp vibration).

Concerning durability, wood can undergo biological deterioration. Properly treated with preservatives, wood can be used successfully for permanent structures, as is shown by many examples throughout the world. Gojkovic (1991) gives examples of durable timber construction, such as bridges over

the Danube river built at the beginning of our era (in A.D. 103-105). Fan (1991) describes ancient construction in China from the 700 and 800's A.D.

The advantages and economy of wood have lead the utility industry to use wood poles to support overhead electrical power systems. As far as wood pole structures are concerned, they have the advantage of requiring a relatively simple foundation system and connections which can be easily fabricated. Installation, maintenance and future modification costs are all relatively low (Goodman et al. Vol 1, 1981; Phillips et al. 1985).

In the United States, the dimensions of single pole structures are governed by a standard (ANSI 1987) in which considerations are based on tests of poles in full size and, when data on full- scale basis were not available, results of tests on small-clear specimens (Wood and Markwardt 1965).

The load capacity of a pole is affected by various factors which make the strength prediction difficult. Factors affecting the load capacity of wood poles are generally related to growth characteristics and, more rarely, to mechanical damages.

Abnormalities (Kollmann and Cote 1968), sometimes a synonym for defect, should be seen according to the end use as it affects the final product. From the economic view point, a defect in wood is any feature that lowers its value on the market. In structural members, abnormalities decrease the strength and limit the wood for a particular purpose. Natural

defects, in a strict sense, are not abnormalities, but the product of natural growth. Knots, reaction wood, cross grain, variations from the normal form are examples of natural defects. Defects due to processing arise during conversion of logs into products (e.g. seasoning defects).

Strength reduction in wood members due to the presence of knots and grain deviation are well documented in textbooks and papers (Wangaard 1981; Bodig and Jayne 1982; Kollmann and Cote 1968; Panshin and deZeeuw 1968; Cramer 1981, 1984; Wang 1987). Two different sources of grain deviation, spiral grain and that associated with knots, were objects of study by several researchers (Phillips 1980; Dabholkar 1980; Cramer 1981, 1984; Zandbergs 1985).

Among the growth characteristics, cross grain is one of the major factors because of the high degree of anisotropy in wood. Wood members are often used as linear elements where the normal stresses are typically parallel to the lengthwise dimension. It is highly desirable that wood stresses are oriented parallel to the longitudinal direction where the strength of wood is greatest.

Finite element techniques taking into account the effect of knot-associated grain deviation and spiral grain have been used by many researchers to model structural wood members (Cramer 1981, 1984; Zandbergs 1985; Wang 1987; Dabholkar 1980). These studies analyzed the stress field in boards. The knowledge of knot and grain deviation characteristics are

fundamental in modeling techniques to obtain accurate and reliable results.

2.2 WOOD CHARACTERISTICS AND THEIR EFFECT ON POLE STRUCTURES

Single-pole and some framed-pole structures utilize round wood members as it is found in nature. Because wood is a natural material, poles have natural defects (knots, cross grain) variation in shape, variation in weight (density), etc. In most cases, a single pole in a structure is designed as a cantilever beam with a concentrated load applied near the tip.

For electrical distribution and transmission lines, poles are always installed in an upright position subjected to an axial load due to its own and conductor weight, as well as one or more horizontal loads originating from the line itself and wind. Ignoring other possible lateral (horizontal) loads on the pole and assuming a linear pole taper, the moment along the pole and below the groundline, generated by a concentrated load applied to the tip, varies linearly being zero at the top and maximum at the groundline section. The normal stresses due to normal load are generally very small when compared with the bending stresses caused by the applied horizontal loads, thus in most cases the axial loads can be neglected with little error resulting.

The maximum stress at any section along the pole (considering wood as an homogeneous, isotropic and defect free material), using the basic theory of linear mechanics of materials, is evaluated by the expression:

$$F_b = M/S \quad [2,1]$$

where: F_b - maximum stress at any section

M - applied moment

S - section modulus

2.2.1 KNOTS

Kollmann and Cote (1968) and Wangaard (1950, 1981) describe a knot as a portion of branch that is included in the stem of a tree during growth around the branch's base. Knots cause the cells around them to be arranged at angles, sometimes at right angles, to the local grain direction. They are considered the principal natural defect affecting mechanical properties. As stated by Wangaard (1950), the weakening effect of knots is caused not by the inferiority of the material composing them, but by the combined effect of local cross grain and the checking which may develop in and around them during drying. The presence of a knot in a piece of wood causes a discontinuity of the material and cross grain (grain is distorted or deflected around it), both contributing to stress concentration. The presence of a knot causes the grain distortion that can extend to a distance at least three times the knot diameter. In the zone of grain distortion, a severe stress concentration may be induced by bending loads. Loaded members containing knots may fail at stresses which are a fraction of clear wood strength.

With respect to pole structures, Bodig (1986) studied the influence of knots while analyzing the modulus of rupture

(MOR) at groundline of new, green, untreated, 40 foot long Douglas-fir poles, as a function of maximum knot diameter and maximum sum of knot diameters in a one foot section. The results showed that the effect of a single knot is not highly significant, but the tendency of decreasing strength with increasing maximum knot diameter was observed. A similar tendency was observed when the maximum sum of knot diameters in a one foot section increased.

Concerning location of the failure, little correlation was observed between the location of the maximum sum of knots and the break point. The conclusion reached was that the maximum sum of knots did not predict the failure location. It was mentioned that in cantilever beams in bending, the stresses are not uniform along the pole length. Knots closer to the tip are expected to have less influence in pole failure (Bodig 1986).

A model considering the net moment of inertia, i. e. the moment of inertia of the section less the moment of inertia of the knots taken out with triangular shape, was studied by Dashiell (1985). The model was based on several assumptions which affected the analysis in terms of predictor parameter. The assumptions made in his study included: to evaluate the moment of inertia, knots at the cross section were represented by triangular shape rather than circular sectors; the stress distribution across a pole section was assumed to be linear; all knots in one foot pole section were assumed to lie on a single plane.

The following facts were cited by Dashiell that appear to influence the lack of sensitivity: knots were not the only characteristic involved in failure mechanism; the apparent failure location may not have been the actual location in every case since the initial location of the failure is difficult to detect; the knot diameter alone was used in computing the moment of inertia and no measure of grain deviation around the knot was incorporated into the analysis.

The principal conclusions of his study were: the use of knot data to reduce the moment of inertia of pole cross section give insufficient quality as a strength predictor.

Wang (1987) analytically studied, in 2-D analysis, the interaction between knots by applying the principle of superposition. In bending, the outermost fibers in tension usually control the strength of a pole. When a knot is present at the pole surface, the stress distribution can be obtained from computer programs developed by Cramer (1984) and Zandbergs (1985). Based on this research, Wang (1987) studied the possible interaction between knots by defining a least distance at which two knots have an appreciable effect on each other. The approach of superposition did not appear to be successful in a prediction method of pole strength, as was verified by experimental data.

2.2.2 SPIRAL GRAIN

Bodig and Jayne (1982) define spiral grain as the inclination of the fibers in the plane of a growth ring with

respect to the longitudinal axis of the member. It occurs naturally in trees of nearly all species.

The most used formula to account for spiral grain was developed by Hankinson (Kollmann and Cote 1968):

$$\sigma_{\theta} = \frac{\sigma_n * \sigma_p}{\sigma_n * (\cos\theta)^2 + \sigma_p * (\sin\theta)^2} \quad [2,2]$$

where σ_p and σ_n are stresses perpendicular and parallel to grain respectively. This equation is suitable for computing the compressive strength of wood, σ_{θ} , in a plane where the direction of the grain is inclined to the direction of load, by an angle θ .

Since spiral grain is a deviation of the fibers from a straight line drawn in the outer surface parallel to the longitudinal axis of growth, its effect in pole structures is to reduce the strength (Harris 1989). Spiral grain as viewed by a person facing a standing pole, can be left handed (spiral twists upwards to the left) or right handed.

As cited by Dashiell (1985), a study conducted by Lowery and Erickson (1967) showed significant difference in results between poles with left and right hand spiral grain. The spiral grain angle can change from pith to periphery. In right hand spiral grained poles, there is often a left hand spiral at the pith which gradually decreases to zero and then develops right hand spiral towards the periphery. Poles with left hand spiral grain in the periphery are likely to contain left hand spiral grain throughout. This may explain torsional

stability of right handed spiraled poles. In terms of bending strength, a 25% reduction in strength from straight grained poles was observed in poles with right hand spiral grain, and 40-50% reduction was found in poles with left hand spiral grain with slope greater than 1:12. For slopes 1:12 or smaller, spiral grain has negligible effect on bending strength. In their study, Lowery and Erickson (1967) concluded that among the variables considered, spiral grain was the least influential for strength prediction and the influence of spiral grain on bending strength does not appear to be as significant for poles as for lumber. The conclusion of a study from Wood, Erickson and Dohr (1960), covered in detail by Wang (1987), is that according to the ASTM Wood Pole Research Program, spiral grain meeting ASA (American Standards Association) limitations has little effect on pole strength. Data from experiments show that strength of poles with spiral grain is almost the same strength of poles with straight grain. One possible explanation for this is that sloping fibers are not cut at the pole surface as they are on the surface of lumber. Test results of a study conducted on Douglas-fir and western redcedar (Bodig et al. 1986, Bodig and Goodman 1986) showed that spiral grain, mean of 2.7° at surface (standard deviation of 1.92°) for Douglas-fir and mean of 1.31° (standard deviation of 1.04°) for western redcedar, has little effect on pole strength.

2.2.3 TAPER

The geometrical shape of a pole, here approximated by a frustum of a right circular cone, plays an important role, since it determines the position along the pole where the maximum flexural stress occurs. The variation of the diameter along the length of the pole, can be represented by the taper coefficient, T , (assuming linear variation), is defined as:

$$T = (D_2 - D_1)/L \quad [2,3]$$

where D_2 is the diameter at ground line, D_1 is the diameter at load section and L is the distance between these two sections. The section modulus, S , for a circle of radius R and moment of inertia I , is :

$$S = I/R = \pi R^3/4 = \pi D^3/32 \quad [2,4]$$

and moment at any point, for a concentrated load applied at the tip of a pole, is equal to:

$$M = P*(L-x) \quad [2,5]$$

the radius at any section is calculated by:

$$R = D_1/2 + (T/2)*(L-x) \quad [2,6]$$

placing these values in the equation [2,1], one obtains:

$$F_b = (4*P*(L-x))/(\pi R^3) \quad [2,7]$$

then taking the derivative of [2,6] in respect to x , and setting it equal to zero, the point of maximum stress is found to be:

$$x = ((2D_2-3D_1)/(2(D_2-D_1)))*L \quad [2,8]$$

or $L-x = D_1/2T \quad [2,9]$

evaluating the diameter at the point of maximum stress:

$$D = 1.5*D_1 \quad [2,10]$$

the diagram in Figure 2.1 (from Vol 2 of Goodman et al. 1981), shows the stress distribution when taper goes up gradually starting at T=0 (cylinder)

The maximum stress, in terms of the geometric parameters, can be expressed as:

$$F_{\max} = (32/27) * (P/A_t * T), \quad [2,11]$$

where A_t is the pole cross sectional area where the concentrated load is applied. At the groundline the stress developed by application of load P is:

$$F_{gl} = 4 * P * l / \pi * (R_2)^3 \quad [2,12]$$

and for a fixed length, it is possible to evaluate the ratio between the maximum stress and the stress at ground line:

$$\alpha = F_{\max} / F_{gl} = 4 (D_2)^3 / 27 (D_1)^2 * (D_2 - D_1) \quad [2,13]$$

and,

D_2/D_1	α	$\beta = 1/\alpha$
<1.500	1.000	1.000
1.625	1.017	0.983
1.750	1.059	0.944
1.875	1.116	0.896
2.000	1.185	0.844
2.125	1.264	0.791
2.250	1.350	0.741
2.375	1.443	0.693

2.2.4 DENSITY AND SPECIFIC GRAVITY

Density is defined as the quotient of the mass of a substance and its volume. For wood, when both mass and volume

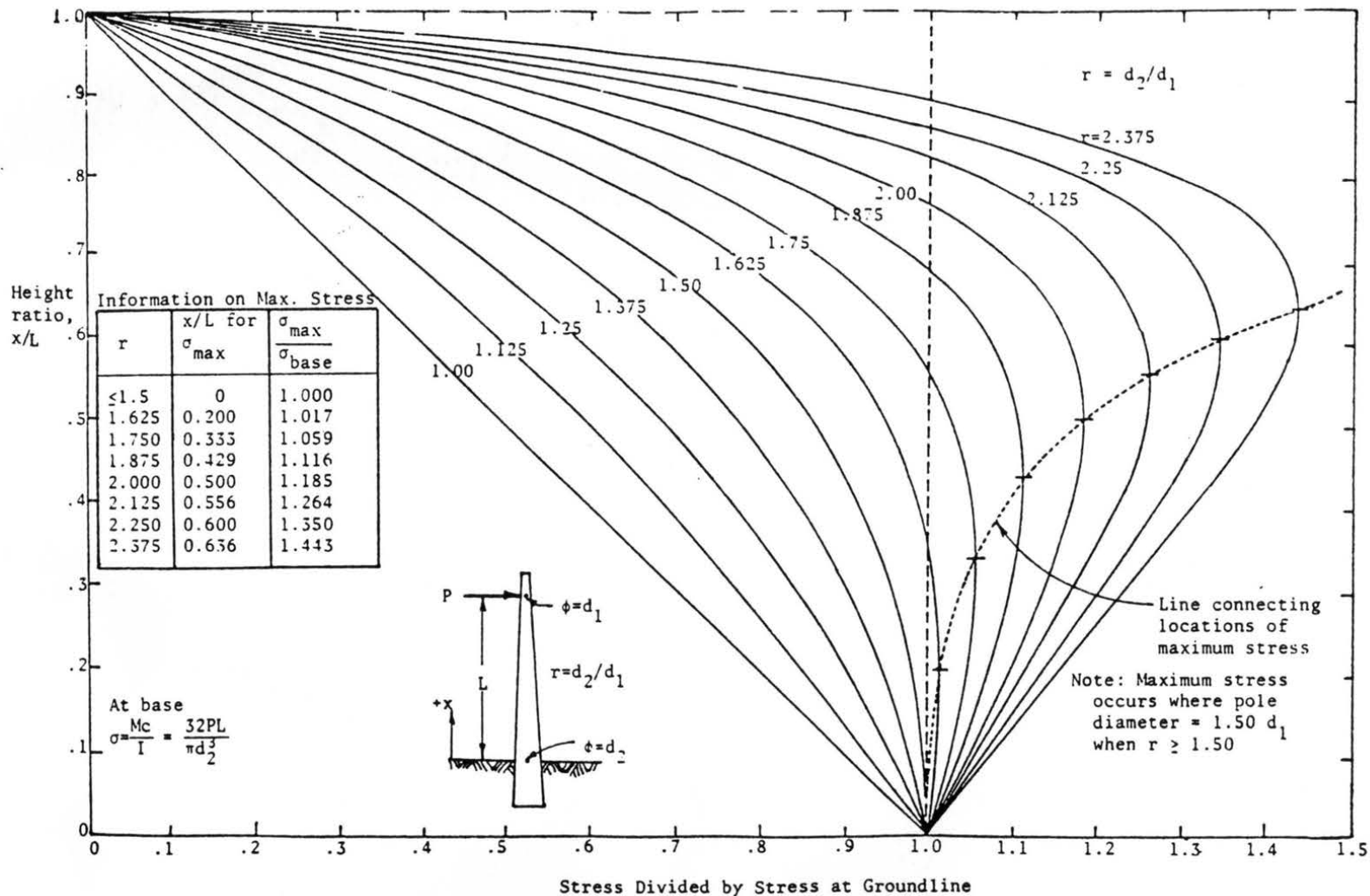


Figure 2.1. Flexural Stress Patterns for Linearly Tapered Pole.
 (After Goodman et al. Vol. 2, 1981).

are measured at the same moisture content, the apparent density is obtained. For 15% moisture content, the generic term D_{15} is used for density in Brazil. The weight density of wood is the quotient of the oven-dry weight and its volume at a specified moisture content; the specific gravity of wood is the relative measure of the weight density to the density of an equivalent volume of water. Of all properties of wood, specific gravity is the most important in accounting for wood characteristics (Bodig and Jayne 1982). Almost all mechanical and physical characteristics are correlated to specific gravity (Kollmann and Cote 1968).

Density and specific gravity are highly sensitive to moisture content. It is necessary to establish a standard or reference value for moisture content in order to make possible valid comparisons between values. ASTM has established 12% moisture content for North America; in Brazil, the moisture content value is set to 15% by ABNT. For all timber, it has been found that the density (oven-dry) of the solid wood substance of cell walls is very similar having the value of 1.5 g/cm^3 . Differences in the wood structure and the presence of extractives may cause variations in the specific gravity of wood. The amount of the different components in the wood structure as fibers, tracheids, vessels, resin ducts, wood rays and their dimensions, especially the wall thickness, is that which characterizes a wood species. Variation in environmental factors such as wind, soil, heat, precipitation, and hereditary tendencies can affect the structure of wood and

its density. Besides these factors, the age and position in the trunk have considerable effect on the density of the wood (Kollmann and Cote 1968).

2.2.4.1 INFLUENCE OF POSITION IN THE TREE ON DENSITY

Based on literature and studies carried out by many scientists, the general rule (Kollmann and Cote 1968) is that the greatest density is found at the butt log and the lowest at the upper portion. For cylindrical shaped stems the density at the butt is greater than in highly tapered trees.

Kollmann and Cote (1968) presents diagrams showing the variation of specific gravity with height in the tree in which a general tendency of decreasing specific gravity up to the height of 10m is evident (Figure 2.2). In a study conducted by Wangaard and Zumwalt, Douglas-fir shows the same tendency and a curve fitted looks like a parabola (Figure 2.3). Koch (1972) also presents results of studies for softwoods, showing variation on specific gravity along the height above the ground. The data reported confirm the tendency of decreasing in specific gravity with increasing the height. A curve fitting for linear, reciprocal or exponential may be fitted to the data to represent the variation. For hardwoods to represent the variation within trees, Koch (1985) presents results by species. For ring porous species, the variation follows a somewhat complex pattern. For diffuse porous species the pattern is similar to that presented by softwoods

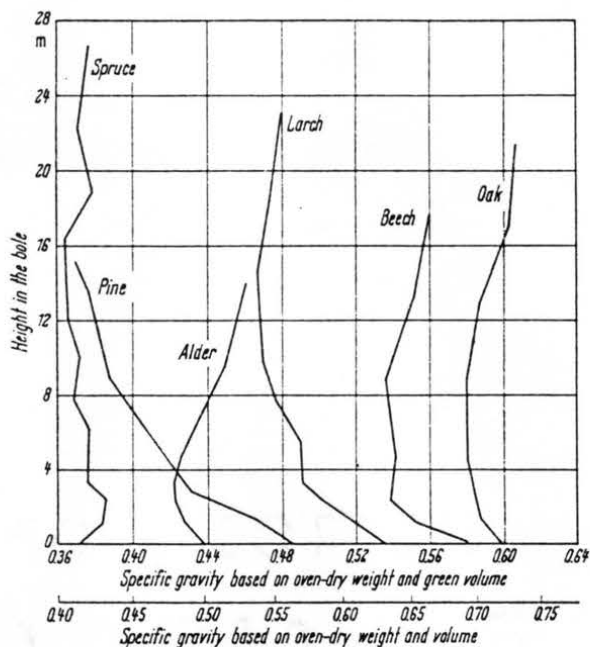


Figure 2.2. Variation of Specific Gravity With Height in the Tree. (After Kollmann and Cote 1968).

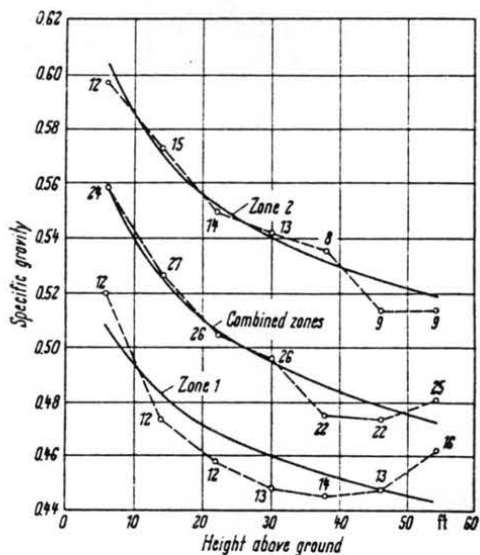


Figure 2.3. Effect of Position in the Tree on Specific Gravity of Second Growth Douglas Fir. (After Wangaard and Zumwalt 1949)

which is decreasing in specific gravity with increasing the height above ground.

2.2.4.2 VARIATION IN SPECIFIC GRAVITY THROUGHOUT THE CROSS SECTION

At any particular cross section, variations in specific gravity are less pronounced than those in height (Kollmann and Cote 1968). Variations in specific gravity are very much affected by the width of the growth rings and on the latewood percentage. For broadleaf species, the general rule is that denser wood is produced near the center.

Koch (1972) reported that the specific gravity for slash pine wood containing both earlywood and latewood increases sharply with radial distance from the pith until the 5th to 10th growth ring (Figure 2.4); it may increase slowly to about the 30th growth ring. For other species, specific gravity changes relatively little beyond the first 10 to 15 years. The same author (Koch 1985) presents data for hardwoods related to variation of specific gravity across the radial direction. The general tendency is that specific gravity increases or remains constant up to the age of 25-30 years (rings from the pith) and then decreases towards the bark as illustrated in Figure 2.5.

2.2.4.3 VARIATION OF SPECIFIC GRAVITY WITHIN SPECIES

Due to differences in structure, different cell types - fibers, tracheids, vessels, rays - and wall thickness, the

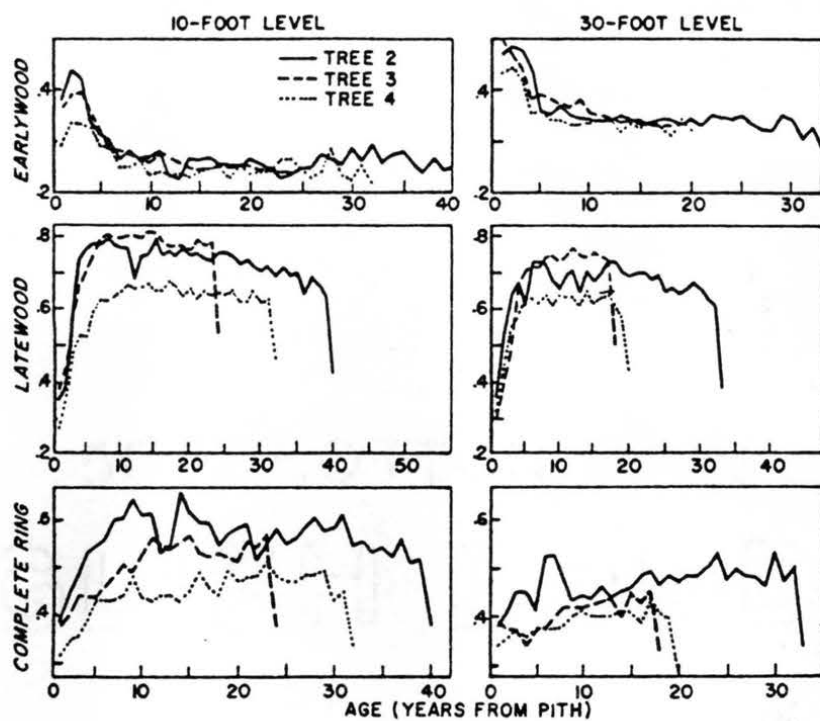


Figure 2.4. Radial Variation of Specific Gravity in Earlywood and Latewood and Complete Growth Ring of Slash Pine at Two Height Levels. (After Koch 1972).

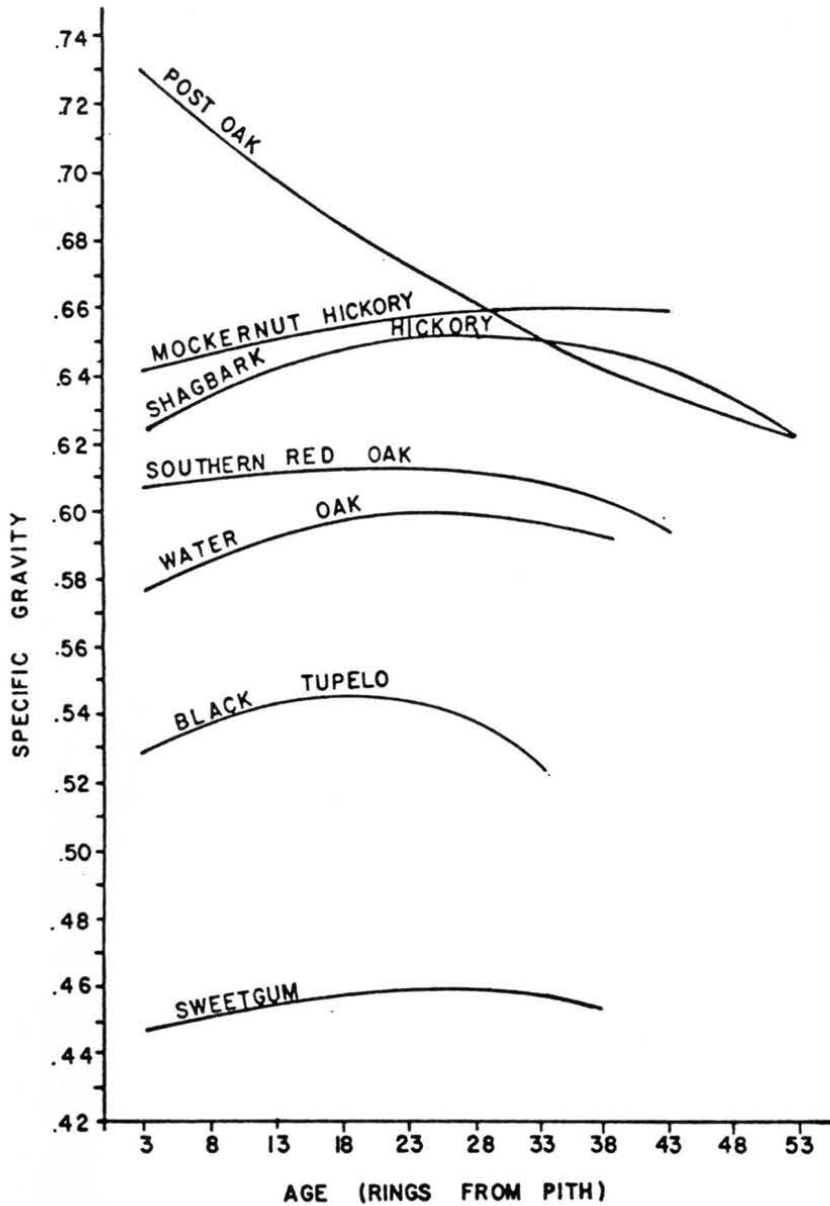


Figure 2.5. Relationship Between Stemwood Specific Gravity Five Feet Ground Level in Seven Species and Number of Annual Rings Distance From Pith. (After Koch 1985).

specific gravity is subjected to variations. Based on studies of characterization of wood species, a coefficient of variation of about 10 percent describes the variability within species (Wood Handbook US-FPL 1974). Koch (1985) reported the average specific gravity and the standard deviation for 22 hardwood species growing on southern pine sites. The average coefficient of variation (COV) was found to be 5.73%, which is in agreement with the Wood Handbook (US-FPL 1974). De Freitas (1978) evaluated the average and the COV's of wood properties for 23 Brazilian species, for which the Brazilian Standard NBR-6230 was followed to determine the properties. From this study, an average COV of the specific gravity of 8.1% was found, which also agrees with the Wood Handbook (US-FPL 1974).

2.3 TESTS FOR WOOD CHARACTERIZATION

2.3.1 METHODS

The testing methods to characterize the physical and mechanical wood species can be classified into two broad groups (Bodig and Jayne 1982): exploratory and standard.

The purposes of the exploratory methods are to obtain data for a particular problem, whereas the standard methods are developed to guarantee reproducibility of the data obtained by different investigators. It should be considered that the methods that yield results comparable to those already available, as well as which facilitate the adoption of improvements that have been shown desirable by experience, are most useful. Of great importance is knowledge of how the data

are used, the population to be represented, data accuracy and range of various variables. In order to account for these, a representative sample must be defined for use.

Since the model presented in Chapter 3 calls for the input of various wood properties, it is convenient here to mention some considerations about sampling techniques from related papers.

Material grown under uncontrolled conditions in nature has more variability than those materials manufactured under controlled conditions (Kollmann and Cote 1968). Wood, as a natural material, grows under conditions which are dependent on many diverse factors, such as locality, climate, group of species, etc. Due to the diversity of growing conditions, it is difficult to characterize this source of all the variability. Bendtsen et al. (1970), stated:

"No structural material can be safely and efficiently used without a knowledge of its strength properties and their variation. Obtaining such information for wood is extremely difficult because of the variation within trees, between trees and between forest areas".

The traditional methods to determine the mechanical properties for wood in small clear specimens and data available provide a basis for establishing stress grades and material properties which are included in the standards for wood products. Methods to estimate wood properties have been proposed based on random sampling techniques, where attention has been given to the dispersion of the tests results, to the precision of the estimates and to the sampling requirements.

The Double Sampling method involves predicting one property by carefully observing a well correlated auxiliary property that is presumably easier or cheaper to measure. For wood, the specific gravity is obtained with a high degree of precision by sampling the population. A smaller subsample of the large sample is used to establish the relationship between the specific gravity and a particular mechanical property. This relationship is generally described by a linear regression equation.

The Direct Random Sampling basically makes use of the statistical theory in planning and conducting a sample experiment so that precision and confidence can be associated with property estimates.

Noack (1971) describes a method to evaluate some of the physical and mechanical properties of little known or unknown species present in tropical forests where it is often necessary to determine the wood properties in short time. These types of studies must be carried out very carefully and special consideration has to be given to sampling, test methods, and wood properties to be determined. A preliminary study is important to assess the potential utilization of the species and to obtain sound knowledge of their properties before the timber can be commercialized. In many cases, it is necessary to determine properties of wood species with the smallest possible expense in personnel and equipment.

The sampling procedures are very important and should be developed to provide an economical determination of certain

basic strength and related physical properties as well as to obtain estimates of average strength and the variability of the measured properties.

It has been shown that the variations of properties between trees are more significant than are variations within a tree. A greater precision of the observed mean values is obtained by taking more trees and fewer pieces from each tree, certainly more so than is prescribed in the systematic sampling plan used in many standards. The number of sampled trees of wood species to reach different accuracy ranges of mean values is presented in Table 2.1.

For practical purposes, an accuracy of the mean value of 15% is usually sufficient. For a better accuracy of 10%, about 10 to 12 trees, with one test per tree, will give the required information.

Kauman and Kloot (1968) presented a program for sampling and testing which consisted of: 1.- preliminary survey where sampling, observation in the forest, close observation of the tree (color, smell, density, identification, etc), are employed; 2.- exploratory assessment; using simple tests which can be performed using sawmill equipment, visual characteristics can be observed; 3.- industrial trials, where workability can be evaluated, feasibility to produce composites as plywood, particleboard, pulp and paper are investigated, etc; 4.- full scale testing to evaluate the performance of the final product. This multi-phase approach is very important in order to evaluate the little known or

Table 2.1. Number of Randomly Sampled Trees of a Wood Species to Reach Different Accuracy Ranges of the Mean Value (After Noack 1971).

Error range of Mean Value, at 95% confidence Interval	Number of Pieces per Tree			
	one		two	
	Density	Strength Property	Density	Strength Property
+/- 15%	4	6	3	5
+/- 10%	5	12	4	80
+/- 5%	20	35	12	20
+/- 2.5%	70	150	40	80

unknown timber species with respect to the potential utilization of these species.

A review of methods for the sampling of timber prepared by Pearson and Williams (1958) states as its main conclusion:

"Accurate estimates of species properties depend mainly on the number of trees properly sampled and not in the total number of specimens tested."

To account for the inherent variability, a larger quantity of material needs to be tested. The determination of the mechanical properties presents a sample problem. The standard error (S_i) of the unweighted mean (x_i) for mean values of different trees is determined from the mean values of the trees themselves as:

$$S_i = \text{SQRT}((\Sigma(x_i)^2 - (\Sigma x_i)^2/m)/(m*(m-1))). \quad [2,14]$$

This expression shows that the standard error of the species mean depends mainly on m , the number of trees, and that N , the total sample size does not appear explicitly. An increase in the total sample size, N , without any change in the number of the trees, m , (that is an increase only in the number of specimens from each tree) will increase some the accuracy of each x_i and will thereby reduce the standard error somewhat, but not below a limit which depends on the inherent variation between trees. It is more satisfactory to include more trees in the sample than to sample a given number of trees more intensively.

2.3.2 DATA AVAILABLE FROM WOOD STANDARD METHODS

The characterization of wood species (physical and mechanical) in Brazil started in 1930 at the Instituto de Pesquisas Tecnologicas do Estado de Sao Paulo (IPT) (Sao Paulo State Institute for Technological Research), where a testing method for small clear specimens was developed and adopted in the study of wood species (Brotero 1956). In 1940, this method was standardized by the Associacao Brasileira de Normas Tecnicas (ABNT) (Brazilian Standard Association), as Metodo Brasileiro 26 (Method MB-26) which corresponds today to the Norma Brasileira 6230 (Standard NBR-6230) Ensaio Fisicos e Mecanicos de Madeira (Physical and Mechanical Tests for Wood).

Basically, two series of specimens are cut from a bole, for both green and air-dry conditions. For each moisture condition, specimens with 2 cm X 2 cm and 6 cm X 6 cm cross sections are tested to allow the derivation of the material resistance. Since 1930, more than 400 trees (more than 200 species) have been tested at the IPT, and the results have been published in Bulletin 31 (Brotero 1956-updated in 1975).

Linear regression curves correlating modulus of rupture (MOR) with modulus of elasticity (MOE), MOR with apparent density (D) at 15% moisture content, defined as the density of wood (in g/cm³), and MOE with D were evaluated using data for several tropical and Eucalypti species by de Freitas (1978). The following equations were obtained:

$$\text{MOR} = 0.918 + 6.46\text{E-}3 \text{ MOE} \quad (\text{MPa}) \quad (r^2 = .673)$$

$$\text{MOR} = -14.55 + 119.2 \text{ D} \quad (\text{MPa}) \quad (r^2 = .789)$$

$$\text{MOE} = 1260 + 13340 D \quad (\text{MPa}) \quad (r^2 = .656)$$

In this study, only species with three or more trees tested were considered, a total of 97 trees involving 23 species.

The apparent density at 15% moisture content and the basic specific gravity can be related and the equations above can be rewritten in terms of specific gravity.

For American species, the ASTM Standard D-143 (ASTM, 1990) is used to evaluate the wood properties in small-clear specimens.

The mechanical properties and the specific gravity at green volume basis, G , for American species can be related by the following exponential equations (Bodig and Jayne, 1982):

$$FS_p = 10200 G^{1.25} \quad (\text{psi})$$

$$\text{MOR} = 17600 G^{1.25} \quad (\text{psi})$$

$$\text{MOE} = 2360 G \quad (\text{psi})$$

or:

$$FS_p = 70.33 G^{1.25} \quad (\text{MPa})$$

$$\text{MOR} = 121.35 G^{1.25} \quad (\text{MPa})$$

$$\text{MOE} = 16.27 G \quad (\text{MPa})$$

where: FS_p - shear stress at proportional limit;

MOR - modulus of rupture;

MOE - modulus of elasticity.

2.4 TEST METHODS FOR POLE CHARACTERIZATION

The classical deterministic design method has been long utilized for single and complex pole structures. Presently,

both deterministic and probabilistic approaches can be used with the pole data presented in the 1987 version of ANSI-05.1.

In the deterministic design approach, safety is assured by designing for designated strength values and maximum nominal load values; load and resistance are assumed to be deterministic values. Consequently, providing an adequate factor of safety in design is assumed sufficient to prevent failure. However, material properties and loads are both random variables. There always exists a finite, although sometimes very low, chance of occurrence of extremely high loads and unusual low resistance; thus there is always some possibility of failure. The probabilistic method is more adequate for dealing with safety in structures. Although the probabilistic method has certain advantages, it requires information on the resistance distribution curve and the distribution of extreme load values; in other words, at least the mean and standard deviation for the material and load (Goodman et al. Vol 1 1981).

In the current ANSI-05.1. Standard Method (ANSI, 1987), the designated fiber stress value F_b for a given species is derived from full size pole test data; this fiber stress value can be expressed as:

$$F_b = MOR_{gl} * K1 * K2 * K3 \quad [2,15]$$

where: MOR_{gl} = mean groundline modulus of rupture;

$K1$ = correction factor for variability, oversize,
and load sharing;

K2 = correction factor adjusting to 20% moisture content;

K3 = correction factor for high temperature drying.

In the case of the Brazilian standard governing the wood pole design values (ABNT 1973, 1984), the current fiber stress (MOR) is specified only for Eucalypti which is the reforested genus most used to produce poles in Brazil. The average fiber stress was obtained experimentally, where a small number of representative poles were tested. A deterministic design approach was adopted in the development of this standard.

2.5 STRENGTH GRADING OF WOOD POLES

For utilization of wood poles, it is required that some knowledge related to species, resistance, dimensions, and growth characteristics be known in order to grade or estimate pole strength.

For specific species, the pole resistance can be estimated in different ways depending on the availability of data, laboratory facilities, equipment, etc. The resistance data can therefore be obtained by:

- testing a limited number of full size poles to determine the average strength, combined with previous results of small clear specimens tests;

- testing full size poles to determine the mean strength and the variability;

- using simulation procedures combined with

non-destructive evaluation and testing a limited number of full size poles.

To develop the strength grade or grading rules, some assumptions have been established (Wood and Markwardt, 1965). A simplified model is a single pole treated as a cantilever beam. The loading is represented by a concentrated load applied two feet from the tip.

Following is presented the basic concepts related to each method mentioned above:

2.5.1 CLASSICAL DETERMINISTIC METHOD

Some standards, ABNT (1973, 1984), utilize the deterministic method to derive the tables that provide values for structural designers.

Poles are usually separated by classes, which concept is to define the range of average load, ultimate or allowable, that the pole can resist. The design loads are based on parameters specifically for the lines, such as space between poles, weight of wires, etc, and environmental conditions like snow, wind, etc.

In the U.S., 15 classes are recognized for distribution and transmission lines and the designated load varies from 370 lbs to 11400 lbs. In Brazil, five classes are recognized for distribution lines and the allowable load varies from 150 kgf (330 lbs) to 800 kgf (1800 lbs)

For each class, depending on the species considered, different ranges of lengths can be found in the standards,

according to availability. Poles are placed in classes by tip dimensions and circumferences at groundline (ABNT 1980) and at six feet from butt (ANSI 1987).

The Brazilian standards (ABNT 1973; 1984) are concerned only with the use of poles of Eucalyptus genus. The fiber stress value for the Eucalypti species was determined in bending tests performed on a small sample size (few poles tested) in the green condition. Five levels of concentrated allowable loads applied at 60 cm from tip are used to classify the poles in extra light, light, medium, heavy and extra heavy load conditions, in 14 different lengths varying from 7 to 20 meters. The standards assume that this type of structure is exposed to weather, i. e. green values for the mechanical properties should be used, therefore no correction factor is allowed for moisture content; loads are for individual poles, no load sharing among adjacent poles; no effect of deterioration (new poles); and no vertical loads on poles.

ANSI 05.1 (ANSI 1987) - Specifications and Dimensions for Wood Poles - the strength grading criteria is based on designated fiber stress value for the species considered. The values currently found in ANSI 05.1 were obtained by testing a limited number of full size poles (mostly of distribution sizes, 25-30 foot long) and small clear specimens. For a given class, it is implied that poles of different lengths should carry the same amount of load regardless of the species.

It is assumed that the in-service moisture content of poles is the same for the whole country, 20% at four feet above the ground line; existence of load sharing among three adjacent poles; no direct effect of deterioration; and negligible vertical load on poles.

In deriving the values for fiber stress (Wood and Markwardt 1965), ANSI considered a normal distribution and coefficient of variation of 14% to represent material variability. The dimensions of the poles are normally greater than the minimum specified. Load sharing among three adjacent poles leads to smaller variation. In this case ANSI assumes the effective standard deviation as one-half of that assigned for material variability, i.e., 7%.

The result of having the moisture content of 20% is strength increase of 16% over the average value for green poles.

Lastly, it is recognized that the method used for conditioning affects strength, and the following factors are applied for the cases shown:

0.85 for steaming conditioning $T < 245^{\circ}\text{F}$

0.90 for bulking $T < 220^{\circ}\text{F}$

1.00 for air dry.

When data generated by testing full size poles were not available, then ANSI adopted values from small-clear specimens. An additional form factor of 1.08 was selected as a multiplier to small-clear specimens strength values to reflect full-size pole strength.

As a result ANSI presents a table containing fiber stress values for species or groups of species. Defects such as knots, spiral grain, checks, etc. are recognized and permitted in limited sizes and extensions or locations. Defects such as marine borer, decay, cross break, etc. are prohibited.

The standard does not specify limits for the specific gravity, but does provide a minimum growth rate in number of rings per inch. For the species specified in the standard, two entry tables are provided indicating, for each class and length, the minimum circumference at tip and at six feet from the butt (using standard taper values).

To account for the decrease in strength with height resulting from the combined effect of decreasing specific gravity and increasing frequency of natural defects towards the tip, the ANSI 05.1 Appendix A presents the following equation (ANSI 1987):

$$F_2 = F_1 * (1 - 0.5 * H / L_g) \quad [2,16]$$

where the maximum value of H is $L_g/2$;

F_1 = tabulated fiber stress value;

F_2 = calculated fiber stress value at distance H;

H = distance from the groundline;

L_g = length of pole (from groundline to tip).

Phillips et al. (1985), Bodig et al. (1986) and Bodig and Goodman (1986) present the results of studies conducted with southern pine, Douglas-fir and western redcedar and the following equations are presented to relate the modulus of rupture to the height fraction, H/L_g , respectively:

$$\text{MOR}_{\text{BR}} = 8252 - 4615 \text{ H/L}_g \quad (\text{SEE} = 1198)$$

$$\text{MOR}_{\text{BR}} = 4442 - 436 \text{ H/L}_g \quad (\text{SEE} = 794)$$

$$\text{MOR}_{\text{BR}} = 6823 - 1953 \text{ H/L}_g \quad (\text{SEE} = 941)$$

Bohannan (1971) presents graphically the height-strength relationship where the decrease in strength with height is clear for the species studied.

To relate the strength of a material with its size (the volume effect), experiments have been conducted to explain the strength decrease with increasing specimen size as observed by Pierce (Pellicane 1980). Weibull 1937, derived a generic equation:

$$\sigma_u = \int_{\sigma_{\min}}^{\infty} \exp(-V * ((\sigma - \sigma_{\min}) / \sigma_0)^m) * d\sigma \quad [2,17]$$

where:

V - volume

σ - stress

σ_{\min} - minimum value of stress

σ_u - ultimate stress.

for an estimate of the ultimate strength, where m and σ_0 are experimental constants relating to the distribution shape and scale, and σ_{\min} is an estimate of the population lower bound. This is known as the three parameter Weibull cumulative frequency distribution function. Some studies cited by Pellicane (1980) confirm the theory by comparison of experimental and predicted values.

2.5.2 RELIABILITY BASED DESIGN (RBD)

The application of the procedures of RBD involves the specification of the distribution of expected loads Q and the distribution of material for structural resistance R (Zahn 1977; Bodig and Jayne 1982). For both variables the probability functions are required. The concept of structural safety can be visualized in the Figure 2.6 (Goodman et al. 1981; Bodig and Phillips 1983; Phillips et al. 1985).

As can be seen there always exists the probability of occurrence of low resistance and high load; therefore, the absolute safety can not be guaranteed.

The failure probability (which is a function of the degree of overlapped area of the two distributions) is the probability that the load effect for a structural member exceeds its resistance. The Load Resistance Factor Design approach allows a desired level of reliability to be achieved by use of the relationship:

$$\phi * R_m = \sum_{i=1}^n * \gamma_i * Q_{mi} \quad [2, 18]$$

where:

- ϕ = resistance factor (usually <1);
- R_m = nominal mean resistance;
- γ_i = load effect factor (usually >1);
- Q_{mi} = load effect;
- n = number of load types.

The values assigned to the factors vary according to the reliability design. These factors, γ and ϕ , for load and

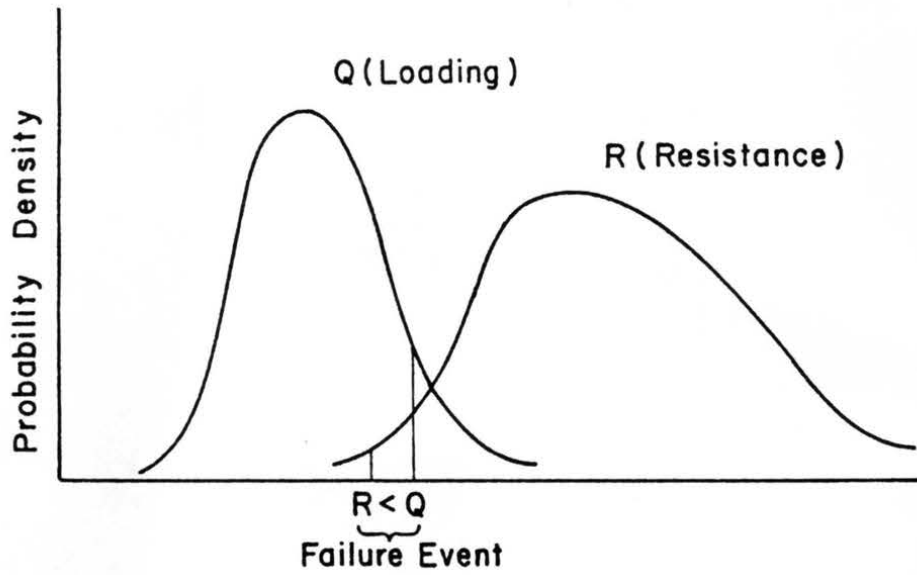


Figure 2.6. Probability Density functions of Loading (Q) and Resistance (R), Showing Typical Failure Location. (After Zahn 1977)

resistance reflect the variability of the load and resistance (material), data uncertainty and reliability level. They can be evaluated by

$$\phi = \exp(-0.75 \beta \text{COV}(R) K_R) \quad [2,19]$$

$$\gamma_W = \exp(+0.75 \beta \text{COV}(W) K_W) \quad [\text{wind}] \quad [2,20]$$

$$\gamma_I = \exp(+0.30 \beta \text{COV}(I) K_I) \quad [\text{ice}] \quad [2,21]$$

$$\gamma_D = 1.2 \quad [\text{dead load}] \quad [2,22]$$

where:

β = the index of structural reliability;

COV = coefficient of variation;

K = correction factor for data
uncertainty.

In order to obtain data for poles to be used in the equations derived in the reliability-based design method, a search resulted in identification of 3002 laboratory tests of North American wood poles, mostly of distribution sizes. Later, the EPRI sponsored a project where data were obtained for Douglas-fir, southern pine and western redcedar (Phillips et al. 1985; Bodig et al. 1986; Bodig and Goodman 1986) by testing full-size poles and determining the mean and variability of MOR and effective modulus of elasticity (MOE) of green untreated transmission size poles.

The Appendix C of the 1987 ANSI 05.1 code provides data to be used in reliability-base design method. The data in this code were originated from "Wood Pole Properties, Review and Recommendations for Design Resistance Data", Volumes I, II and III (Phillips et al. 1985; Bodig et al. 1986; Bodig and

Goodman 1986). The sizes and classes mentioned in the ANSI code 05.1 apply for the data presented. The circumference defined by this standard, however, should be used with data provided in that appendix. The strength at groundline and stiffness values are presented for new, green, untreated poles. Some adjustments, treatment effect, height effect, etc.) may apply to the general formula:

$$R_m = MOR_m * K_1 * K_2 * \dots * K_n \quad [2,23]$$

$$E_m = MOE_m * K_1 * K_2 * \dots * K_n \quad [2,24]$$

where:

- R_m = Adjusted mean groundline strength;
- MOR_m = Mean modulus of rupture based on pole class dimensions given in ANSI tables;
- E_m = Adjusted mean groundline modulus of elasticity;
- MOE_m = Mean modulus of elasticity, based on pole class dimensions given in ANSI tables;
- K_i = Adjustment factor to account for effect of characteristics and processes influencing pole strength and stiffness.

2.5.3 SIMULATION PROCEDURES COMBINED WITH NON-DESTRUCTIVE EVALUATION (NDE) OF WOOD POLES

Non-destructive evaluation (NDE) techniques can be used successfully to predict properties of materials with low variability and uniform properties (Goodman et al. 1981). In

the case of wood, because of its high variability, the use of this technique is more difficult.

The uses of NDE procedures are often based on empirical relationships between the properties, e. g. MOR and its dynamic modulus of elasticity, the latter may be evaluated as:

$$E_d = v^2 * \rho / g \quad [2,25]$$

where:

E_d = dynamic modulus of elasticity (psi);

v = speed of sound (in/sec);

ρ = density of wood (lbs/in³);

g = gravitational acceleration (in/sec²).

The speed of sound, v , can be measured directly on poles tested to destruction, then v and the pole strength, F_b , can be correlated.

As described, the NDE methods can be used to evaluate the strength and the stiffness, which are the data most often required for designing engineered structures (Phillips et al. 1985). To estimate these properties for poles, full-scale destructive tests or NDE can be used. Both methods require the definition of a population such as species, pole class, geographical area, and others, from which samples are taken and assumed representative.

The full-scale testing may involve a large number of variables and requires evaluating a great number of poles to determine the parameters of the population.

The NDE can be combined with Monte Carlo simulation adapted for wood poles to predict statistical distribution for a given destructive property (Pellicane 1982).

The Monte Carlo method uses the probabilistic approach to solve problems where the analytical process is too complicated to solve directly (Pellicane 1980). Some fundamental data on a probability distribution function is needed to apply the Monte Carlo technique and the sampling process is usually accomplished with the help of a pseudo-random number generator with which repeated trials are used to produce data from which statistical information can be obtained.

Data from the parent relationship which relates the destructive property and the NDE variable is necessary (Pellicane 1984; 1985). With the parent relationship data, the field NDE can be performed on those poles and a simulated distribution obtained for the destructive property of interest. For the application of NDE techniques it is assumed that:

- requires the definition of population;
- from each population representative samples taken and evaluated;
- all future members of a population will behave as do representative samples.

The process is adequate to predict the strength distribution of a large group of poles, but not suitable to predict the strength of individual poles. A process is recommended (Goodman et al. 1981) in order to accomplish the

simulation and the generation of strength distribution. The steps needed to predict strength of a population of different products, as a group of poles for example, are:

1. basic information for the group of poles such as number of poles, sizes, species, treatment, etc;
2. transverse stress wave (NDE) obtained for each pole (or a representative number of poles). Determine the distribution function to fit NDE data;
3. determine the MOR vs NDE correlation by testing the sample to destruction. Existing data may be used if available;
4. prediction of pole strength by simulation using computer programs;
5. the output of simulation will be a list of generated MOR values. The statistical distribution can be represented by a curve or histogram.

2.6 PREVIOUS STUDIES RELATED TO WOOD

The presence of knots and associated grain deviation are the most important factor contributing to stress concentration in structural wood members (Wangaard 1950; Kollmman and Cote 1968).

Modeling wood members with single knots and associated grain deviation using finite element theory was reported by

Dabholkar (1980). In his model, he used the similarity between wood grain pattern around a knot with flow stream lines. To predict the grain deviation, equations from fluid mechanics describing fluid flow around an elliptical cylinder in a laminar cross flow were used.

By analogy the longitudinal axis is taken as the main flow direction and the tangential axis as the cross direction. The stream lines can be represented by the following equation (Milne 1950):

$$\psi = v*(a+b)*\sinh(\xi-\xi_0)*\sin(\eta-\alpha) \quad [2,26]$$

where:

ψ - stream function (grain direction analogy);

v - speed of flow (taken as unity in analogy);

a, b - lengths of major and minor axes of ellipse of flow obstacle (represent knot in analogy);

ξ, η - elliptical coordinates, around the elliptical flow obstacle at which the value of ψ is sought;

α - angle of attack of flow (cross grain angle for wood member in analogy), and;

ξ_0 - constant.

The mathematical procedure shown above involves the use of elliptical coordinates. Dabholkar (1980) developed an interactive routine to solve the equation since no direct solution exists in elliptical coordinates. He wrote the program KMESSH to generate the mesh around a knot which was

used in combination with the program SAP-IV to analyze the stress-strain behavior of a wood member containing a single knot.

Cramer (1981) continued this work introducing adjustments in the program KMESH. The program KMESH1 was capable of generating finer meshes, as well as accounting for partial edge knots. Later, based on KMESH1, Cramer (1984) developed the STARW (STrength Analysis Routine for Wood) a program with a more powerful mesh generation and finite element/fracture mechanics algorithm. One more important improvement was made in the program STARW by Zandbergs (1985), introducing a refinement in the finite element mesh to model global cross grain. The resulting version was entitled STARWX.

2.7 FINITE ELEMENT APPROACH FOR ORTHOTROPIC PROBLEMS

Closed-form solutions for 2-D and 3-D problems are limited to simple problems with specific boundary conditions and load cases. For orthotropic materials, solutions exist for only a few problems when the load is applied in the direction of the orthotropic axes of the material. Solutions are even fewer for anisotropic materials and limited to certain shapes of solid and loading conditions (Al Dabbagh 1970).

Numerical techniques to solve more general and complicated engineering problems are used in most of the cases with the aid of computers. The finite element method is a very popular tool to solve 2-D and 3-D problems which present

complicated loadings, boundary conditions, shapes and material properties.

With the development of digital computers the finite element method has become very popular and most used to solve all sorts of engineering problems.

Studies were conducted at CSU which modeled wood members as an orthotropic material using 2-D finite element method, by Dabholkar (1980), Phillips (1980), Cramer (1981, 1984), Zandbergs (1985). To characterize the tension behavior of wood containing a knot, Pugel (1980) and Anthony (1986) studied the properties of knotty wood. Cramer and McDonald (1989) used a finite element model for predicting tensile stiffness and strength of 2" x 4" wood containing a single surface knot. In this study the grain angles were obtained through electrical scanning of the board surface.

For 3-D problems, a fundamental study was carried out by Al Dabbagh (1970) applied to solid blocks. The constitutive law with 21 elastic compliances was used and some examples, including wood orthotropy were presented. A method for simulating tension performance of lumber members was developed by Stahl et al. (1990), in which grain angle maps were obtained by scanning technique and wood characteristic determined in small clear specimens. The methodology uses a 2-D finite element approach, but to include the 3-D fiber orientation (diving angle), transformations for plane analysis in the wide face were performed.

2.8 CONSTITUTIVE LAW IN ORTHOTROPIC ELASTICITY

In mechanics of materials the study of the behavior of bodies can be divided into two cases:

- a. the study of rigid bodies - the shape or volume deformation is not significant. Newtonian laws are used to determine the forces acting on a body in a body in equilibrium;
- b. the study of deformable bodies - in which the deformation of the body under a given force must be known.

The study of mechanics of deformable bodies starts with the force-displacement relationship. Depending on the material in question, the relationship is linear or non-linear. In addition, the deformation after removal of the load system may be completely recoverable or not. For most materials, some deformation is permanent. If the deformation of a material is completely and instantaneously recoverable, the material is said to be elastic, and the deformation called elastic.

In order to apply the constitutive relationships, to conform to Hooke's law, the force-displacement characteristic of wood in bending is assumed to be linear to failure. Also wood is among the fibrous materials classified as orthotropic in 3-D (Jayne and Suddarth 1966; Wood handbook US-FPL 1974). An orthotropic solid denotes an internal structure which is characterized by the existence of three mutually perpendicular planes of structural symmetry. These three planes imply the

existence of a system of mutually perpendicular axes, Figure 2.7:

- (L) - longitudinal axis parallel to the grain;
- (R) - radial is normal to the rings in the cross section;
- (T) - tangential axis perpendicular to grain and tangent to growth rings.

The 3-D Hooke's law mathematically relates all components of stress to all components of strain (Bodig and Jayne 1982). The relationship can be either strain as a linear function of stress with a set of parameters called the compliance coefficients, or a stress as a linear function of strain and the set of parameters called stiffness coefficients.

The tensor expression of Hooke's law for a general anisotropic body connects the nine components of stress to the nine components of strain, or vice-versa, identifying in either case 81 stiffness or compliance coefficients (Jayne and Suddarth 1966; Goodman and Bodig 1970; and Jayne 1974):

$$\sigma_{ij} = C_{ijkl} * \epsilon_{kl} \quad [2,27]$$

and similarly,

$$\epsilon_{ij} = S_{ijkl} * \sigma_{kl} \quad [2,28]$$

where:

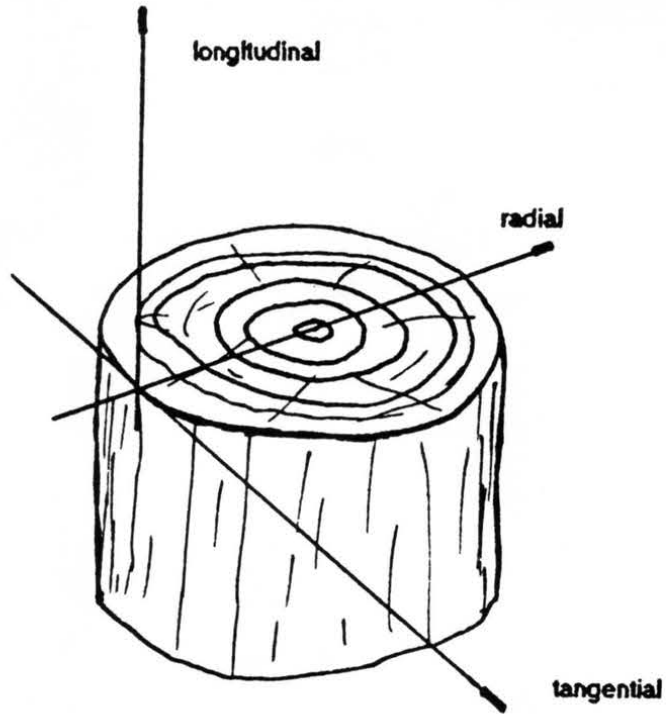
σ_{ij} - stress tensor;

ϵ_{ij} - strain tensor;

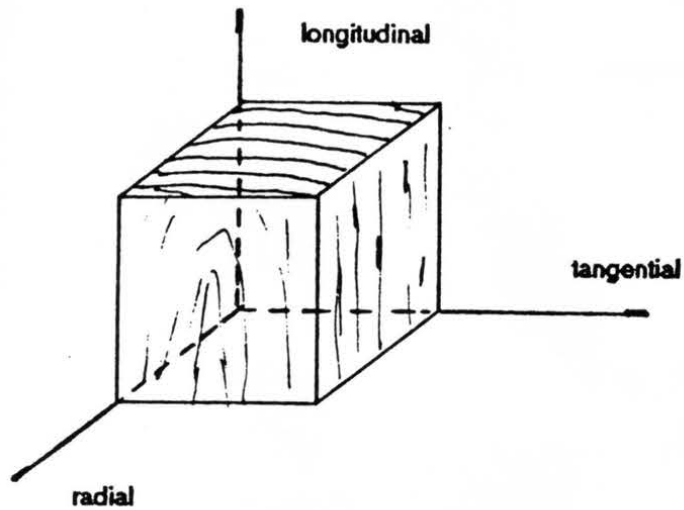
S_{ijkl} - compliance tensor;

C_{ijkl} - stiffness tensor;

i, j, k, l - coordinate index (each can be 1, 2, 3 independently).



(a)



(b)

Figure 2.7. Three Mutually Perpendicular Axes of symmetry with Reference to a) Cylindrical Bole, and b) Lumber.

Stress is represented by a second order tensor defined at a point. For any 3-D orthogonal coordinate system, the nine stress components are:

$$\begin{vmatrix} \sigma_{11} & \sigma_{12} & \sigma_{13} \\ \sigma_{21} & \sigma_{22} & \sigma_{23} \\ \sigma_{31} & \sigma_{32} & \sigma_{33} \end{vmatrix} \quad [2,29]$$

and similarly for strain:

$$\begin{vmatrix} \epsilon_{11} & \epsilon_{12} & \epsilon_{13} \\ \epsilon_{21} & \epsilon_{22} & \epsilon_{23} \\ \epsilon_{31} & \epsilon_{32} & \epsilon_{33} \end{vmatrix} \quad [2,30]$$

Because of the symmetry, the matrices [2,29] and [2,30] have six independent coefficients and for the matrices [2,27] and [2,28] 21 coefficients out of 36 are independent. One more simplification can be obtained when the orthotropic axes of symmetry of wood coincide with the axes of reference. The simplest form of the Hooke's law is obtained setting the axes longitudinal, radial and tangential as x, y and z (Figure 2.7).

Wood, or any other orthotropic material, is characterized by six elastic moduli and six poisson coefficients:

E_L, E_R, E_T - Young's moduli of elasticity in
longitudinal, radial and tangential axis;

G_{LR}, G_{LT}, G_{TR} - Shear or rigidity moduli in the planes LR, LT
and RT;

$\nu_{LR}, \nu_{LT}, \nu_{TL}, \nu_{RL}, \nu_{RT}, \nu_{TR}$ - Poisson's ratios, where $\nu_{ij} =$
 (strain on the j axis)/(strain on the i axis)
 for a uniform normal stress in the i axis
 direction.

The constitutive law for wood, then takes the following
 form:

$$\begin{array}{c}
 \gamma_L \\
 \gamma_R \\
 \gamma_T \\
 \gamma_{LR} \\
 \gamma_{LT} \\
 \gamma_{RT}
 \end{array}
 =
 \begin{array}{ccccccc}
 \frac{1}{E_L} & -\frac{\nu_{RL}}{E_R} & -\frac{\nu_{TL}}{E_T} & 0 & 0 & 0 & \\
 \frac{\nu_{LR}}{E_L} & \frac{1}{E_R} & -\frac{\nu_{TR}}{E_T} & 0 & 0 & 0 & \\
 \frac{\nu_{LT}}{E_L} & -\frac{\nu_{RT}}{E_R} & \frac{1}{E_T} & 0 & 0 & 0 & \\
 0 & 0 & 0 & \frac{1}{G_{LR}} & 0 & 0 & \\
 0 & 0 & 0 & 0 & \frac{1}{G_{LT}} & 0 & \\
 0 & 0 & 0 & 0 & 0 & \frac{1}{G_{RT}} &
 \end{array}
 \begin{array}{c}
 \sigma_L \\
 \sigma_R \\
 \sigma_T \\
 \sigma_{LR} \\
 \sigma_{LT} \\
 \sigma_{RT}
 \end{array}
 \quad * \quad [2,31]$$

As stated before the Hooke's law has the form [2,31], when the geometric axes are coincident with the material axes. If the material axes are different from the geometrical axes, then the orthotropic law must be transformed accordingly using the tensor transformation law. Appendix A shows the final matrix with 36 parameters after the transformation.

2.9 ELASTIC PARAMETERS OF WOOD

As seen in Equation [2,31], 12 elastic parameters are needed for complete characterization of the 3-D compliance or stiffness matrix of an orthotropic material. Considering the

symmetry due to strain energy, three Poisson ratios can be computed using the following identities:

$$\frac{\nu_{LR}}{E_L} = \frac{\nu_{RL}}{E_R}; \frac{\nu_{LT}}{E_L} = \frac{\nu_{TL}}{E_T}; \frac{\nu_{RT}}{E_R} = \frac{\nu_{TR}}{E_T} \quad [2,32]$$

thus, only nine elastic parameters are independent and necessary to be determined. The method to determine these parameters are based on plate tests and are described by Gunnerson et al. 1973.

Bodig and Goodman (1973) describe the test difficulties in determining these parameters in terms of instrumentations, time to prepare and test specimen preparation. This paper includes the results of tests performed on some American softwoods and the results from other sources as well, using plate bending and compression tests. A very useful section is included in this paper describing the relationship between combinations of the elastic parameters and density. For the Poisson ratios, however, due to the small variation of six different values, a table is presented, including the average values for hardwoods and softwoods, regardless of the species. These values are given in Table 2.2.

TABLE 2.2. Average Poisson's Ratios for Hardwoods and Softwoods Determined in Small Specimens Tests (After Bodig and Goodman (1973))

Poisson's ratio	Softwood	Hardwoods
ν_{LR}	0.37	0.37
ν_{LT}	0.42	0.50
ν_{RT}	0.47	0.67
ν_{TR}	0.35	0.33
ν_{RL}	0.041	0.044
ν_{TL}	0.033	0.027

CHAPTER 3

MATHEMATICAL MODEL FOR WOOD POLES

3.1 GENERAL

In solid mechanics, three basic requirements need to be satisfied for stress-strain analysis (Boresi and Sidebottom 1985; Criswell 1988):

- a. Equilibrium;
- b. Geometric conditions or continuity (compatibility);
- c. Material properties (constitutive relations, stress-strain properties).

Mathematical models are usually categorized by means of two different solutions: closed-form and numerical techniques. The latter includes finite element, finite difference and matrix methods. Closed-form solutions are exact solutions and are often limited to problems with special loads, boundary conditions, and generally assume material isotropy. Timoshenko (1962), Coates et al. (1988), Gutkowski (1981) and others present the closed form solution approach to solve engineering problems related to structural analysis.

In general, a numerical solution formulates a discrete element mathematical model, equivalent to an actual continuous structure. The formulation of such a model called "structure idealization" is accomplished essentially by equating energies

of the continuous and discrete element systems (Przemienieck 1985).

For structures with irregular shape, the finite element method is recognized as the best approach in order to evaluate the stresses generated by loading systems.

Being a natural material, poles always present growth characteristics such as knots, spiral grain, and variable taper (barrel shape). Therefore, a pole is a very complex 3-D structure that, for the purpose of this study, will be modeled using a finite element method.

The loading of single pole structures for distribution and transmission lines are schematically represented as cantilever beams with a concentrated load applied to the tip (ANSI 1987; ABNT 1980). To account for local effect of natural defects such as knots, spiral grain, and material inhomogeneity producing MOE and MOR variations along the length and across the diameter of a pole, pole segments were studied to create data useful in incorporating these effects.

The 3-D modeled segment represents a real segment of a pole, which includes anisotropy, defects (knots and spiral grain) and material inhomogeneity.

Literature related to the finite element method (Weaver and Gere 1965; Weaver and Johnson 1984; Przemienieck 1985; GTSTRU DL 1985); studies concerning knot sizes and wood characteristics (Bodig 1986; Phillips et al. 1981; Dashiell 1985; Wang 1987) and pole geometry and dimensions (ANSI 1987; Phillips et al. 1985) were followed as guidelines to define

the mesh pattern, dimensions of elements, element types and other details. Loading and boundary conditions at the segment ends were modeled using static equilibrium and the tools (variable loading using stresses applied at joints, elastically restrained supports, etc.) offered by the finite element software used.

3.2 THREE-DIMENSIONAL MODEL FOR WOOD POLES WITH NATURAL DEFECTS

3.2.1 FINITE ELEMENT MODEL

For continuum problems using finite element methods, the computer program Georgia Tech STRUctural Design Language (GTSTRUDL) from Georgia Institute of Technology version 8701 CDC, released in March 1988, available at the CSU Control Data CYBER 840 computer center, was used. This program contains an element library with a multitude of diverse element types that can be mixed in the same analysis to provide a most rational structure idealization. GTSTRUDL performs static and dynamic analyses assuming linear elastic material properties and small-displacement theory. Appropriate considerations for geometry, topology, boundary conditions, element and material properties must be made. Basically, a matrix formulation is used to solve the stiffness equations expressed in terms of unknowns displacements:

$$U = F/K \quad [3,1]$$

where: K = structure stiffness matrix;

U = unknown joint displacement components;

F = equivalent applied joint force components.

3.2.2 ELEMENT DEFINITION

To analyze a pole, 18 inch long segments were taken along the length and modeled with 3-D analysis and appropriate boundary conditions, as detailed in the subsequent sections.

To define the mesh over any segment, some assumptions were made based upon the analysis method, material characteristics and current pole standards:

A) For 3-D analysis, parallelepiped elements are recommended (GTSTRUDL 1985) with element aspect ratios as close as possible to 1:1:1. Analyzing the geometry and dimensions of Douglas-fir, western redcedar and southern pine poles of different lengths (ANSI 05.1) the width and height of the elements could be fixed. As an example, Table 3.1 shows typical element dimensions for poles of 45 ft and 60 ft in length and the cross section angles 15° and 22.5°, located at 6 ft from butt (Figure 3.1).

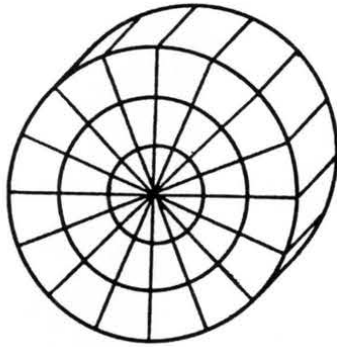
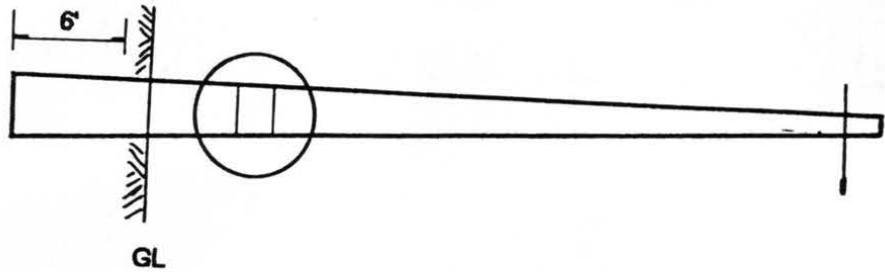
The circular cross section can be divided into an even number of equal angles for symmetry. Therefore the mesh generation and the process to assign the elastic properties on elements are simplified;

B) Knot diameters were limited according to the standards. ANSI 05.1 specifies for poles up to 45 feet long the maximum knot diameter in the lower half of 2 and 3 inches

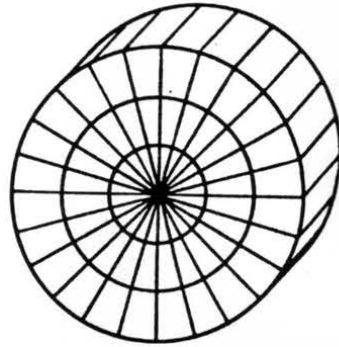
Table 3.1. Element Dimensions for Poles of 49' and 60',
and Cross Section Angles of 15° and 22.5°

<i>l</i>	<i>c</i>	<i>d</i>	<i>a</i>	<i>b</i>	class
DOUGLAS FIR/SOUTHERN PINE					
45	43.0	2.28	2.69	1.79	1
60	48.0	2.55	3.00	2.48	1
WESTERN REDCEDAR					
45	47.5	2.52	2.97	1.97	1
60	46.5	2.47	2.91	1.94	3

- l* - Pole length, feet
c - Circumference at 6' from butt, inches
d - Element depth, inches
a - Element width for 15.0°, inches
b - Element width for 22.5°, inches



22.5 deg. angle



15 deg. angle

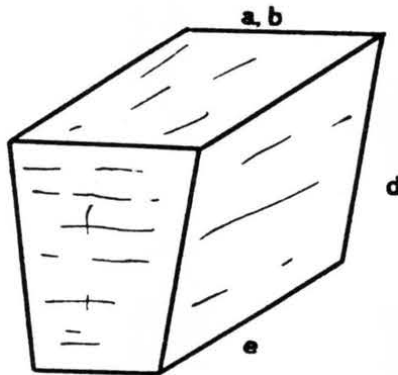


Figure 3.1. Idealization of Elements for Central Angles of 15.0° and 22.5°.

for classes 10 to 4 and 3 to H6 respectively, and ABNT, 8.5 cm (3.3 in) for all classes;

- C) Knots normally have elliptical shape. Measurements of knot diameters perpendicular and parallel to the pole length for all poles were made and presented in Tables 4.2 (Chapter 4.).

The guidelines A) and B) above lead to the definition of the angle of 22.5° (16 divisions), and B) and C) make reasonable an element length of 3 inches. For the outermost surface the ratio width/length fell close to the ratio recommended for 3-D analysis.

Multiple knots are commonly referred to in standards as the sum of knots in any one foot segment. Hence, any 12 inch length may be represented as four discs of three-inch elements. However, preliminary runs of the model using isotropic material showed that the stresses at end sections were influenced by load and boundary conditions. As discussed in Chapter 5, the stresses along a pole segment are graphically presented showing the effect of the boundary conditions and loadings on end sections. To avoid difficulties created by load and boundary effects along to the longitudinal axis of the one foot segment and to smooth out the stresses as well, two more discs were added. These two discs serve as transition discs or transition elements. Figure 3.2 shows the 3-D finite element segment mesh to represent any section along the pole.

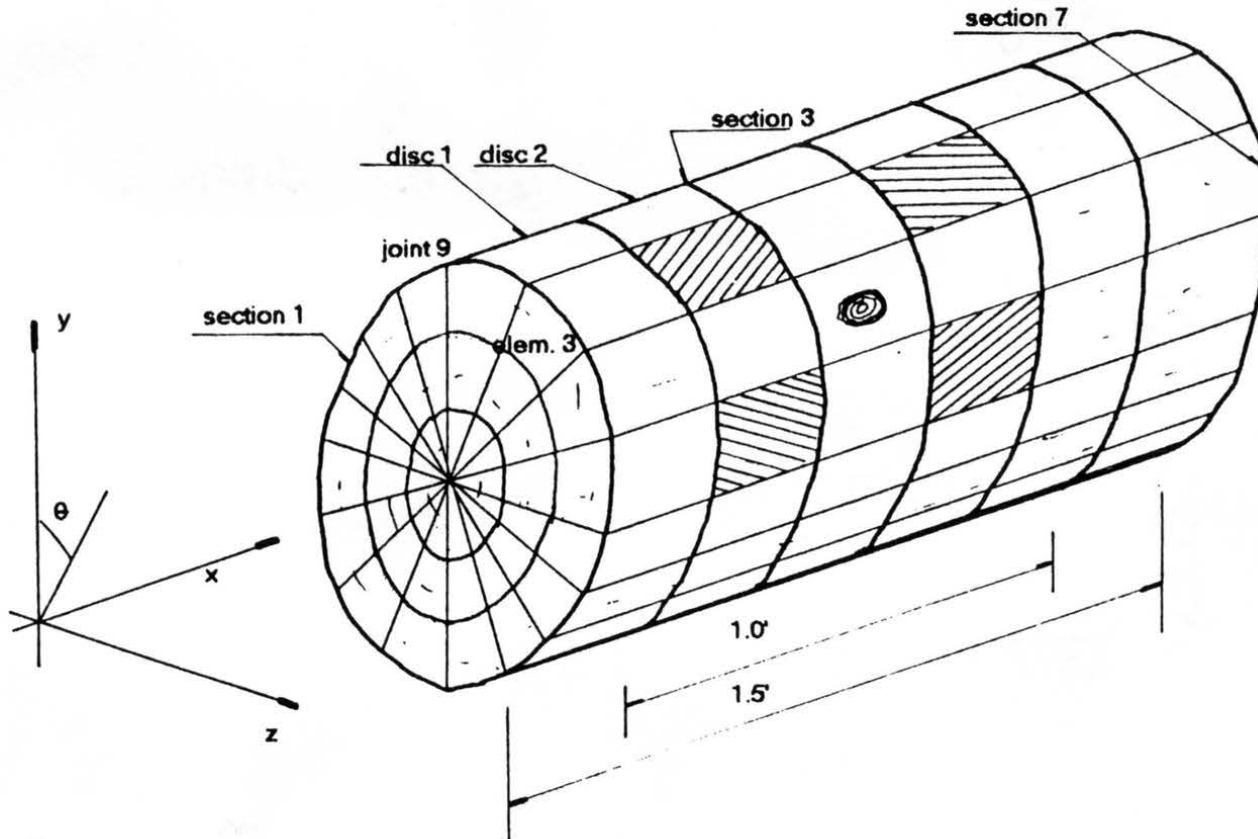


Figure 3.2. Finite Element Mesh to Represent a Pole Section of 18 inches in Length.

3.2.3 LOADING REPRESENTATION

Poles are often analyzed as statically-determinant cantilever beams with a concentrated load applied two feet from the pole tip. Thus, at any section the bending moment and shear force can be evaluated. According to the hypothesis mentioned earlier, the stresses developed by the applied moment and shear forces were evaluated and applied to each of the 145 joints located at the far section (the section of a segment closer to the pole tip, Figure 3.3) of the 18 inch segment. A FORTRAN program (Appendix B) was written to calculate the stresses at any section along the pole. Figure 3.3 presents schematically the loading representation.

For a circular section of area A, adopting a load of 1000 lbs, the shear is evaluated as $f_v = VQ/Ib$, where Q is the moment area about the horizontal line $y=y_0$, b is the chord at the same line and I is the moment of inertia of the circle:

$$Q = \int_A y dA = \int_{-a}^a \int_{y_0}^{\sqrt{R^2-x^2}} y dy dx = \quad [3,2]$$

$$Q = \frac{1}{2} \left((R^2 - y_0^2)x - \frac{x^3}{3} \right) \Big|_{-a}^{+a} \quad [3,3]$$

$$Q = a^3 - \frac{a^3}{3} = 2 \frac{a^3}{3} \quad [3,4]$$

since $b=2a$, $V=1000$ lbs,

$$f_v = \frac{1000(2a^3)/3}{2aI} = \frac{4000a^2}{3\pi R^4} \quad [3,5]$$

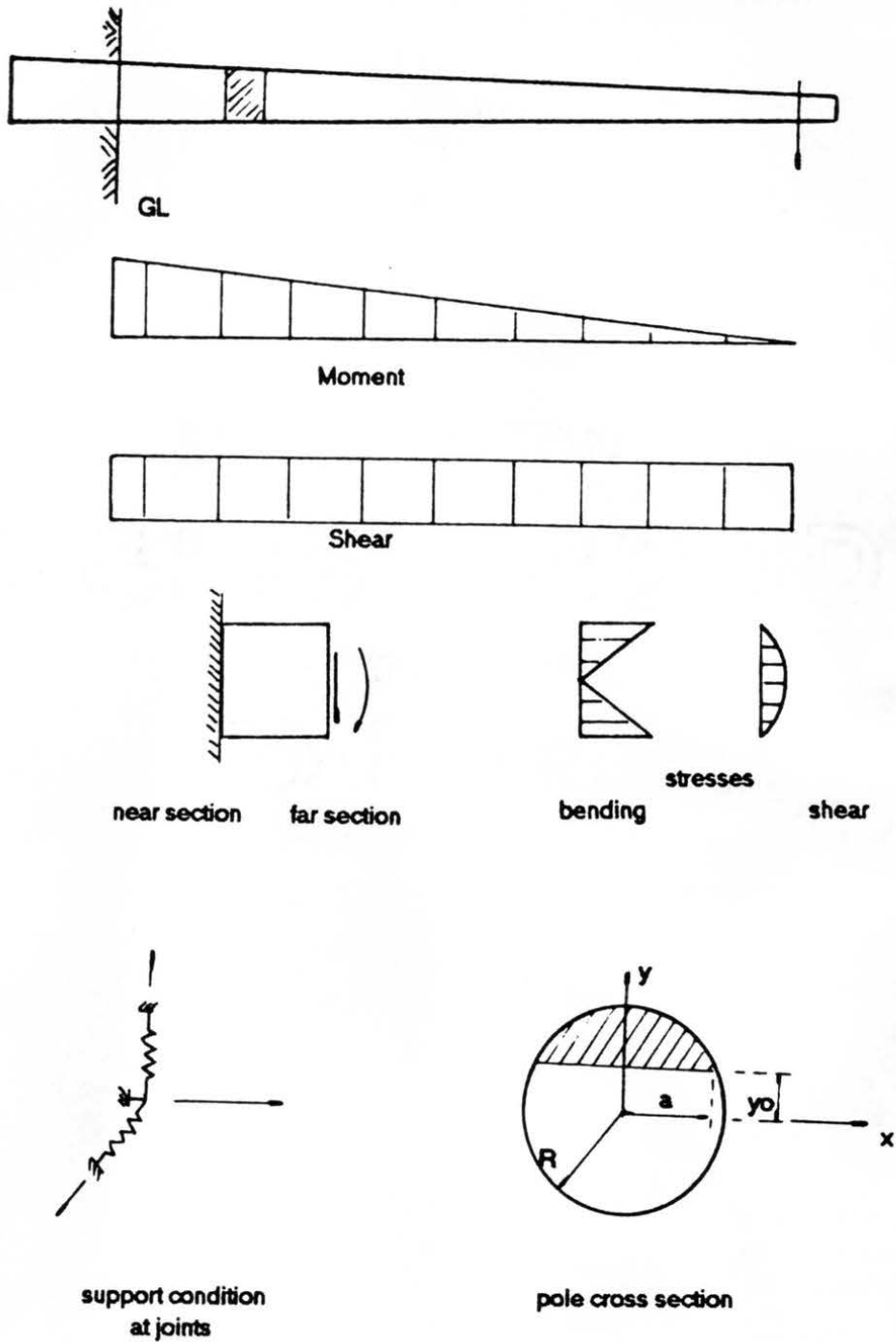


Figure 3.3. (Top) Representation of Loading on Pole Segments. (Bottom) Support Condition at Joints and Pole Cross Section.

At the near section (the section of segment closer to the butt, Figure 3.3), at each joint a system of springs was applied in order to permit movement in the y and z directions, Figure 3.3. A stiffness coefficient equivalent to $k=(A_c/L)*E$, was set for the springs. Due to some practical difficulties in determining k for each joint, it was taken as a unique coefficient numerically equal to the average E of radial and tangential directions, by setting $A_c/L=1$, where A_c is the element area parallel to grain and L is the depth of element perpendicular to grain. The loading and support conditions are illustrated in Figure 3.3.

3.2.4 KNOT MODELING

Knots and their associated cross-grain deviation have been modeled by several researchers (Dabholkar 1980; Phillips 1981; Cramer 1981, 1984; Zandbergs 1985) using flow-grain analogy. In the flow-grain analogy, the mesh is generated according to the knot size, the spacing of flow grain lines and by the number of rows of element within the knot. A typical half mesh generated by the flow-grain analogy is shown in Figure 3.4.

The mesh pattern for the pole segment as shown in Figure 3.2 is a function of the pole segment diameter only. The GTSTRU DL program automatically generates the mesh provided the pole radius and the radial increment are provided. Details of GTSTRU DL of mesh generation is given in the Appendix C.

In the mesh, over the pole segment generated by the

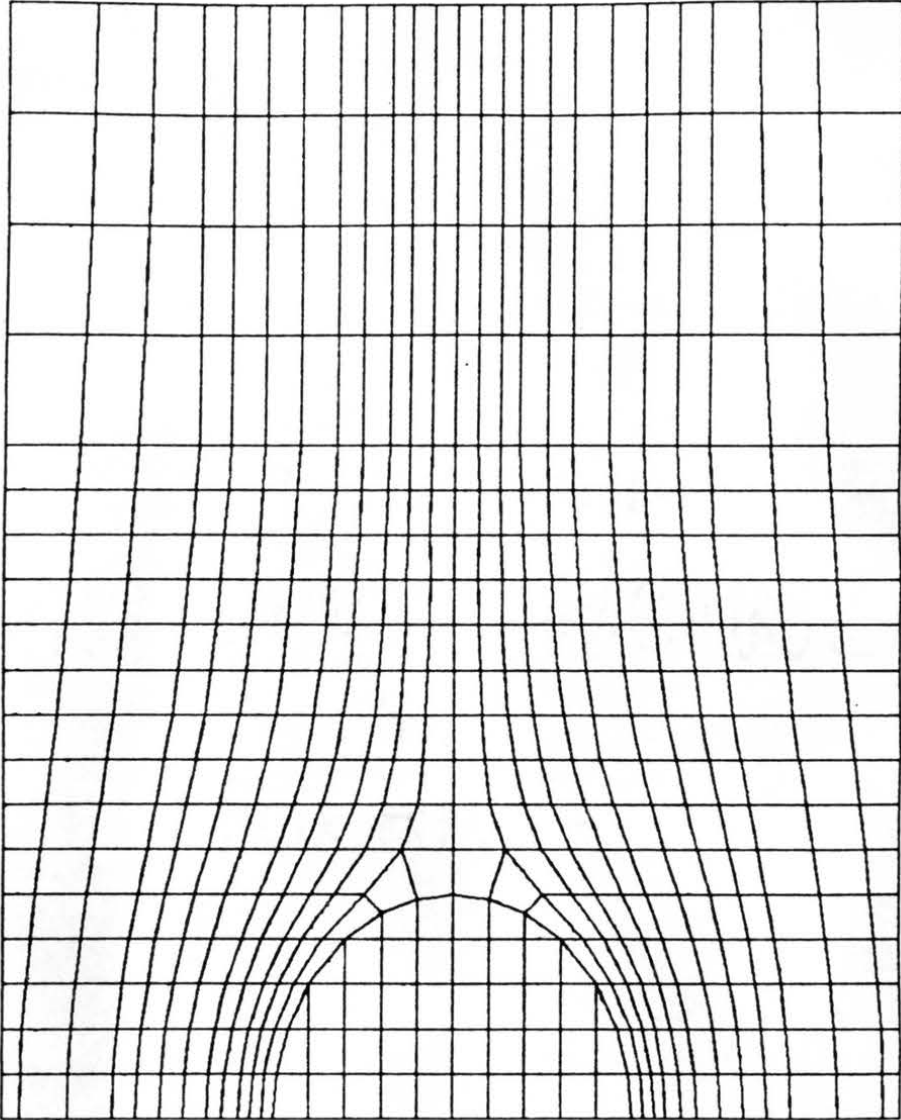
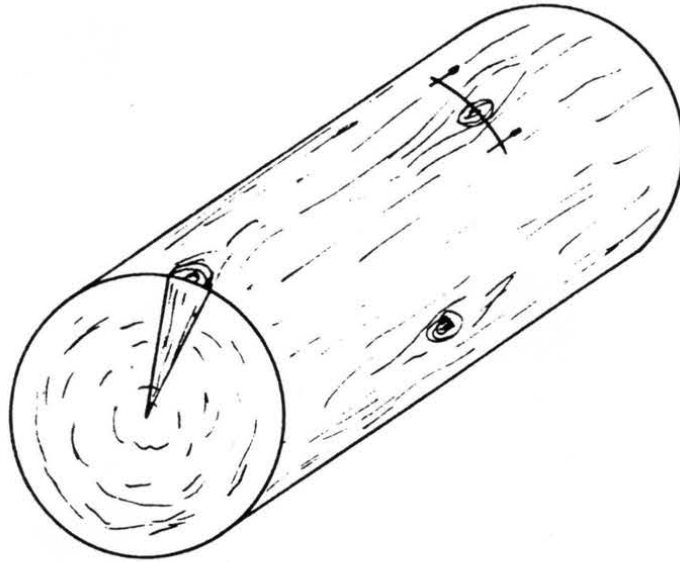


Figure 3.4. Typical Finite Element Mesh Generated by the Flow-Grain Analogy

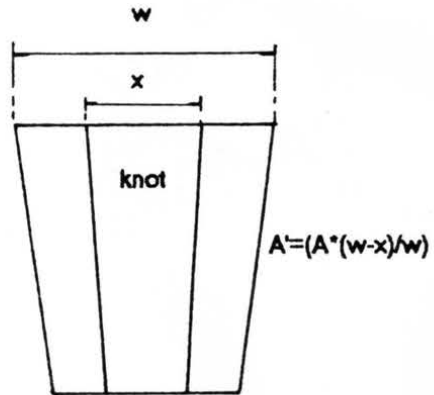
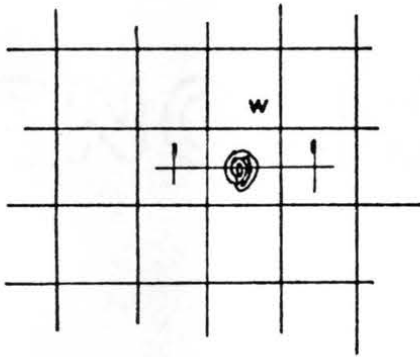
finite element program, knots could be modeled. To represent a knot and the associated fiber deviation (fiber angles) around it, knots were modeled as a cone shape which is centered in the element, with the vertex located in the pith and perpendicular to the longitudinal direction of the pole (Figure 3.5.a). Grain deviation around a knot was assigned to the four elements most affected by the presence of a knot, Figure 3.2, depending upon the knot diameter according to the function developed in Section 3.2.5, using the flow-grain analogy program. When more than one knot were presented in the same segment (cluster of knots) the superposition effect for grain deviation was adopted as shown schematically in Figure 3.6. Whenever a knot occurred in the outer surface, three elements were affected by it (one in each layer). Its effect on the element stiffness was taken into account by decreasing the MOE, and consequently the element stiffness matrix, by the ratio of the net width (element width minus the knot diameter) to element width. This is illustrated schematically in Figure 3.5.b.

3.2.5 GRAIN DEVIATION REPRESENTATION

As will be described in Section 4.2, all knots (knot map) on the poles analyzed were measured. In order to search for a function to represent the grain deviation around a knot, the frequency of knots was verified. Table 3.2 summarizes these numbers and presents the frequency of knots for poles of all three species and their cumulative distribution. As



(a)



(b)

Figure 3.5. (a) Knot Represented as a Cone; (b) Reduced Area due to the Presence of a Knot.

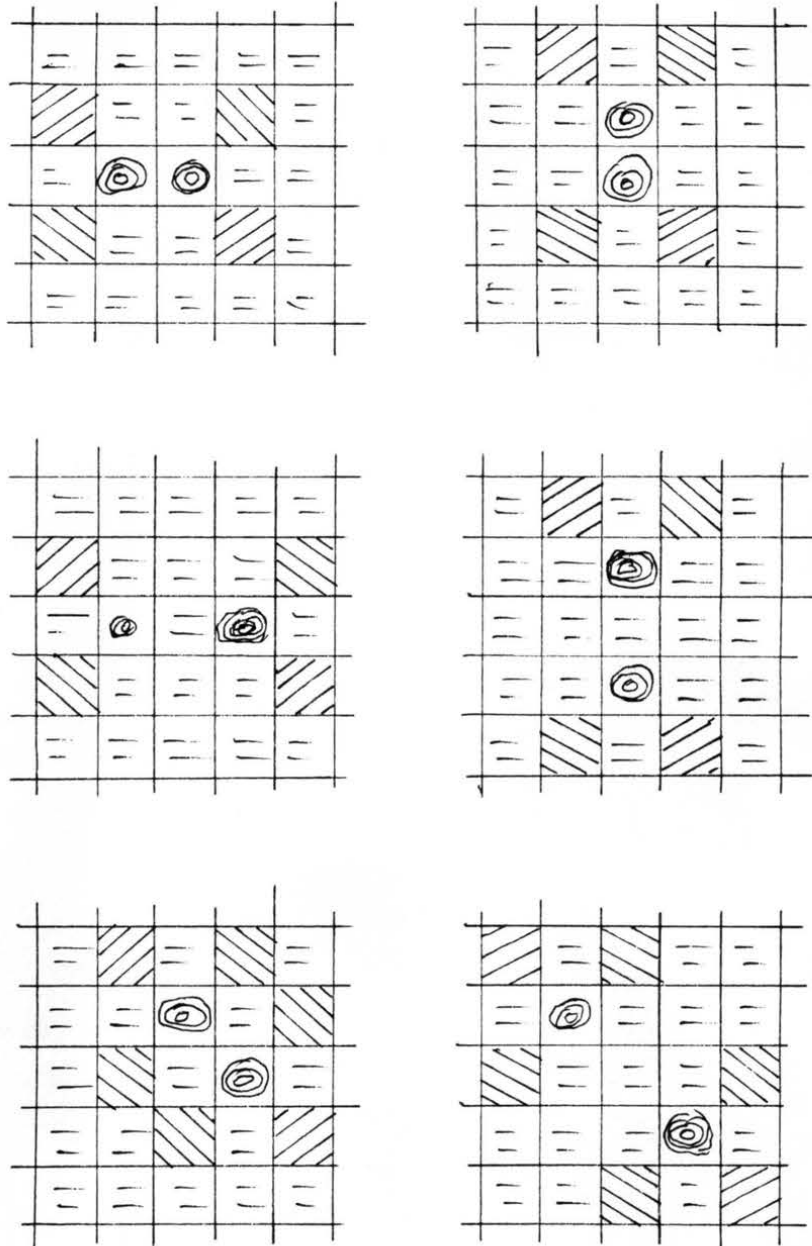


Figure 3.6. Representation of Cluster of Knots on Segment Finite Elements.

Table 3.2. Cumulative Distribution of Knot Diameters for Western Redcedar, Douglas-fir and Southern Pine.

Knot diameter	Western redcedar		Douglas-fir		Southern pine		Total		Percentage
	frequency	accumulated	frequency	accumulated	frequency	accumulated	frequency	accumulated	
0.5	22	22	22	22	0	0	44	44	15.6
0.6	15	37	21	43	1	1	37	81	28.7
0.7	8	45	28	71	4	5	40	121	42.9
0.8	7	52	19	90	0	5	26	147	52.1
0.9	13	65	8	98	1	6	22	169	59.9
1.0	9	74	16	114	2	8	27	196	69.5
1.1	10	84	4	118	3	11	17	213	75.5
1.2	9	93	2	120	0	11	11	224	79.4
1.3	6	99			5	16	11	235	83.3
1.4	12	111			2	18	14	249	88.3
1.5	8	119			0	18	8	257	91.1
1.6	6	125			1	19	7	264	93.6
1.7	7	132			0	19	7	271	94.1
1.8	2	134			1	20	3	274	97.2
1.9	5	139					5	279	98.9
2.0	1	140					1	280	99.3
2.1	2	142					2	282	100.0

seen in this table, all knots measured were of 2.1 inches or less in diameter and 99.3% were less than or equal to 2.0 inches in diameter.

Using the flow-grain analogy program, the grain angles around the knots were obtained and the maximum average grain angle deviation in the stream lines, associated with knot diameters varying from 0.75 to 3.0 inches, were evaluated using 0.13 (stream lines) inches of flow division and 5 divisions per radius within a knot as seen in Figure 3.4. The average maximum angle illustrated in Table 3.3 was 54.5° to represent the fiber deviation.

Having the knot distribution and the maximum angle around a knot, it was assumed for modeling purposes that the grain deviation caused by a 2.0 inches knot was 54.5° . To represent the grain deviation angles for smaller knots in the elements of the model, a function was developed that correlates the area influenced by the presence of the knot and the knot diameter. Figure 3.7 illustrates the area affected by a knot in western redcedar of 1.5 inches of diameter using the mesh and the angles predicted by the flow-grain analogy. Figure 3.8 indicates the curve obtained for different angles and cumulative areas measured on the flow diagram of Figure 3.7, according to Table 3.4.

The measurements were limited to angles greater than 2 degrees, which was the smallest angle represented in the flow diagram, being the limit of the model. Using the flow grain analogy the areas affected by the presence of a knot were

Table 3.3. Maximum Fiber Angle Around a Knot, Generated by the Flow Grain Analogy.

Knot Diameter	western redcedar	Douglas-Fir	southern pine
0.50	45.6	45.5	45.6
0.75	50.5	50.3	50.6
1.00	52.2	52.0	53.2
1.25	52.5	54.6	53.7
1.50	54.9	54.7	54.2
1.75	55.4	56.0	54.1
2.00	55.1	59.0	55.1
2.25	56.0	56.8	55.6
2.50	55.8	56.9	55.8
2.75		56.9	
3.00		56.6	

Obs: Average Fiber Angle = 54.5°
 For knot diameters from 0.75" to 3.0"

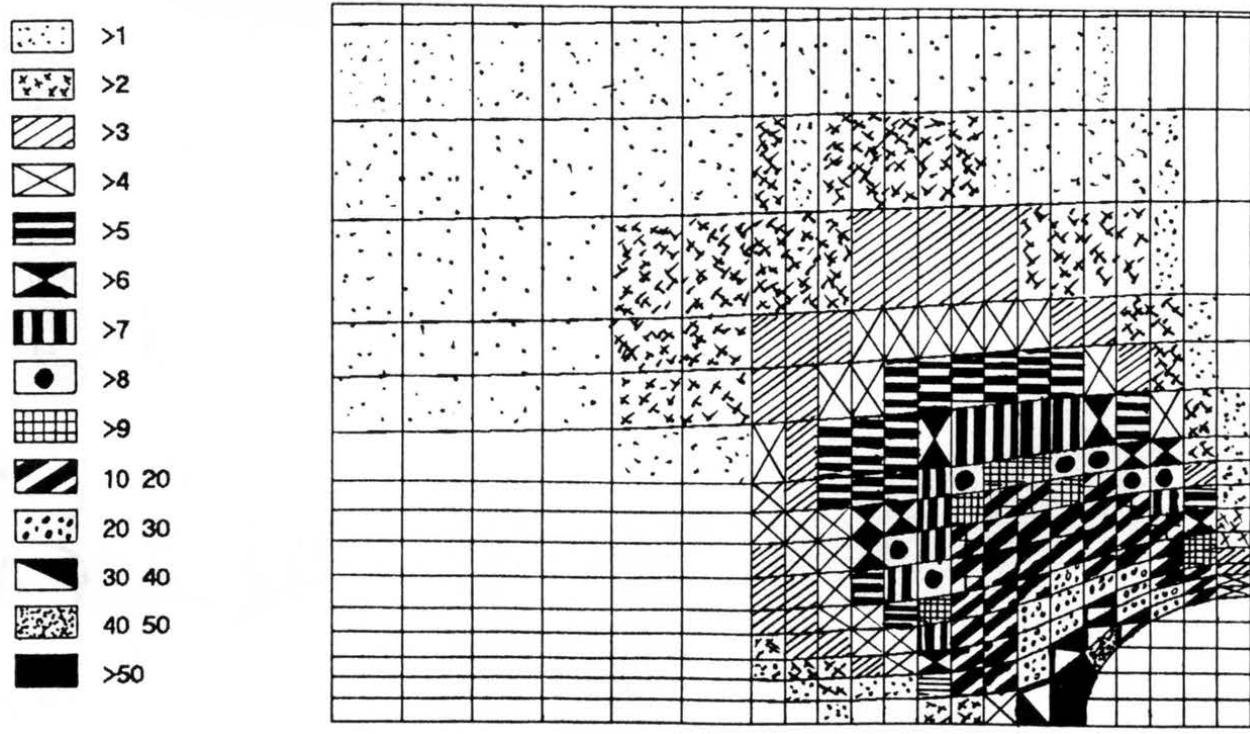


Figure 3.7. Flow Grain Diagram for a Knot of Western Redcedar of Diameter of 1.5 Inches, and Corresponding Fiber Deviation, in degrees, in Surrounding Area.

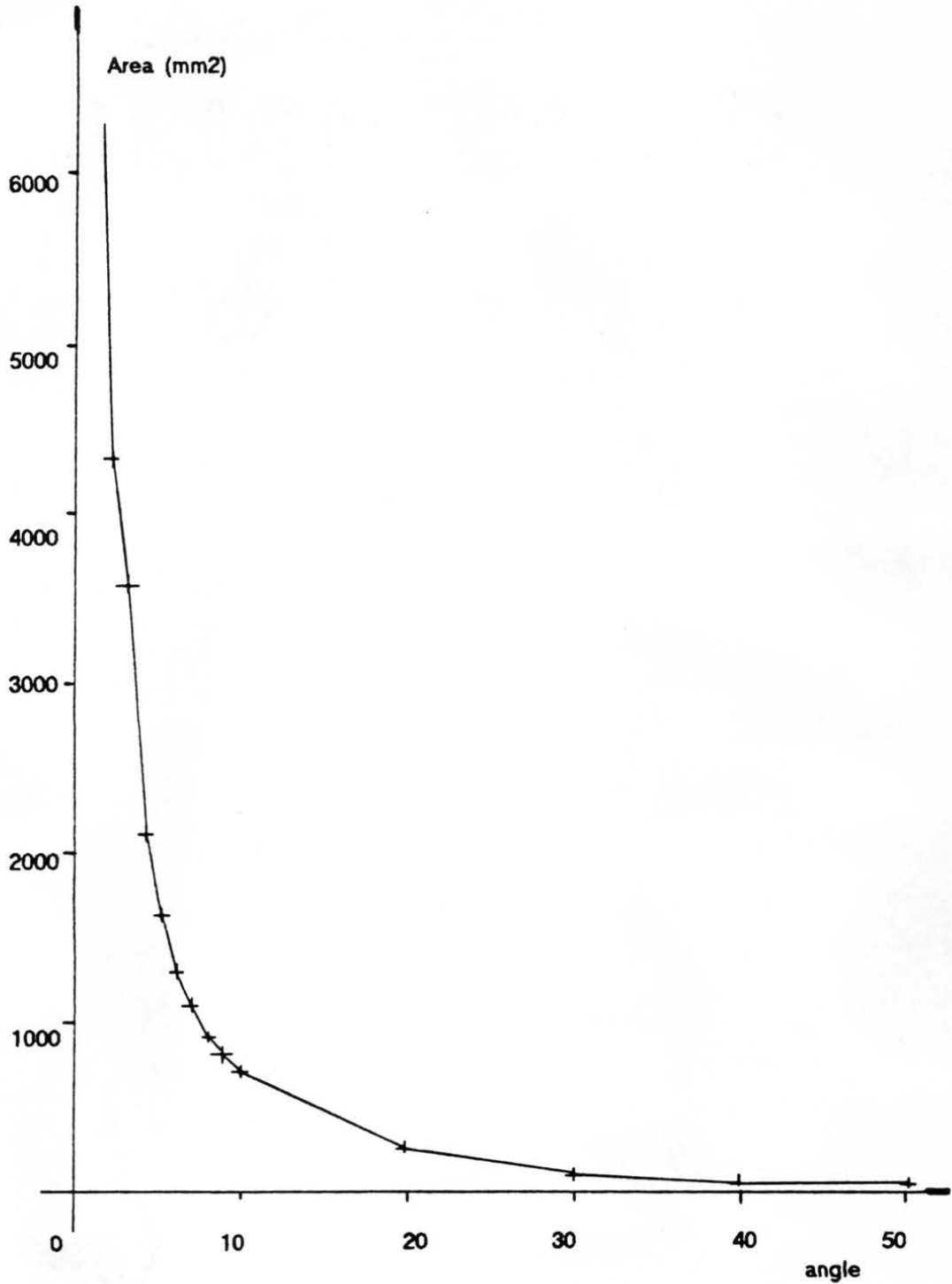


Figure 3.8. Area Around a Knot (diameter = 1.5") Affected by the Presence of Knot, for Different Angles of Deviation.

Table 3.4. Cumulative Area of Influence for a Knot of 1.5" of Diameter of Western Redcedar, using a Mesh Generated by the Flow Grain Analogy.

Angle (degree)	Area (mm ²)	Cumulative Area (mm ²)
>50	43	43
>45	14	57
>35	68	125
>25	137	262
>15	467	729
>9.5	87	816
>8.5	100	916
<7.5	199	1115
>6.5	153	1268
>5.5	357	1625
>4.5	511	2136
>3.5	737	3595
>2.5	1459	4332
>1.5	3756	8088

evaluated for knots of 0.5, 1.0 1.5 and 2.0 inches for Douglas-fir and western redcedar, which were the two first species studied, and are given in Table 3.5. Since poles of southern pine were tested later, data were not available at that time. The curve indicated in Figure 3.9 represents a function relating the knot diameter and the area affected by the presence of a knot.

The ratio between the area of influence of a knot less than 2.0 inches in diameter and one of 2.0 inches in diameter was taken as the coefficient to represent the decreasing factor over the maximum angle of deviation. The following function, which incorporates the decreasing factor, was used to evaluate the angle of deviation for knots less than 2 inches in diameter:

$$\alpha_d = \frac{A_d}{A_{2''}} * \alpha_{\max} = \frac{A_d}{A_{2''}} * 54.5^\circ = K_d * 54.5^\circ$$

The coefficient K_d was evaluated for knot diameters varying from 0.5 to 2.0 inches in increments of 0.1 inch according to the function, and are presented on Table 3.6. This table also includes the angle of deviation for these knots.

3.2.6 THREE DIMENSIONAL SEGMENT MODEL

Using the parallelepiped and wedge shaped element types available in GTSTRU DL, and the parameters defined previously in this chapter, such as number of discs in a segment and

Table 3.5. Area(*) Affected by the Presence of a Knot,
Using the Flow-Grain Analogy.

Knot diameter (inches)	Area (in ²)	
	western redcedar	Douglas-fir
0.5	0.72	0.73
1.0	2.86	2.74
1.5	6.66	6.93
2.0	11.02	11.02

(*) Evaluated in one quarter of the mesh.

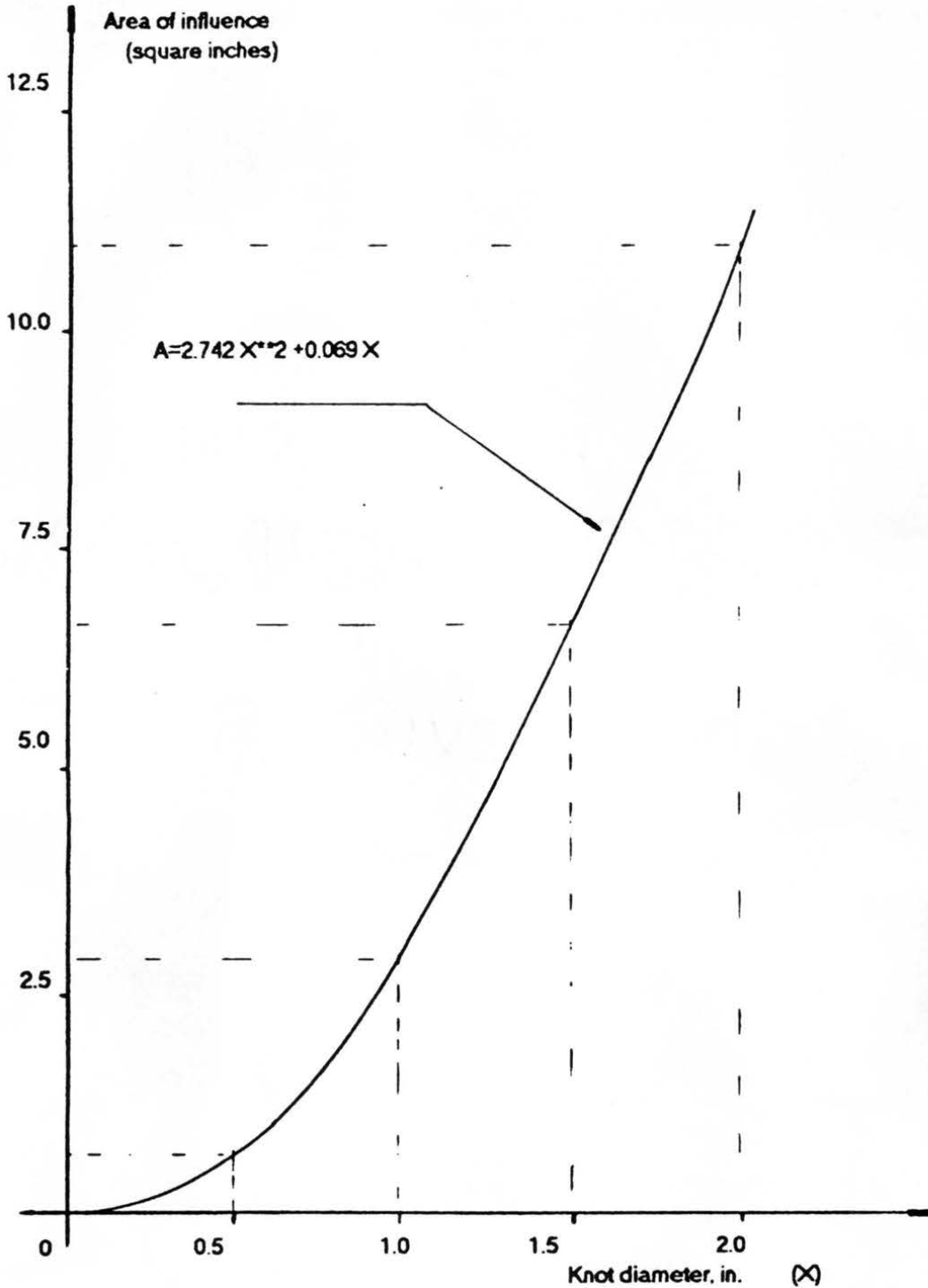


Figure 3.9. Curve Fitted for Area of Influence (Angles of Deviation $\geq 2^\circ$), for Knots of Douglas Fir and Western Redcedar, Using Flow-Grain Analogy.

Table 3.6. Effective Maximum Angle of Deviation for Knot Diameters between 0.5 and 2.0 inches.

Knot diameter in	Area affected in ²	$K = A1/A2$	Effective Angle ($K \cdot 54.5^\circ$)
0.5	0.720	0.065	3.533
0.6	1.029	0.093	5.050
0.7	1.392	0.125	6.831
0.8	1.810	0.163	8.882
0.9	2.283	0.206	11.203
1.0	2.811	0.253	13.794
1.1	3.393	0.306	16.650
1.2	4.031	0.363	19.781
1.3	4.724	0.425	23.182
1.4	5.471	0.493	26.848
1.5	6.273	0.565	30.783
1.6	7.130	0.642	34.988
1.7	8.042	0.724	39.464
1.8	9.008	0.811	44.205
1.9	10.029	0.903	49.215
2.0	11.106	1.000	54.500

A1 - Area affected by a knot

A2 - Area affected by a knot of 2.0" diameter.

number of elements in a disc, the segment idealized to model the pole characteristics was broken down into 288 elements, Figure 3.2. Due to the different shapes of the elements, in the two external rings a parallelepiped shaped element was used, and in the internal ring a wedge shaped element was used. From the GTSTRUDL library the element types IPQS a six face, 20 node (joint) element and the WEDGE15 a four face, 15 node element, were chosen and illustrated in Figure 3.10. For these elements, on each external face 145 joints were necessary and in the intermediate section, 49 joints were necessary, Figure 3.11. For the entire segment, the total of 1309 joints was generated for the 288 elements.

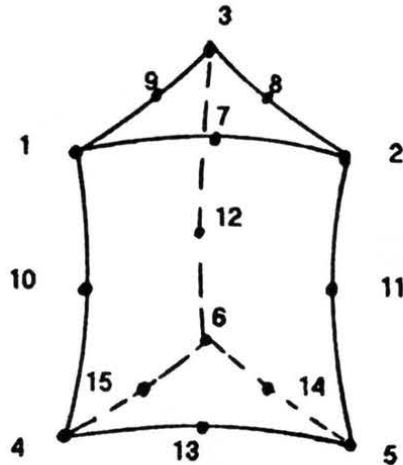
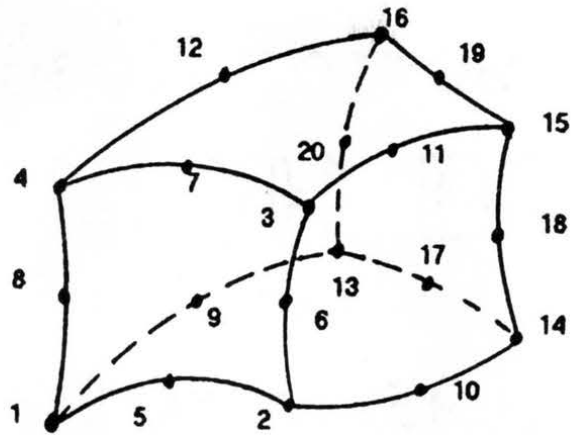


Figure 3.10. Node Numbering for Three-Dimensional Elements. Element Type IPQS (top); Element Type Wedge15 (bottom).

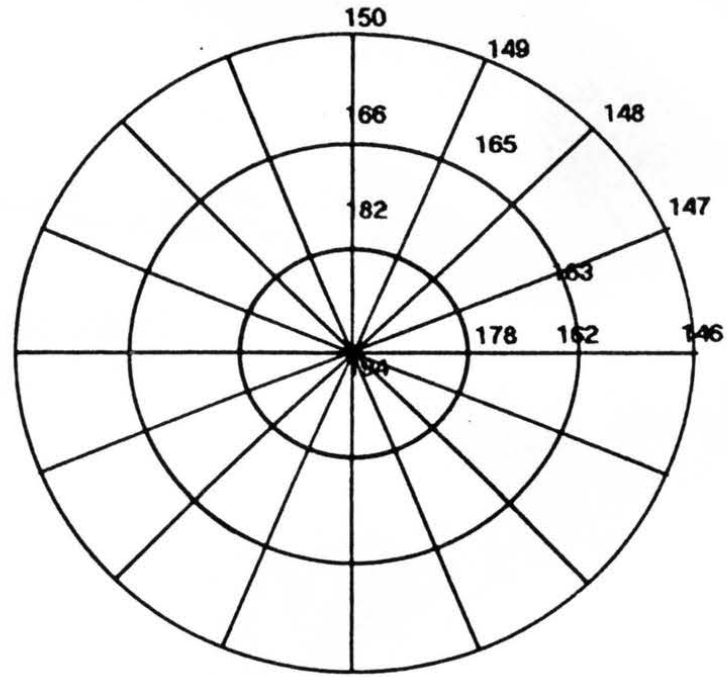
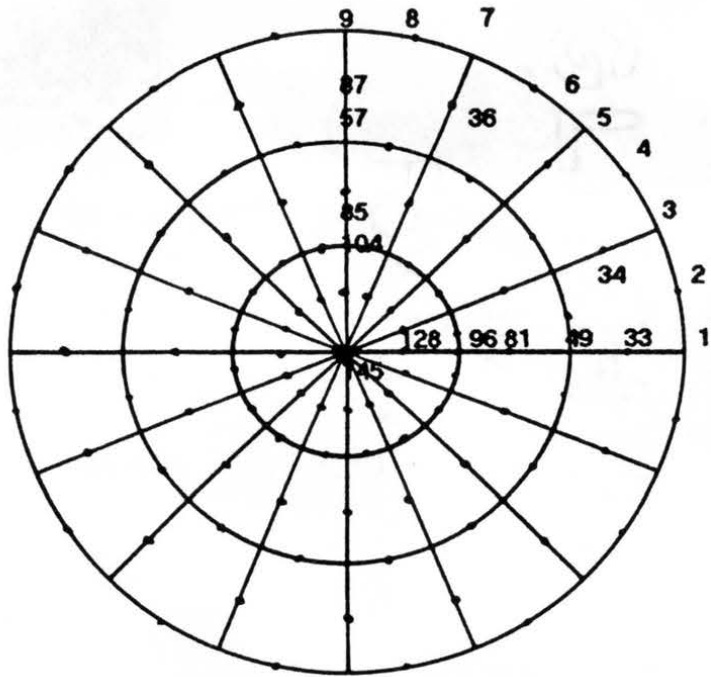


Figure 3.11. Cross Sections of a Pole Segment Showing (a) External Face of Disc 1 with 145 Nodal Points, and (b) Intermediate Face with 49 Nodal Points.

CHAPTER 4

MATERIAL CHARACTERISTICS AND DATA COLLECTION

4.1 GENERAL

All tests on poles for this study were performed at the Structural Laboratory located at the Engineering Research Center (ERC). Bending tests on small-clear specimens were conducted to determine the elastic and mechanical properties of the wood poles at the Wood Science Laboratory (WSL). Pole segments were cut from tested poles and brought to the WSL for evaluation.

The poles chosen for this study were selected from a greater number of poles evaluated in a project sponsored by the EPRI, conducted by the EDM at the ERC. Further information regarding this project can be found in the report entitled "Longitudinal Non-Destructive Evaluation of New Wood Poles" (in print).

A total of 306 poles (102 of western redcedar, Douglas-fir and southern pine) were tested in this project. The poles were debarked, graded and treated (with pentachlorophenol, creosote or CCA) before their shipment to the ERC. Here, they were stored outdoors without any protection or sprinkler system to prevent the poles from drying (Figure 4.1).



Figure 4.1. Poles Stored Outdoor at Engineering Research Center, Prior to Test.

For each species, three poles were selected to verify the 3-D finite element model developed to predict pole strength. Table 4.1 provides general data about each of these poles.

All measurements on the poles (pole profile, spiral grain, knot map and moisture content) were taken before the poles were tested to rupture in bending. After rupture, four-two foot long segments were cut and sent to the WSL-CSU. These segments are illustrated in Figure 4.2.

4.2 GEOMETRY, SPIRAL GRAIN AND KNOT MEASUREMENTS

Various properties were measured for the selected nine poles before full-scale destructive testing. These measurements were taken in order to provide a complete description of the pole profile, spiral grain and knot occurrence. The procedure for measuring a pole started by marking the groundline location according to ANSI 05.1-1987. In most cases, the location is found by adding two feet to one tenth of the pole length.

4.2.1 POLE PROFILE

Starting at the pole butt, the circumference at each three-foot interval was measured to the nearest 0.1 inch, up to the pole tip. Assuming linear variation between measurements, the diameter at any section could be evaluated. Appendix D-1 contains a sample of a pole profile data sheet.

Table 4.1. Characteristics of Poles Selected for the Verification of the Finite Element Model.

Order	Pole number	Length (feet)	Treatment*	Class	Supplier	Moist. cont. %
WESTERN REDCEDAR						
1	85	50	CCA	3	B.C.	23
2	88	50	CCA	H-2	B.C.	26
3	91	40	CCA	5	B.C.	27
DOUGLAS FIR						
4	162	50	PENTA	3	N.M.	24
5	174	50	PENTA	3	N.M.	26
6	188	60	PENTA	3	N.M.	23
SOUTHERN PINE						
7	289	40	CCA	5	A.W.	50
8	292	50	CCA	5	A.W.	80
9	297	50	CCA	3	A.W.	80

- (*) CCA - Chromated-Copper-Arsenate
Penta- Pentachlorophenol
- (**) B.C. - Bell Pole and Lumber Co.
N.M. - Niedemeyer-Martin Co.
A.W. - Atlantic Wood Industries.



Figure 4.2. Segments of Douglas-Fir Taken from Three Poles Tested to Failure.

4.2.2 SPIRAL GRAIN

At the same three-foot interval where the diameters were measured, grain deviation measurements also took place. Figure 4.3 shows how the deviation from the longitudinal straight line was measured and the spiral grain at the outer surface evaluated, approximating the actual angle to a planar angle using the relationship:

$$\theta = (t/36) * (180/\pi) \quad [4,1]$$

where t is the deviation measured. For modeling purposes, the spiral grain angle, θ , was considered constant throughout the segment. A sample of the data sheet used for spiral grain measurements is found in Appendix D-2.

4.2.3 KNOT MAP

For each of the nine poles, the diameters of the knots present were recorded, along with their longitudinal and circumferential locations along the pole. The knot map included all knots from the groundline to the tip with diameter greater than or equal to 0.5 inch.

Before testing, each pole was visually inspected to detect the presence of any sweep or crook. This allowed clamping the pole in such way that the concave side became the tension side during the bending test. The tension and compression faces previously determined, referenced the knot recording. Straight lines (on neutral plane) were drawn on both faces and whenever a knot was found, the longitudinal distance (origin at groundline) and the deviation to the left

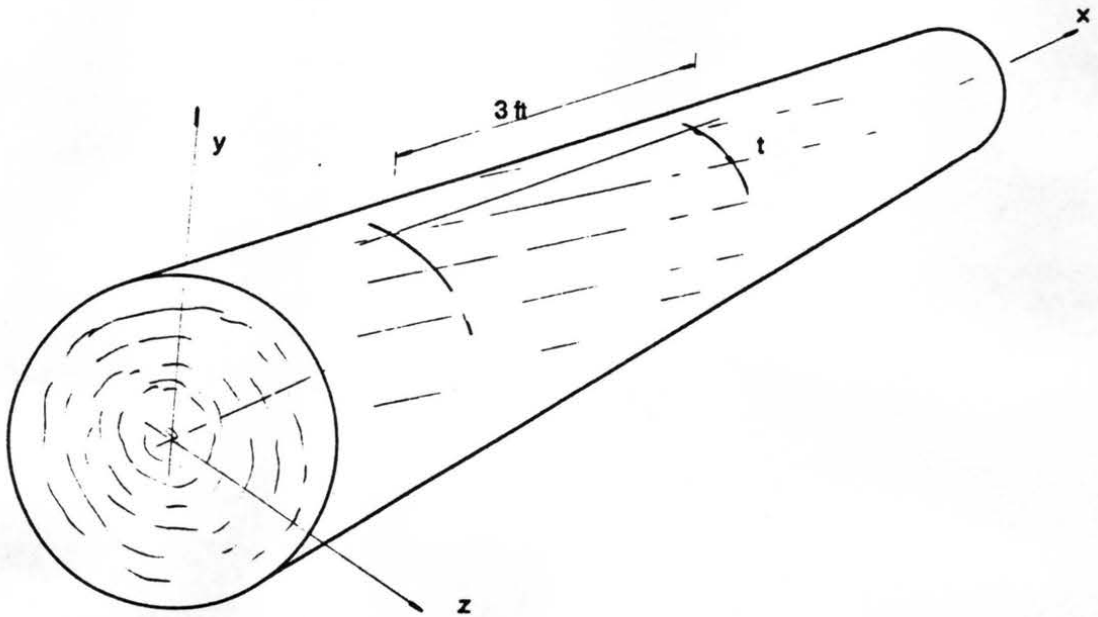


Figure 4.3. Schematic Illustration of Procedures for Spiral Grain Angle Measuring.

or right (circumferential location) were recorded to the nearest 0.5 inch. These details can be visualized by examining Figure 4.4, where TL and TR are the left and right quadrants on tension face and CR and CR the quadrants on compression face, viewed from the butt to the tip of the pole. With these data, the angle of location was calculated using a software program (spread sheet). An example of knot map and the calculations is included in the Appendix D-3.

The diameters of the knots were measured along the external circumference on the pole cross section where they occurred. As knots often possess an elliptical shape, 40, 20 and 40 knots were measured for western redcedar, Douglas-fir and southern pine respectively, with the objective of evaluating the ratio between the major axis A and the minor axis B of the ellipse (knot). Table 4.2 shows the average ratio for each species, based on different sample sizes.

4.3 MECHANICAL CHARACTERISTICS OF POLES

4.3.1 FULL SCALE TESTING OF POLES

After measurements of circumferences, knots and spiral grain were conducted, and NDE data collected, each pole was placed in the clamps of a testing apparatus and loaded as a cantilever beam until rupture. Load was applied using a steel cable attached to the pole tip, pulled by a winch that rested on an elongated frame parallel to the pole. An electrical load cell was used to measure the load. At the loading point, the deflections were measured and recorded using a LDT (large

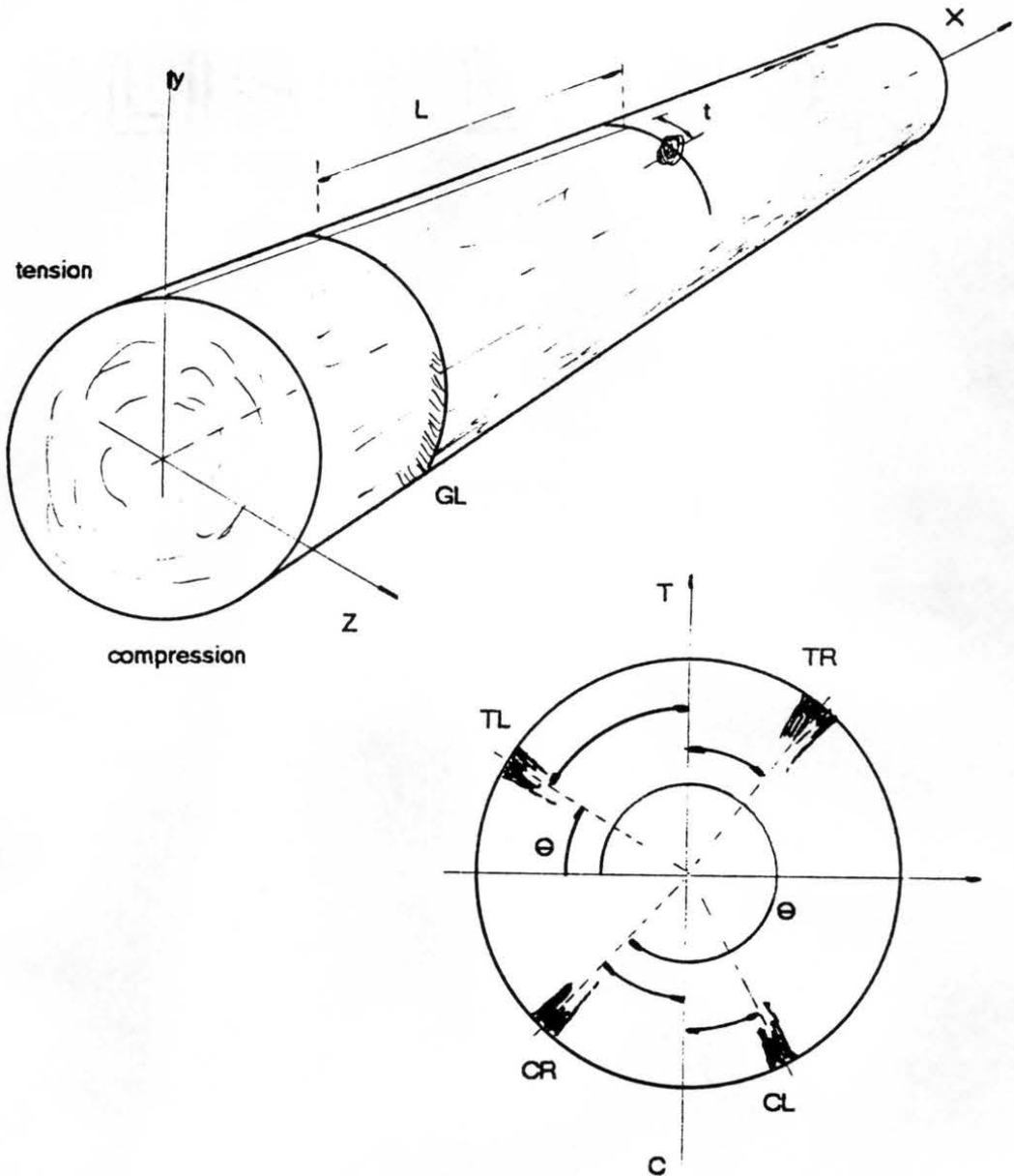


Figure 4.4. Steps Followed to Determine the Longitudinal and Circumferential Distances During Knot Mapping.

Table 4.2. Ratio Between the Major (A) and Minor (B) Axes for Knots of Each Species.

Knot number	Western Red Cedar			Douglas Fir			Southern Pine		
	A (mm)	B (mm)	Ratio A/B	A (mm)	B (mm)	Ratio A/B	A (mm)	B (mm)	Ratio A/B
1	41	30	1.367	19	18	1.056	16	13	1.231
2	47	35	1.343	17	15	1.133	20	17	1.176
3	34	34	1.000	23	21	1.095	16	13	1.231
4	27	25	1.080	23	21	1.095	16	13	1.231
5	48	42	1.143	22	19	1.158	19	15	1.267
6	58	50	1.160	23	21	1.095	17	15	1.133
7	52	42	1.238	38	32	1.188	17	15	1.133
8	24	24	1.000	26	22	1.182	14	14	1.000
9	35	35	1.000	40	32	1.250	30	25	1.200
10	27	20	1.350	15	12	1.250	24	19	1.263
11	43	32	1.344	17	14	1.214	29	22	1.318
12	36	27	1.333	20	17	1.176	32	25	1.280
13	43	32	1.344	23	19	1.211	20	16	1.250
14	37	37	1.000	20	18	1.111	21	18	1.167
15	41	37	1.108	21	18	1.167	19	16	1.188
16	54	45	1.200	24	19	1.263	24	20	1.200
17	57	49	1.163	19	16	1.188	24	20	1.200
18	46	41	1.122	18	15	1.200	43	33	1.303
19	30	28	1.071	15	13	1.154	15	13	1.154
20	34	25	1.360	19	17	1.118	17	13	1.308
21	27	19	1.421				17	16	1.063
22	64	51	1.255				16	15	1.067
23	39	30	1.300				24	19	1.263
24	30	29	1.034				17	14	1.214
25	55	44	1.250				18	15	1.200
26	28	24	1.167				16	13	1.231
27	20	16	1.250				15	12	1.250
28	55	50	1.100				17	14	1.214
29	50	38	1.316				12	11	1.091
30	25	21	1.190				21	17	1.235
31	50	39	1.282				16	13	1.231
32	65	55	1.182				12	10	1.200
33	25	22	1.136				22	18	1.222
34	21	18	1.167				22	18	1.222
35	50	42	1.190				25	20	1.250
36	50	40	1.250				25	20	1.250
37	30	28	1.071				23	18	1.278
38	58	55	1.055				17	14	1.214
39	29	26	1.115				23	19	1.211
40	34	30	1.133				15	13	1.154
	AVERAGE:		1.190			1.165			1.207

displacement transducer) specially designed for this purpose. During the test data on load and deflection were periodically stored onto a computer file for later evaluation of the MOE and MOR. The schematics of the bending test apparatus used for the full-scale destructive testing is illustrated in Figure 4.5.

After rupture, for each pole the pattern of failure was sketched on the data sheet and details observed. Appendix D-4 presents a typical test sheet used to record test data of individual poles. Between the groundline and the tip, four-two foot long segments (see Figure 4.2) were marked on the undamaged regions, cut and sent to the WSL for further evaluation on wood material. The segments were numbered 1,2,3 and 4 from butt to tip.

4.3.2 SMALL CLEAR SPECIMENS FOR MOE AND MOR EVALUATION

The material characteristics determined experimentally on logs cut from the poles included MOE, stress at proportional limit, and MOR in bending. Clear material was selected from the segments from the zone located at the neutral plane. Figure 4.6 shows the specimen locations in segments of western redcedar, for testing in bending. A minimum of 12 specimens per pole were prepared for bending tests (three per each pole segment). On each segment the three specimens were marked in the radial direction centered one at each third of the radius, as illustrated on Figure 4.6. The outermost specimen was designated, A, the central, B, and the innermost, C. The

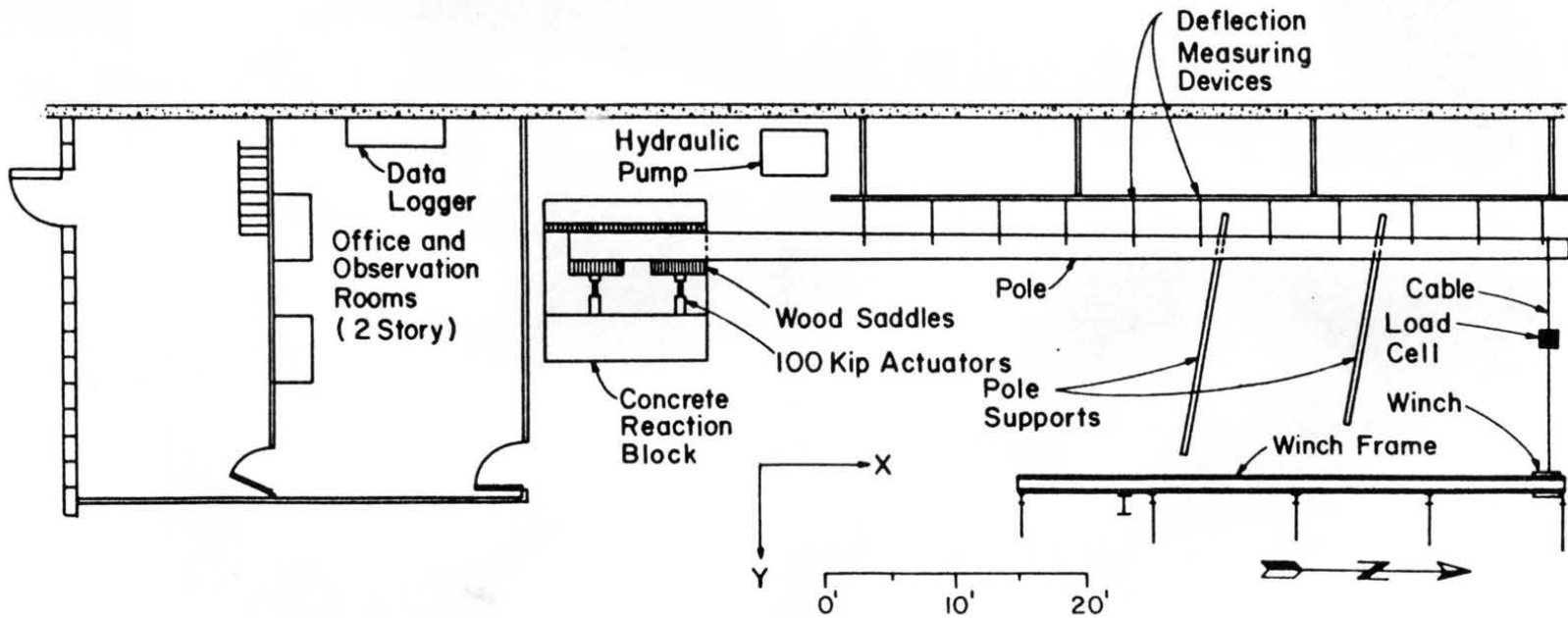


Figure 4.5. Pole Testing Facilities Located at the Engineering Research Center, Colorado State University. (After Goodman et al. 1981)



Figure 4.6. Position of Specimens in the Cross Section of Segments.

bending specimens had nominal dimensions of 1" x 1"x 15".

The next step was to separate the segments into blocks using splitting wedges, as seen in Figure 4.7. Next, the blocks were planed on two faces perpendicular to each other, observing the radial and tangential faces, Figure 4.8. The other two sides were cut using the circular saw, reaching the final cross section dimensions of the specimens. Finally the specimens were cut into the length of 15 inches.

4.3.2.1 BENDING TESTS

The objective of the bending test was to provide data to form the input data file for the finite element program GTSTRU DL.

The specimens cut from the poles were tested on an Instron mechanical testing machine-Model 1137, shown in Figure 4.9, using a constant cross head displacement of 0.05 in/min, equivalent to the strain ratio of 0.0015 in/in*min. The MOE and MOR determination followed the ASTM-D-143, adopting the span of 14" (span to depth ratio 14:1). The actual height and width of specimens were measured prior to test. The Appendix D-5 contains a sample of the load-deflection curve plotted during the bending test.

After rupture one sample of 1" x 1" x 1" was removed from each specimen to evaluate the moisture content during the test. The samples were weighed to the nearest 0.01 g and placed in a convection oven at 105° until constant weight (oven-dry weight), was achieved.



Figure 4.8. Two Faces (Tangential and Radial) of Specimens Planed to Form Perpendicular Surfaces.

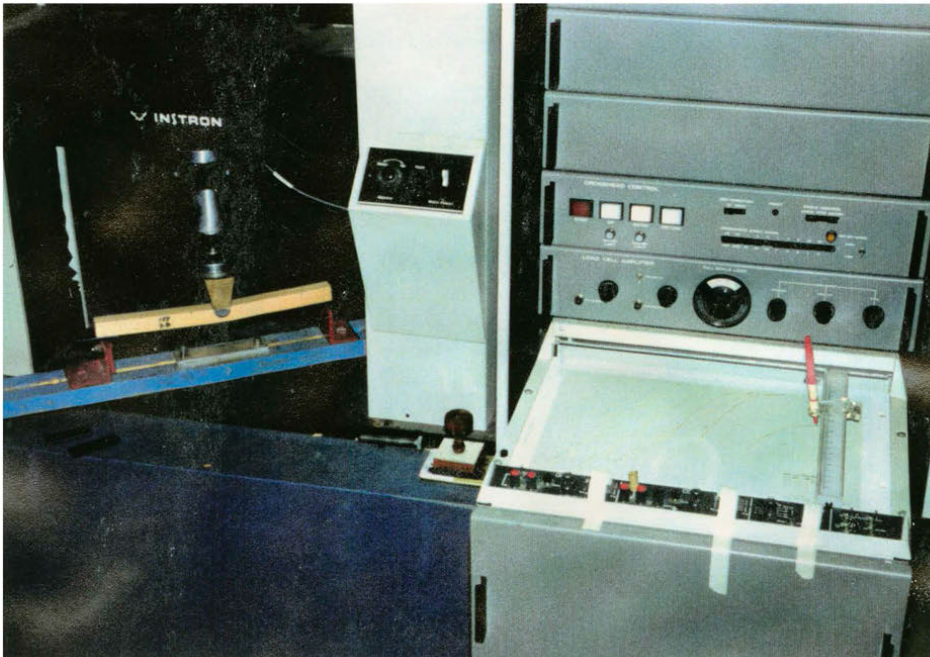


Figure 4.9. INSTRON Testing Machine Used for Bending Tests of Small Clear Specimens.

4.3.2.2 LONGITUDINAL MODULUS OF ELASTICITY AND STRENGTH VALUES

From the bending load-deflection curves and using the actual dimensions of the specimens, the stress at proportional limit, MOR and MOE were calculated with the following equations:

$$\sigma_{pl} = \frac{3 * P_{pl} * L}{2 * b * h^2} \quad [4, 2]$$

$$MOR = \frac{3 * P_u * L}{2 * b * h^2} \quad [4, 3]$$

$$MOE = \frac{P_{pl} * L^3}{4 * \delta_{pl} * b * h^3} \quad [4, 4]$$

Tables 4.3, 4.4 and 4.5 summarize the results obtained in the bending tests for the three wood species. Using the results obtained from small clear specimens, the relationships between MOE and MOR with the position along the poles could be established, assuming linear variation in the intervals. As shown in Figures 4.10 to 4.21, these characteristics could be evaluated at any section of a pole by linear interpolation.

4.3.2.3 ELASTIC PARAMETERS OF WOOD

As described in Chapter 3, to execute the proposed model, nine elastic parameters are necessary to build the element compliance matrix used in the 3-D finite element analysis.

For each wood segment these constants are: E_L , E_T , E_R , G_{LT} , G_{TR} , G_{LR} , ν_{LR} , ν_{LT} , ν_{TR} . According to Bodig and Goodman (1973), the

Table 4.3. Mechanical Properties of Western
redcedar Evaluated Through Bending Tests

Sample number	Stress @ pl psi	MOR psi	MOE (1000)psi	Moisture content (%)
POLE # 85				
85-1-A	1990	7794	1017	16.4
85-1-B	1817	8341	1139	18.0
85-1-C	2808	7598	1004	15.6
85-2-A	2232	8846	1165	16.0
85-2-B	3107	7466	1017	16.3
85-2-C	3155	8480	957	14.5
85-3-A	2929	9134	1092	16.1
85-3-B	2092	7488	988	17.2
85-3-C	2588	7627	1045	16.3
85-4-A	2371	8423	1135	13.9
85-4-B	2298	9298	972	13.5
85-4-C	2704	8937	1081	15.0
POLE # 88				
88-1-A	2046	8185	1132	14.2
88-1-B	1505	7356	1092	14.3
88-1-C	1807	7883	1073	13.1
88-2-A	2062	7529	923	14.0
88-2-B	1534	6241	754	12.6
88-2-C	1894	7380	1149	13.6
88-3-A	2526	5819	783	14.2
88-3-B	1831	6930	1033	13.8
88-3-C	3436	7371	786	13.6
88-4-A	1600	8403	1159	12.9
88-4-B	2245	7755	1058	13.6
88-4-C	1888	7676	976	12.9
POLE # 91				
91-1-A	3556	12006	1318	16.2
91-1-B	2828	9294	1143	15.8
91-1-C	2549	7794	1006	16.2
91-2-A	2811	10308	1442	14.5
91-2-B	2106	8531	1180	16.3
91-2-C	2811	8474	1211	17.1
91-3-A	2985	9846	1419	13.5
91-3-B	2185	8491	1194	15.1
91-3-C	1980	8065	1165	15.1
91-4-A	2899	10976	1438	13.7
91-4-B	2042	9231	1320	14.2
91-4-C	2225	9128	1071	15.1

Table 4.4 Mechanical Properties of Douglas-Fir
Evaluated Through Bending Tests

Sample number	Stress @ pl psi	MOR psi	MOE (1000)psi	Moisture content (%)
POLE # 162				
162-1-A	2950	9651	1742	---
162-1-B	2429	9001	1503	---
162-1-C	2469	7627	1387	---
162-2-A	2556	10159	1802	---
162-2-B	2444	8095	1265	---
162-2-C	2836	7621	1122	---
162-3-A	2516	9478	1678	---
162-3-B	2602	9039	1426	---
162-3-C	2402	6820	1006	---
162-4-A	2657	10220	1597	---
162-4-B	2616	8021	1267	---
162-4-C	2530	7861	1208	---
POLE # 174				
174-1-A	2686	9554	1740	---
174-1-B	2762	7682	1338	---
174-1-C	2481	7156	1062	---
174-2-A	3167	10382	1700	---
174-2-B	2615	8229	1167	---
174-2-C	2429	6614	1038	---
174-3-A	2935	9775	1595	---
174-3-B	2583	6970	1199	---
174-3-C	2547	5780	962	---
174-4-A	2874	7817	1430	---
174-4-B	3168	7259	1148	---
174-4-C	2130	7901	1056	---
POLE # 188				
188-1-A	4206	13846	2172	---
188-1-B	3108	9768	1709	---
188-1-C	3161	8495	1442	---
188-2-A	2706	10692	1727	---
188-2-B	2368	8228	1491	---
188-2-C	1584	7073	1403	---
188-3-A	3370	8389	1659	---
188-3-B	2160	7070	1453	---
188-3-C	2095	7462	1313	---
188-4-A	3123	8979	1468	---
188-4-B	2373	8526	1405	---
188-4-C	2602	8306	1347	---

Table 4.5 Mechanical Properties of Southern
pine Evaluated Through Bending tests

Sample number	Stress @ pl psi	MOR psi	MOE (1000)psi	Moisture content (%)
POLE # 289				
289-1-A	1808	7848	1351	36.5
289-1-B	1896	7356	1418	84.5
289-1-C	2883	7969	1503	50.1
289-2-A	1540	7537	1347	65.2
289-2-B	1472	6997	1236	78.3
289-2-C	2368	7300	1365	71.5
289-3-A	1594	7808	1208	62.8
289-3-B	1973	7089	1258	78.6
289-3-C	2199	7002	1228	37.6
289-4-A	2137	6863	1160	61.6
289-4-B	1634	6047	985	68.1
289-4-C	1510	5483	811	79.2
POLE # 292				
292-1-A	2374	5935	945	71.3
292-1-B	1035	4857	565	145.9
292-1-C	1579	4191	471	75.9
292-2-A	1772	6321	1233	88.1
292-2-B	2369	6133	1231	92.6
292-2-C	2015	5410	1030	115.5
292-3-A	2214	7053	1258	72.9
292-3-B	1750	5021	965	113.9
292-3-C	2312	5402	968	114.1
292-4-A	2002	5068	866	93.9
292-4-B	1575	5806	1093	71.3
292-4-C	1603	5499	1015	105.6
POLE # 297				
297-1-A	1362	8303	1477	82.4
297-1-B	1900	7417	1388	73.1
297-1-C	1389	6270	1069	77.3
297-2-A	1644	6452	1101	104.1
297-2-B	1469	8416	1440	72.6
297-2-C	1378	6258	1200	99.8
297-3-A	2566	7585	1500	74.5
297-3-B	1527	7398	1475	92.6
297-3-C	2313	4621	891	59.5
297-4-A	2071	8012	1402	63.6
297-4-B	2051	6367	1311	117.4
297-4-C	1675	6260	1034	121.9

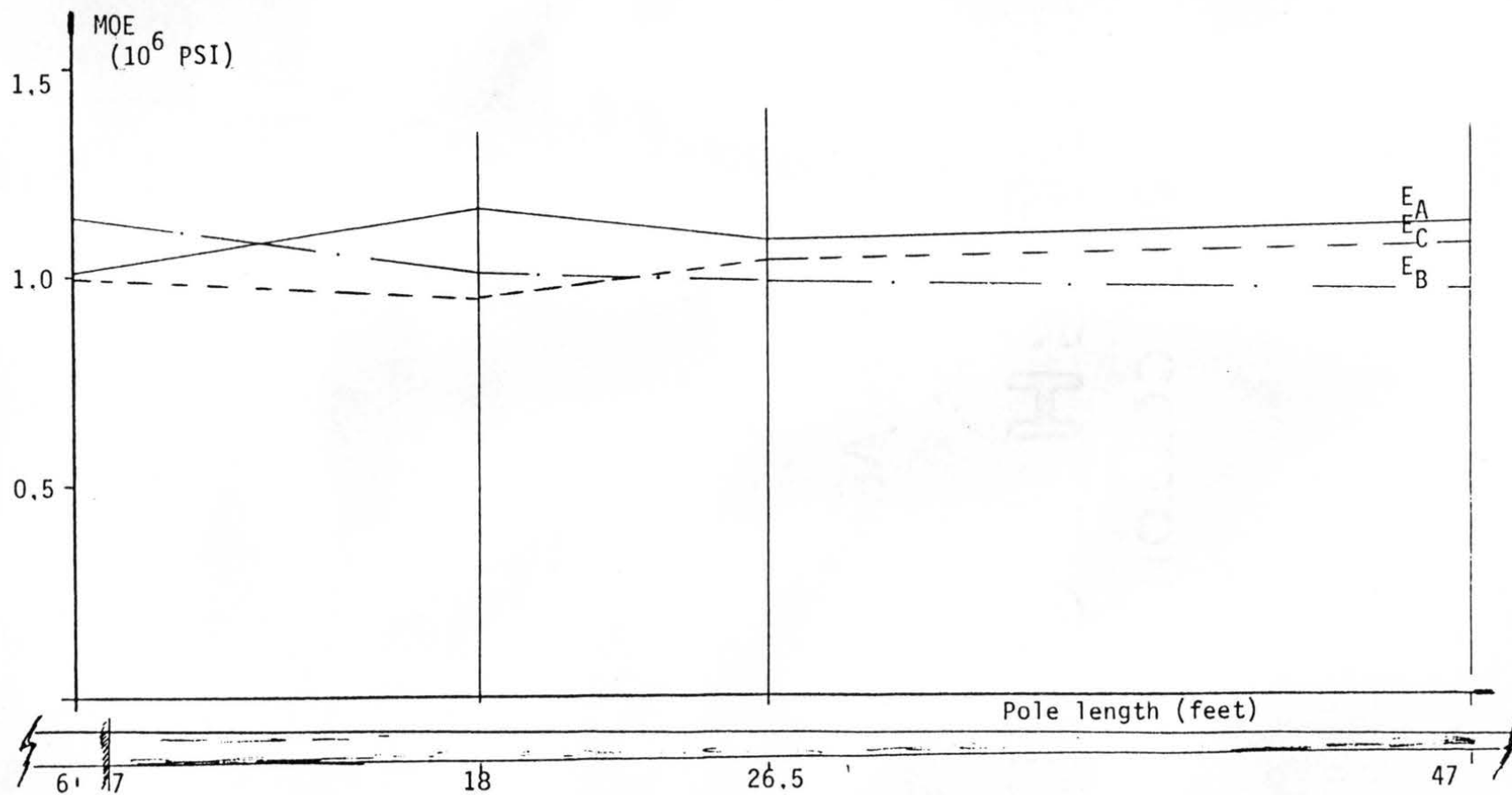


Figure 4.10. Modulus of Elasticity Along the Western Redcedar Pole # 85, Determined in Small Clear Specimens in Bending.

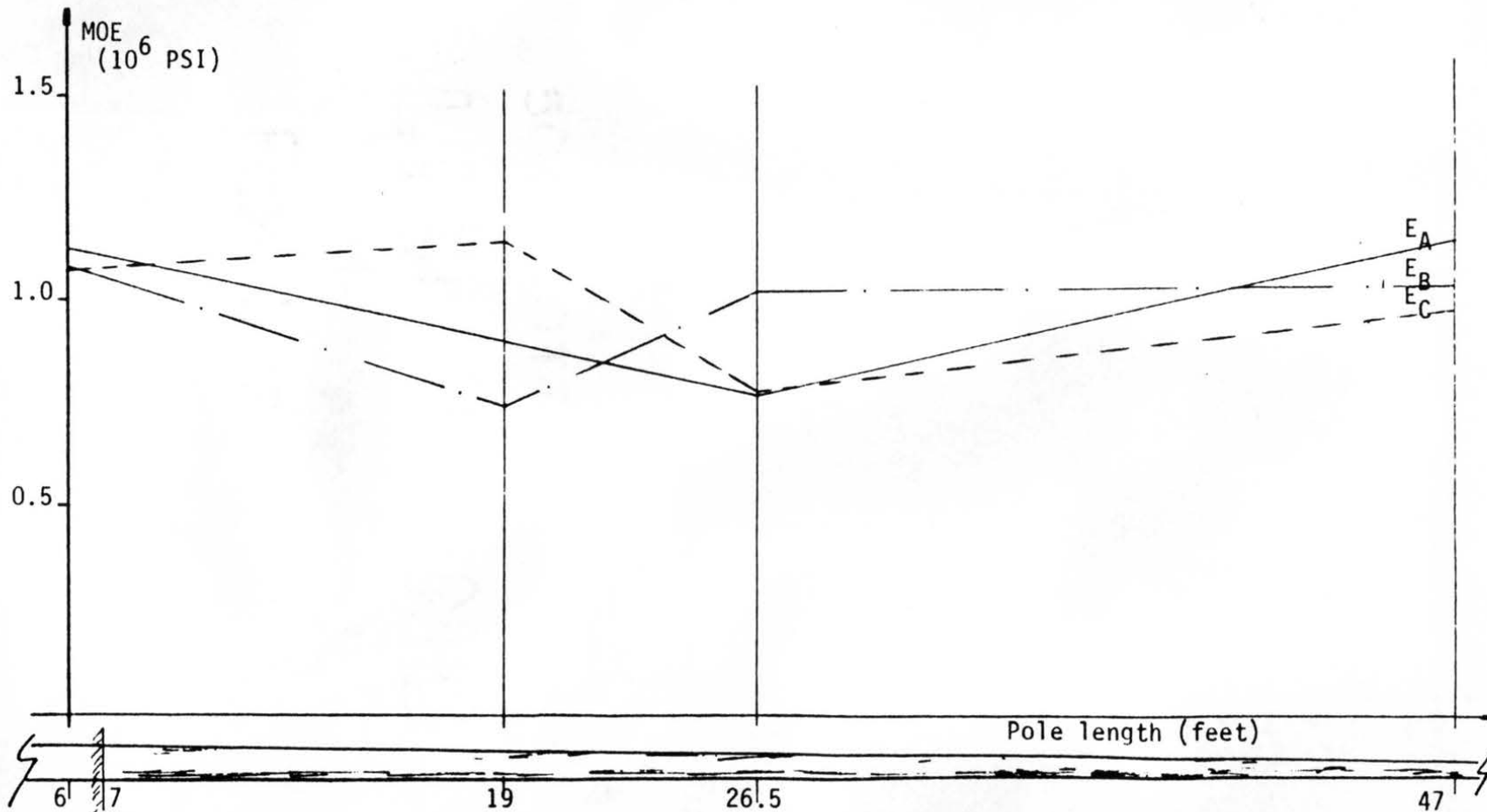


Figure 4.11. Modulus of Elasticity Along the Western Redcedar Pole # 88, Determined in Small Clear Specimens in Bending.

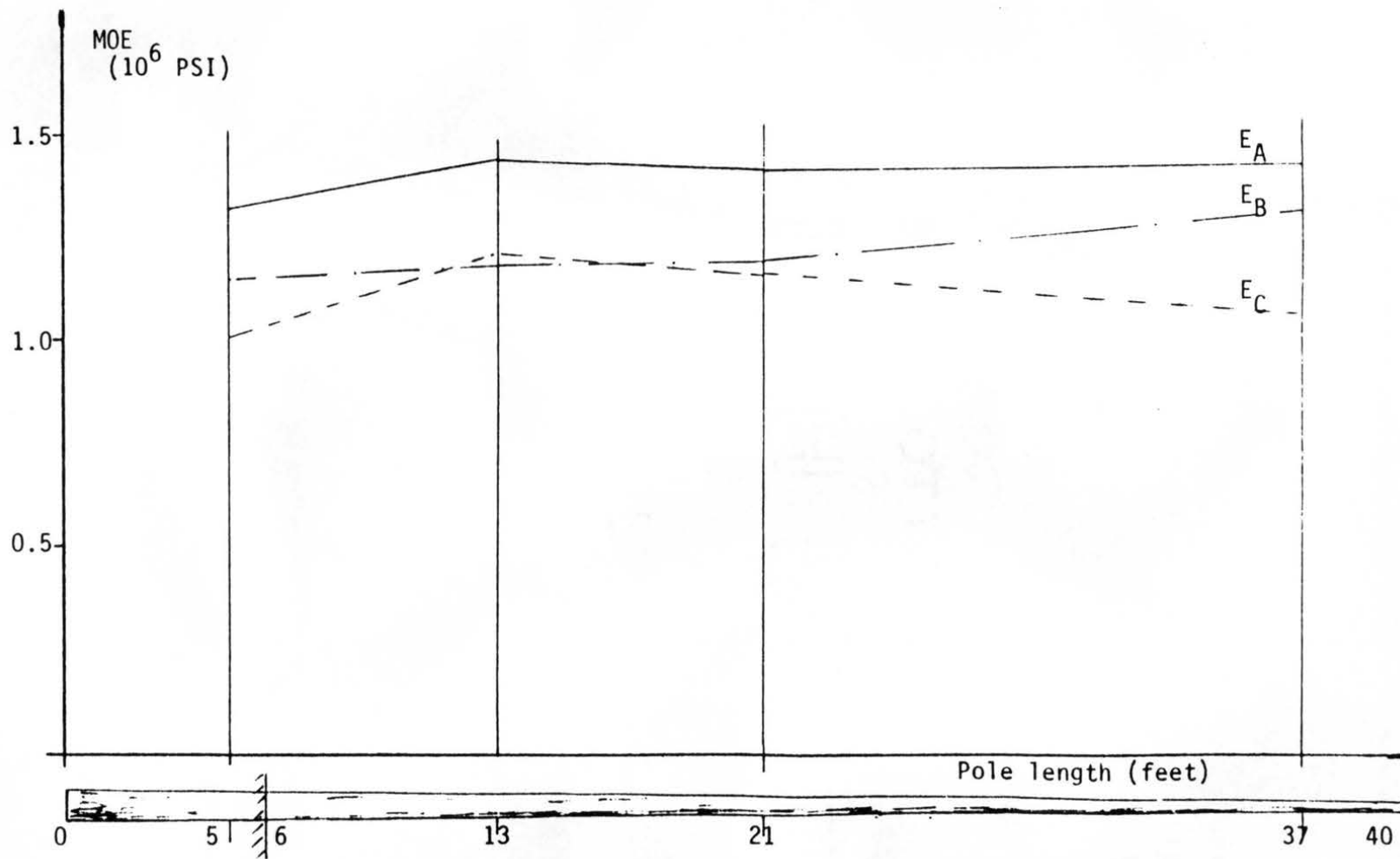


Figure 4.12. Modulus of Elasticity Along the Western Redcedar Pole # 91, Determined in Small Clear Specimens in Bending.

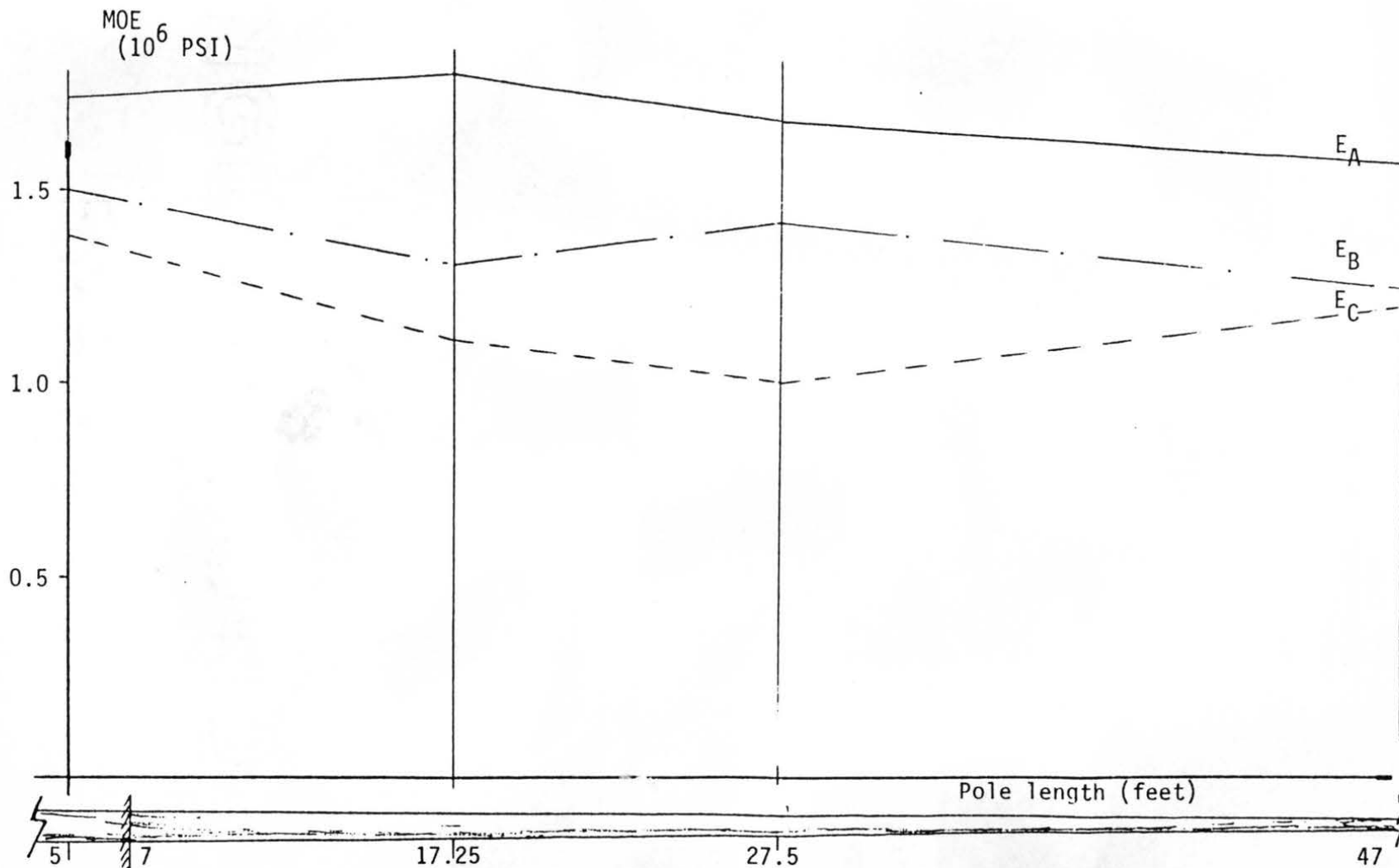


Figure 4.13. Modulus of Elasticity Along the Douglas-Fir, Pole # 162, Determined in Small Clear Specimens in Bending.

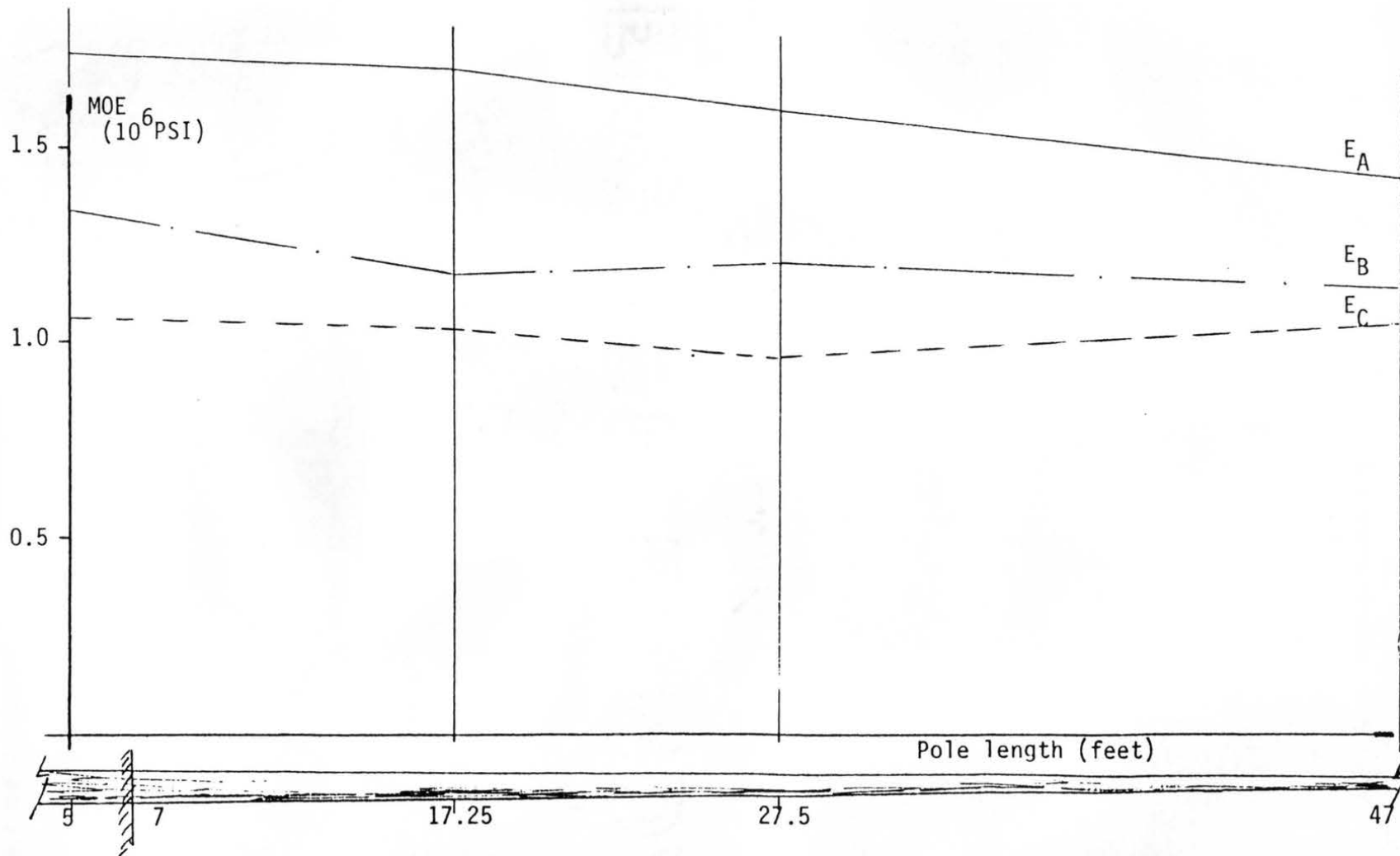


Figure 4.14. Modulus of Elasticity Along the Douglas-Fir, Pole # 174, Determined in Small Clear Specimens in Bending.

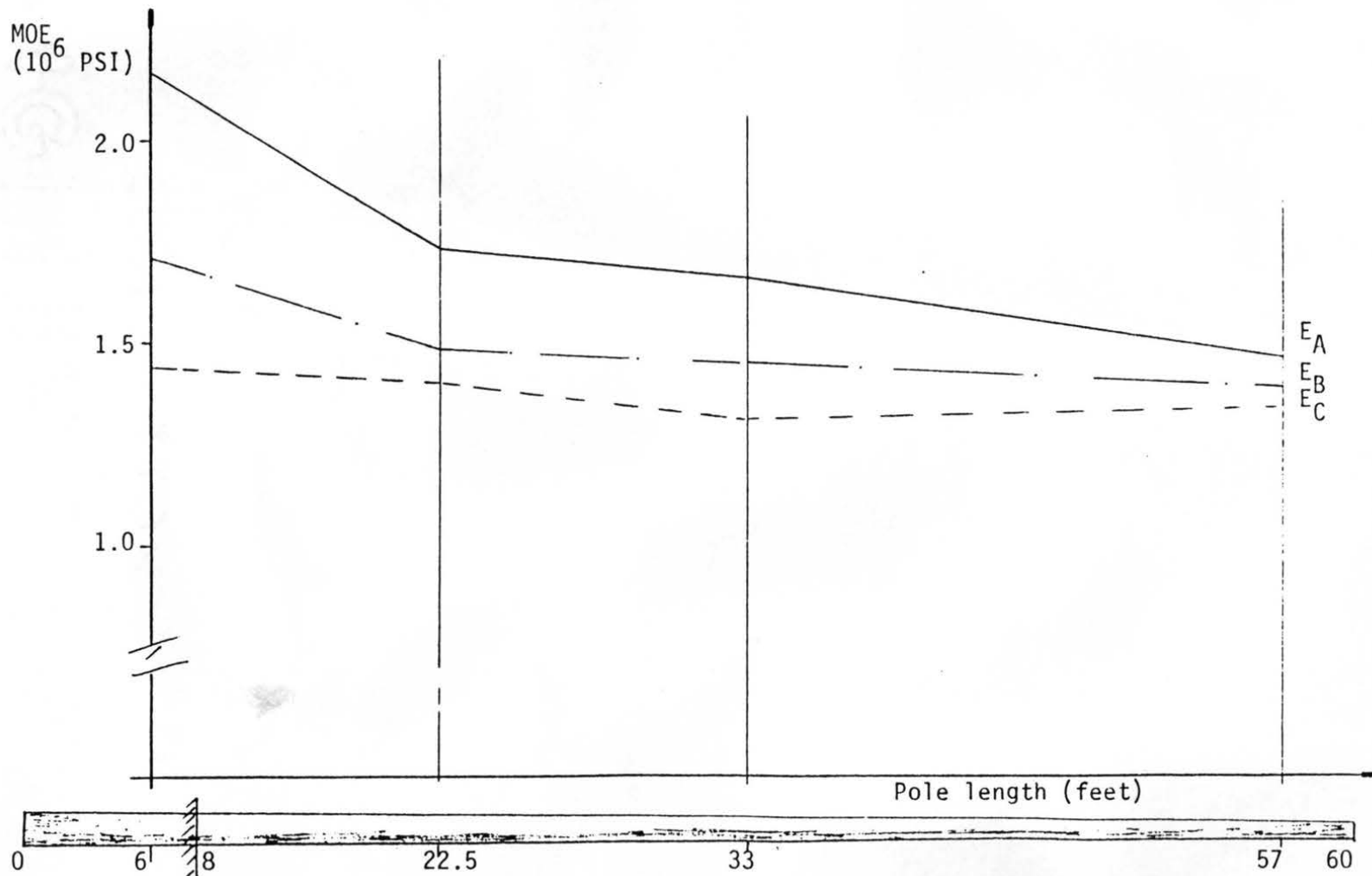


Figure 4.15. Modulus of Elasticity Along the Douglas-Fir, Pole # 188, Determined in Small Clear Specimens in Bending.

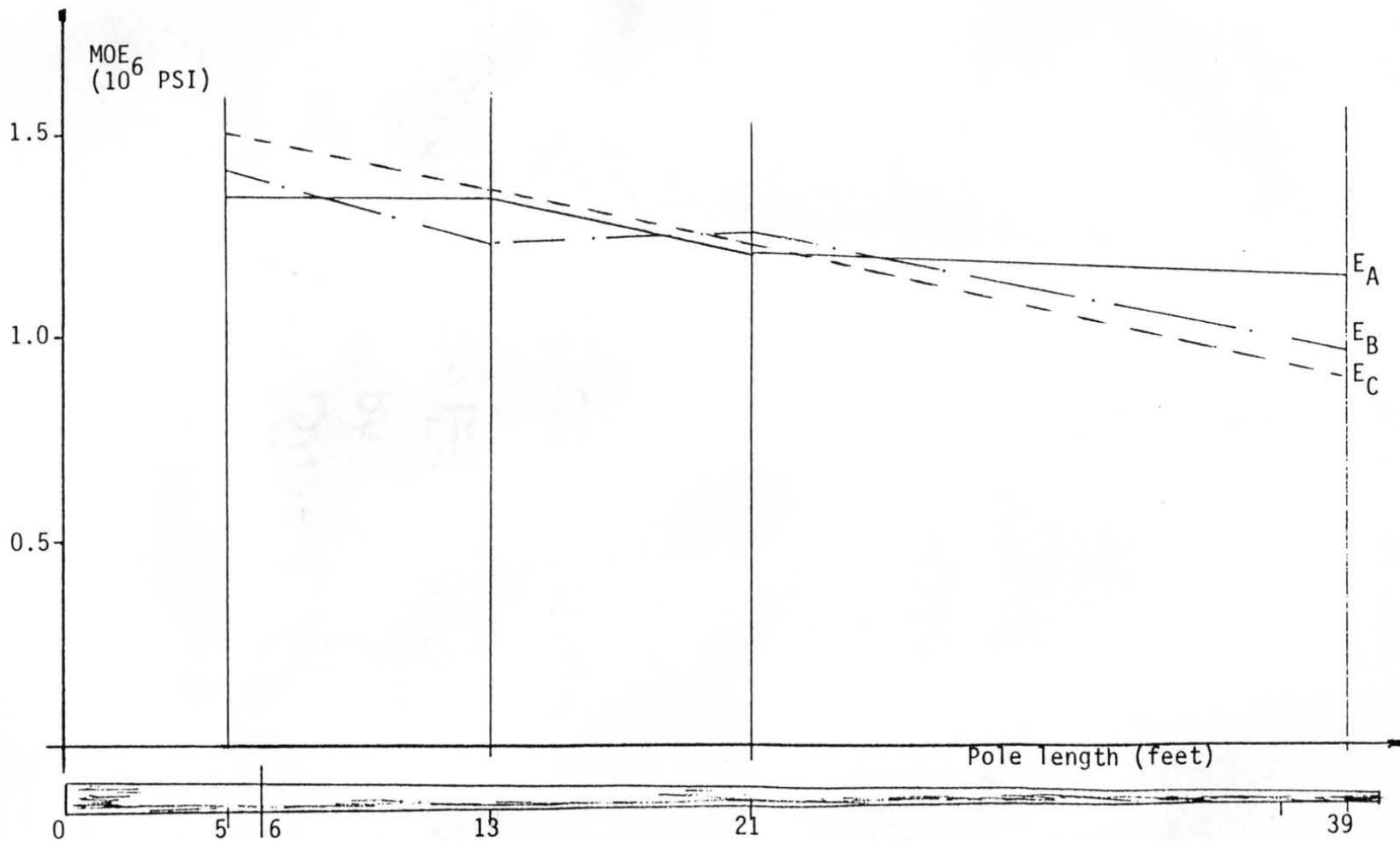


Figure 4.16. Modulus of Elasticity Along the Southern Pine, Pole # 289, Determined in Small Clear Specimens in Bending.

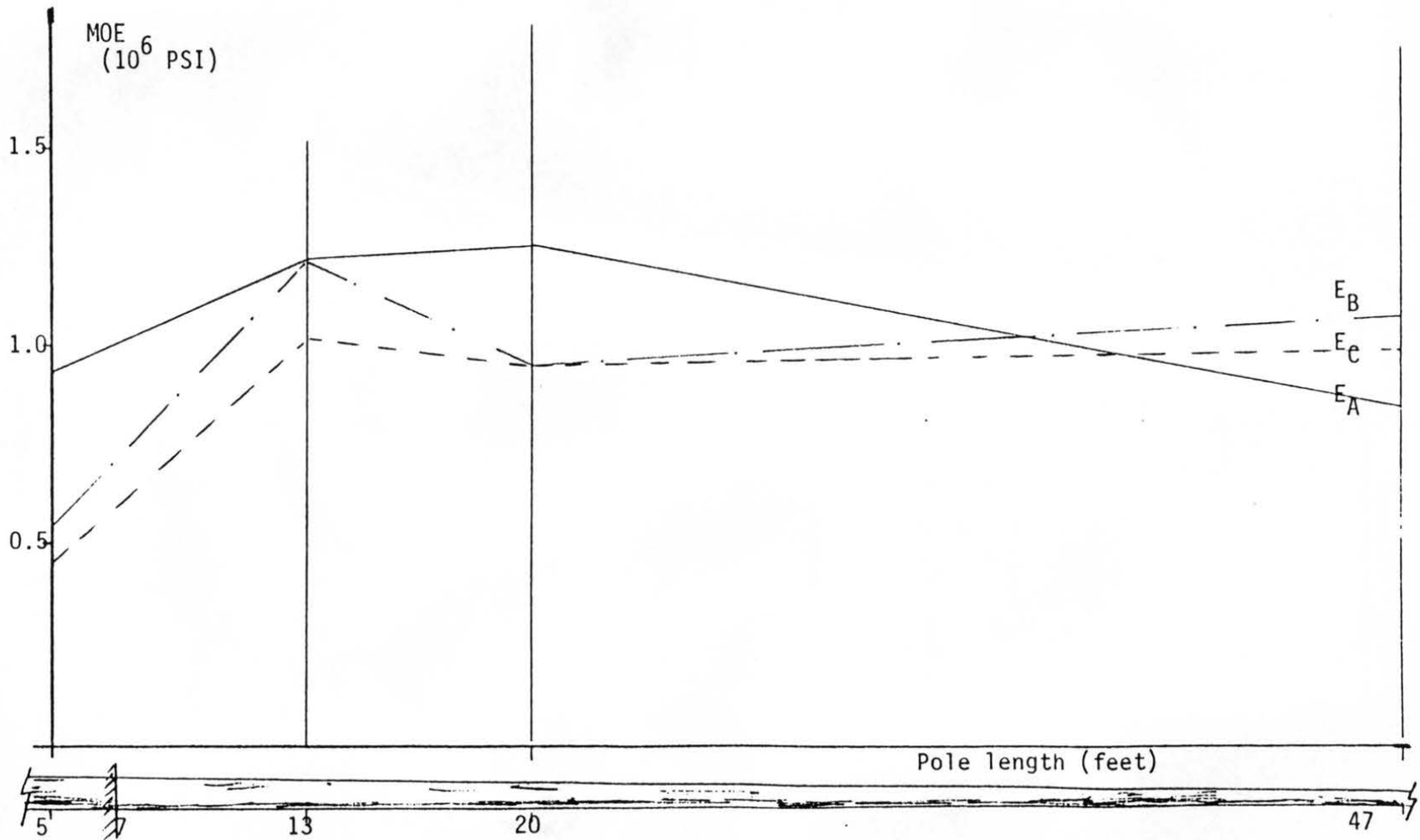


Figure 4.17. Modulus of Elasticity Along the Southern Pine, Pole # 292, Determined in Small Clear Specimens in Bending.

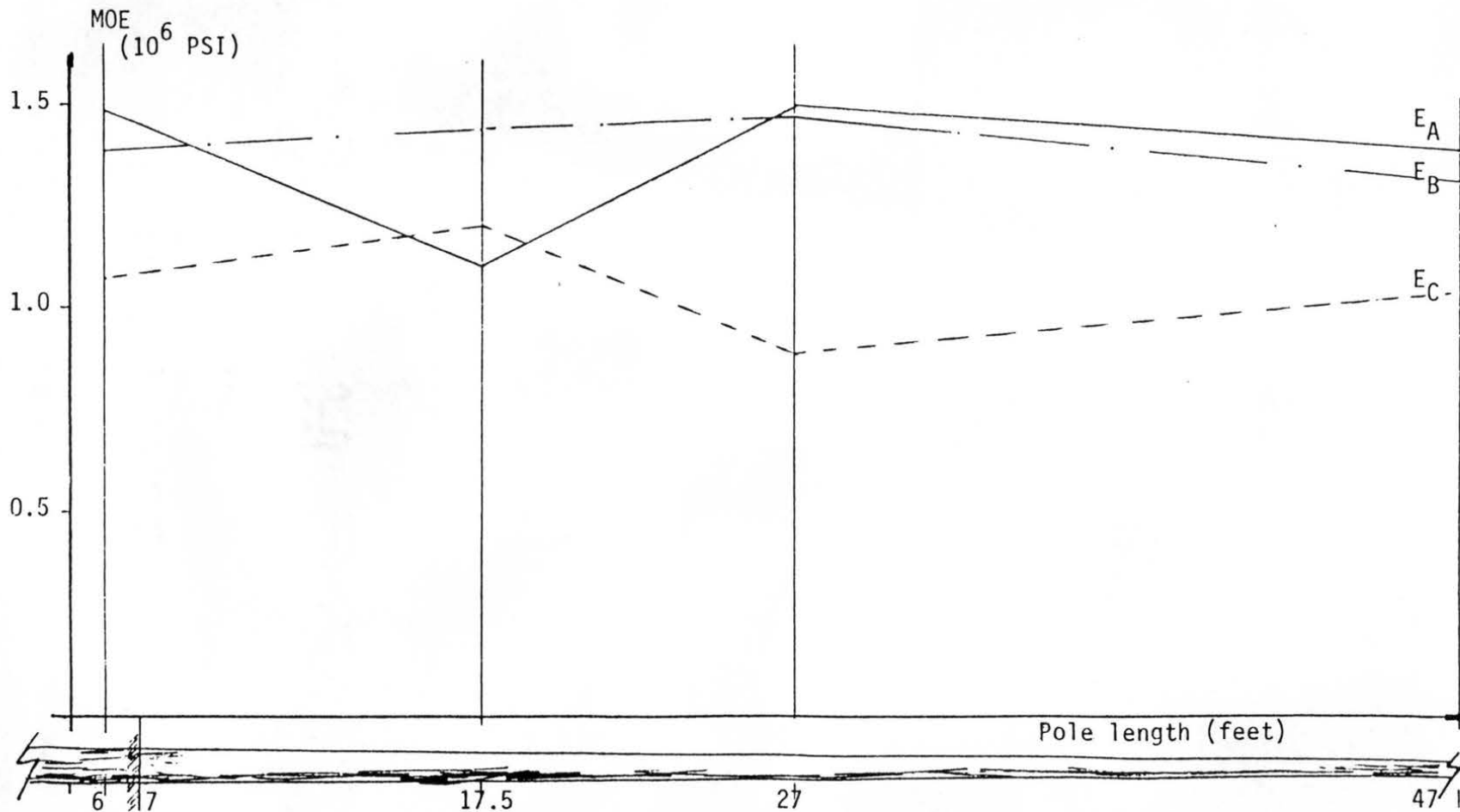


Figure 4.18. Modulus of Elasticity Along the Southern Pine, Pole # 297, Determined in Small Clear Specimens in Bending.

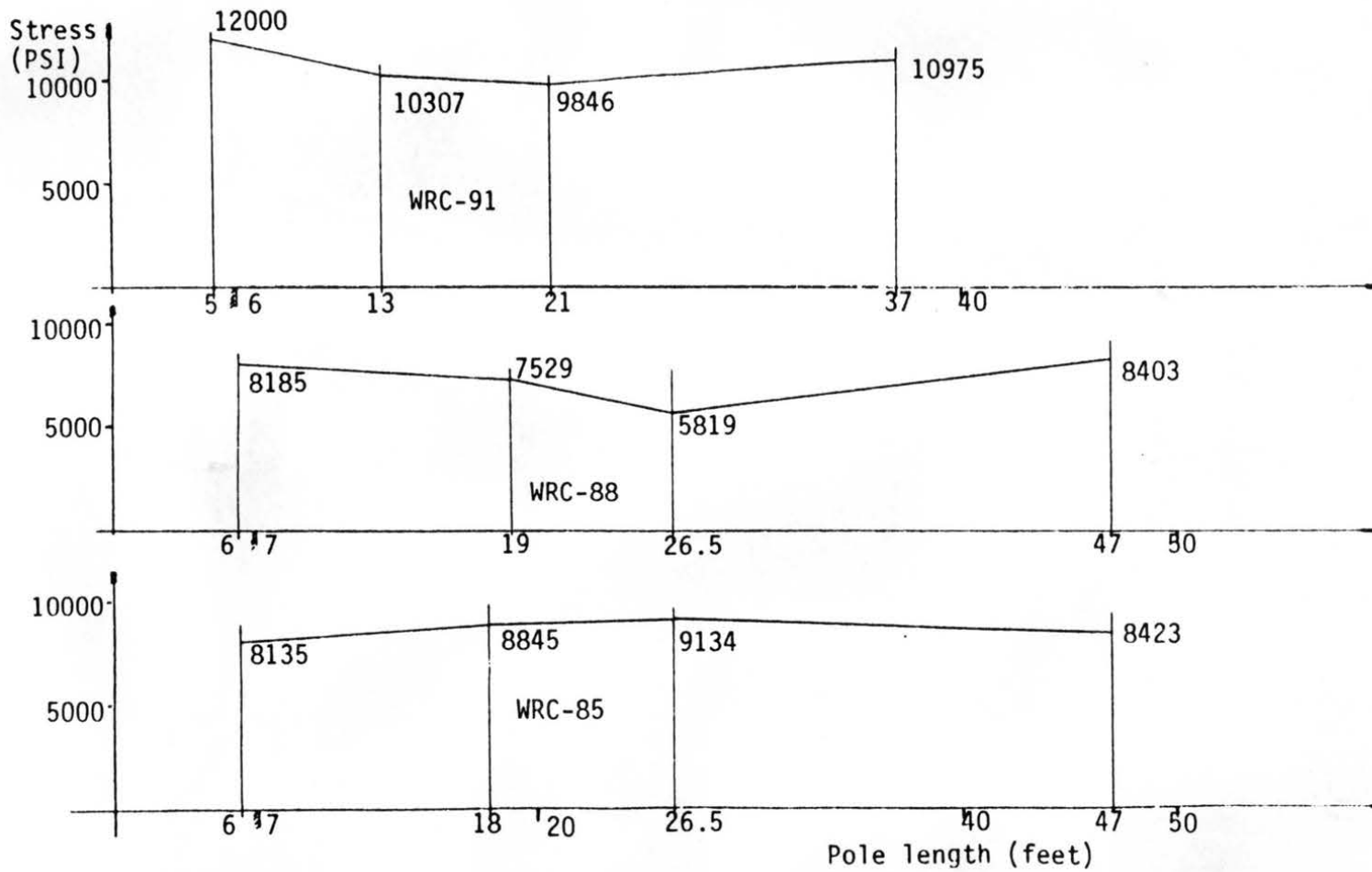


Figure 4.19. Wood Strength at the Outermost Third Along Western Redcedar Poles, Determined in Small Clear Specimens in Bending.

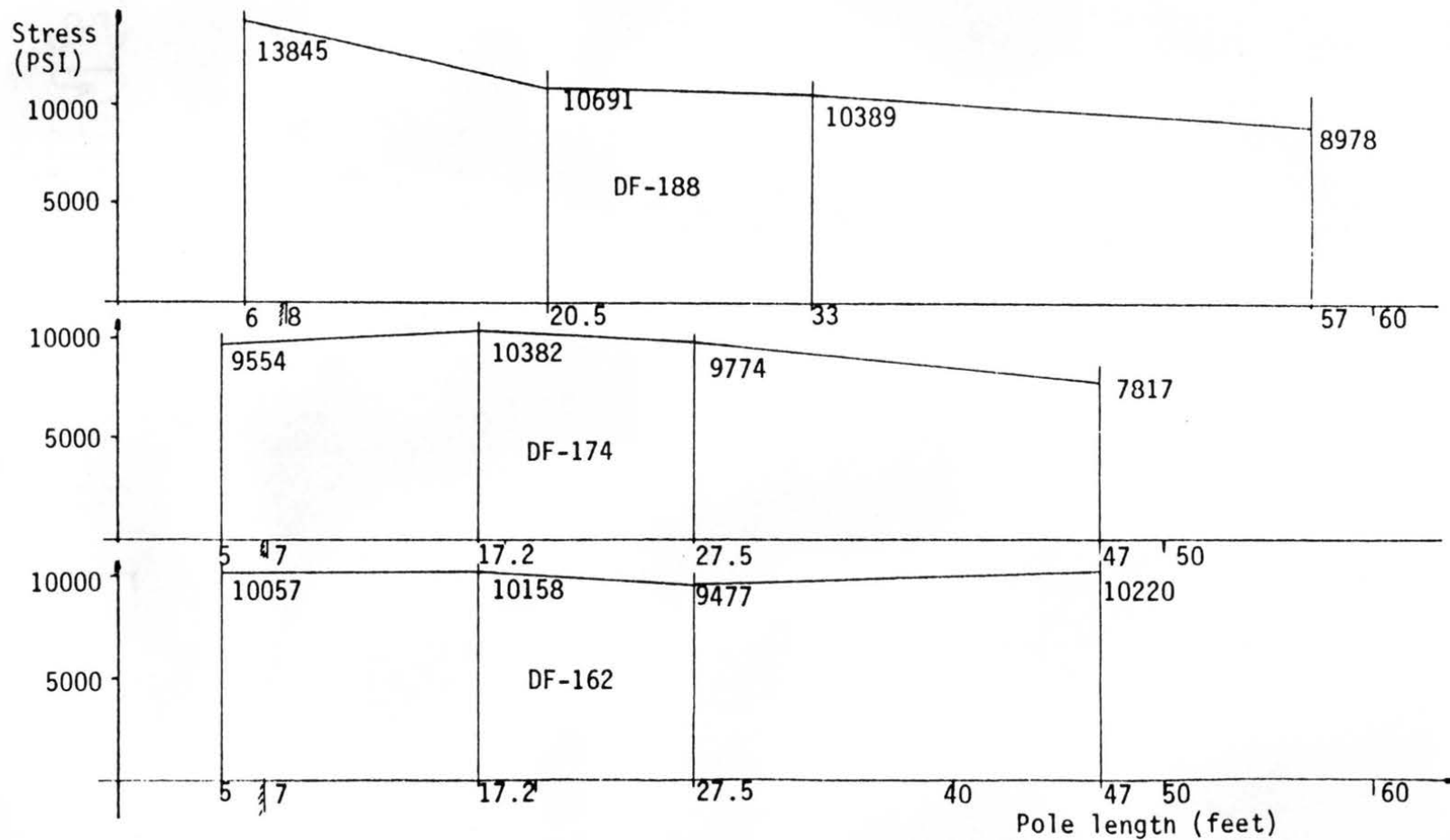


Figure 4.20. Wood Strength at the Outermost Third Along Douglas Fir Poles, Determined in Small Clear Specimens in Bending.

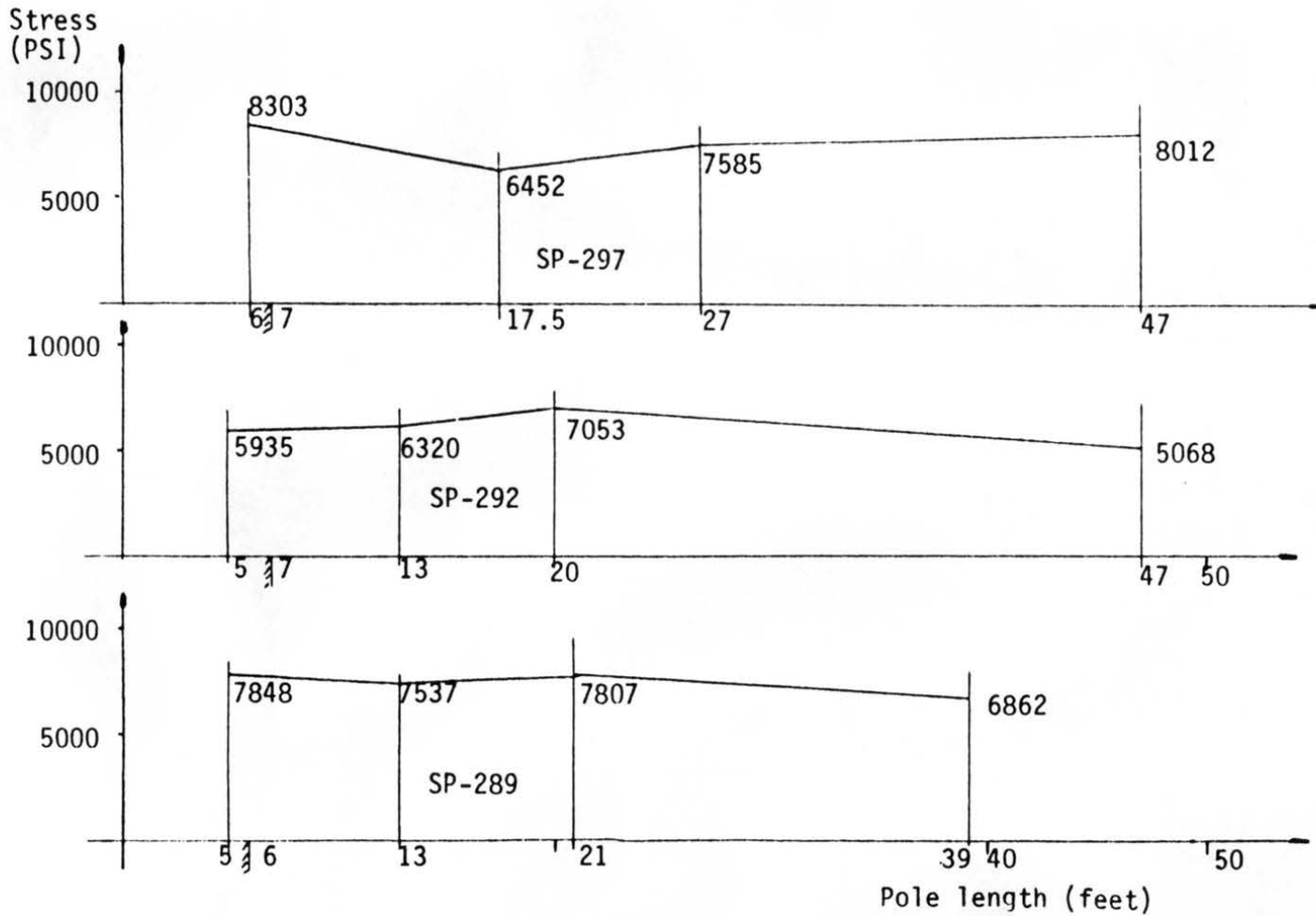


Figure 4.21. Wood Strength at the Outermost Third Along Southern Pine Poles, Determined in Small Clear Specimens in Bending.

elastic properties can be correlated to the true MOE parallel to grain. The MOE parallel to grain was determined for each pole segment and the true modulus was computed using the shear deformation factor $K_s = 1.098$, for the condition where the small clear specimen was tested in bending with the span to depth ratio of 14:1 and modulus of rigidity assumed to be 1/16 of the MOE (Biblis 1965). The equations presented by Bodig and Goodman (1973) were therefore used to predict the other non-measured elastic parameters for each species. The values of the Poisson's ratios were assumed constant and taken from the Table 2.2, according the Bodig and Goodman (1973).

CHAPTER 5

EXPERIMENTAL VERIFICATION OF THE MODEL

5.1 GENERAL

In this chapter, the results obtained from the analysis performed on pole segments using the 3-D finite element program, GTSTRU DL, are presented. Prior to running the program with the actual pole data, some considerations related to the influence of the boundary conditions and loading on the results were made, based on trials with isotropic and orthotropic material models. Comparisons with theoretical results evaluated with formulas from elementary mechanics of materials theory are also presented.

For the finite element analysis in the wood pole segments using GTSTRU DL, information on pole geometry (diameter), material properties (elastic parameters: true modulus of elasticity E , G , ν , included in the element stiffness matrices), support conditions, properties of elements containing knots, and applied loading, are necessary input file data. In trial examples the characteristics of a Douglas-fir pole were taken for the orthotropic case and steel for the isotropic case.

To perform the stiffness analysis in the modeled segment, an input file had to be created to supply data for the mesh

generation, element rigidity matrix assembly, boundary conditions (supports), and loading. Every segment was analyzed as a cylinder, with diameter of the segment butt (near section) evaluated from the pole profile data file. Using the external diameter GTSTRUDL generates all joints on the three concentric cylindrical surfaces necessary to create the mesh around the segment. A total of 1309 joints were created over the segment. Figure 5.1 shows the location of some joints located at the tension side of the segment.

Using an internal routine activated by a statement that requires the joint sequence and joint numbers, the finite element program generates 288 elements (192 elements of IPQS type and 96 elements of WEDGE15 type). Having the elements defined, the next step was to assign material properties to each element. Element type and rigidity specifications are required for each element. In Section 3.2.5, the type of elements used were indicated. The element rigidity matrices were copied to the input file from a file previously built using the longitudinal E and predicted transverse E, G's, and ν 's. For matrix generation, such factors as spiral grain and position of element in the cross section were taken into account. The Appendix E presents the FORTRAN code written to create the rigidity matrices for the elements. When knots were presented in a segment, the elastic properties (previously assigned) for the elements were replaced to include the knot effect on the central element and the associated grain deviation on neighboring elements using the

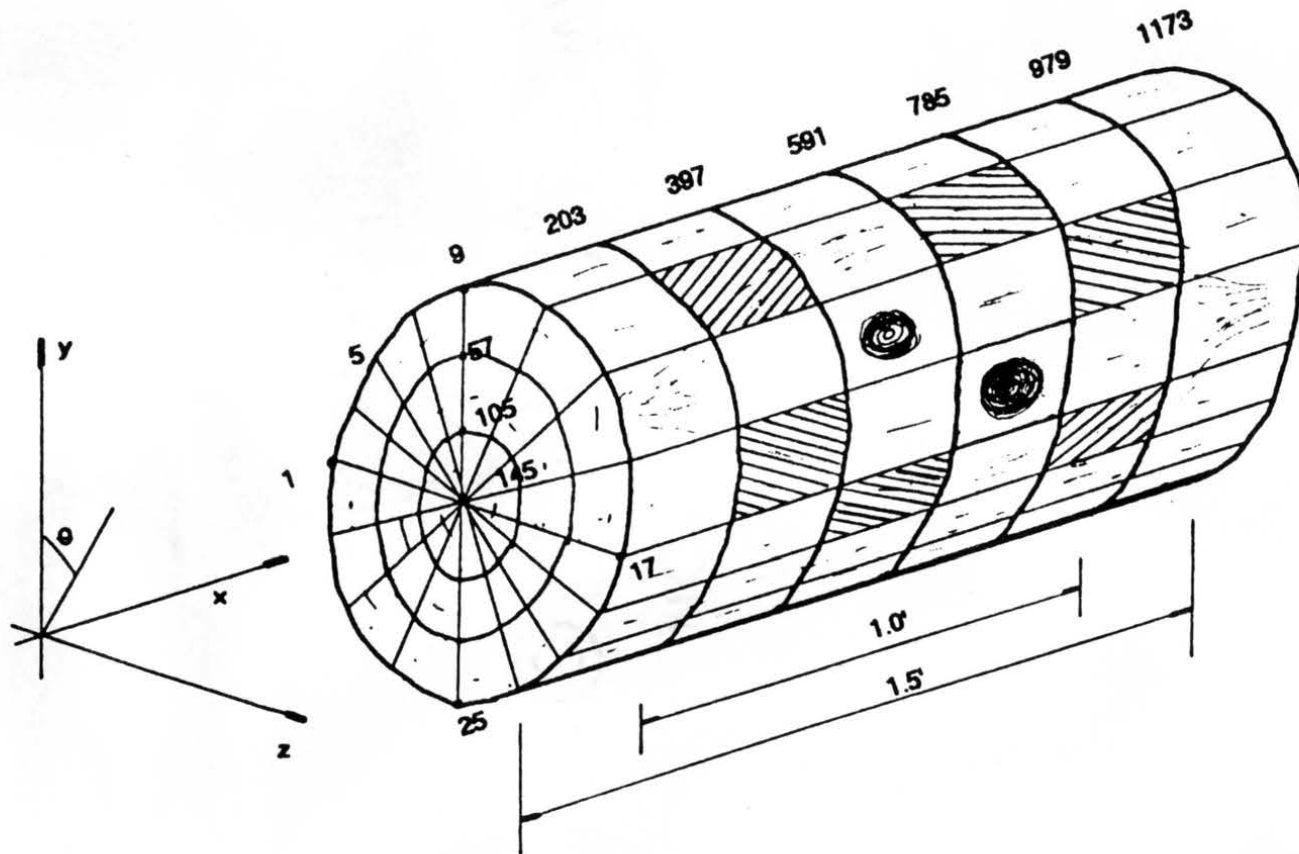


Figure 5.1. Location of the Joints at Top Line of Tension Side of Segment.

algorithm described in Chapter 3 (see also Figure 3.2).

The loading was applied at the far end of the segment using the GTSTRU DL boundary conditions statements. The longitudinal and shear stresses were assigned to each joint of the far section (see Figure 3.3), which were evaluated using another FORTRAN code, see Appendix B, developed for this purpose.

The joint conditions to represent boundary conditions at the near section of the segment are described in Section 3.2.2.

5.2 RESULTS OF TRIAL ANALYSIS WITH ISOTROPIC AND ORTHOTROPIC MATERIALS

In order to compare the theoretical results with those from the GTSTRU DL program, an isotropic material, steel, was considered. Also an orthotropic material, wood, Douglas-fir properties were assigned into the model, assuming no spiral grain and E constant across (D-1) and in each of the three principal directions.

In the preliminary study, the segments considered were taken from a 50-foot long Douglas-fir pole located at the groundline, with actual diameter of 12.49 inches. The same loading system, as described in Section 3.2.2 was applied on these segments.

The results of the finite element analysis for steel are presented in Table 5.1 and for wood in Tables 5.2. These

Table 5.1. Stresses Parallel to x-axis at Joints on xy Plane of a Steel Cylinder Finite Element Segment

joint	9	150	203	344	397	538	591	732	785	926	979	1120	1173
stress	2575	2551	2537	2527	2521	2514	2506	2498	2490	2482	2475	2470	2462
joint	37		231		425		619		813		1007		1201
stress	2134		2118		2104		2091		2078		2064		2052
joint	57	166	251	360	445	554	639	748	833	942	1027	1136	1221
stress	1698	1698	1698	1689	1685	1679	1674	1699	1664	1657	1652	1648	1643
joint	85		279		473		667		861		1055		1249
stress	1267		1269		1261		1253		1245		1236		1229
joint	105	182	299	376	493	570	687	764	881	958	1075	1152	1269
stress	849	848	848	847	844	842	839	836	833	831	827	825	823
joint	133		327		521		715		909		1103		1297
stress	424		422		421		418		415		412		409
joint	145	194	339	388	533	582	727	776	921	970	1115	1164	1309
stress	15	15	14	13	13	12	12	12	12	12	12	12	12

Steel Properties (Criswell 1988)
 E= 29000000 PSI
 G= 11000000 PSI
 ν = 0.3

Table 5.2. Stresses Parallel to Grain at Joints on xy Plane of a Douglas-fir Pole Segment, With Straight Grain and E Constant Throughout the Section (D-1)

joint	9	150	203	344	397	538	591	732	785	926	979	1120	1173
stress	2722	2638	2563	2527	2523	2523	2517	2510	2503	2496	2490	2485	2478
joint	37		231		425		619		813		1007		1201
stress	2147		2133		2120		2103		2088		2075		2063
joint	57	166	251	380	445	554	639	748	833	942	1027	1138	1221
stress	1653	1688	1714	1692	1694	1689	1683	1677	1671	1665	1660	1656	1651
joint	85		279		473		667		861		1055		1249
stress	1234		1272		1269		1261		1253		1244		1238
joint	105	182	299	376	493	570	687	764	881	958	1075	1152	1269
stress	835	834	838	841	843	842	841	838	835	832	830	828	826
joint	133		327		521		715		909		1103		1297
stress	417		418		421		420		418		416		413
joint	145	194	339	388	533	582	727	776	921	970	1115	1164	1309
stress	4	6	15	16	16	16	15	15	15	14	14	13	11

tables contain the stresses developed on the xy plane for the joints on the tension face.

For a similar segment, using the formulas from mechanics of materials, the stresses at the joints located at the top line of the tension side were evaluated and presented in Table 5.3. Comparing the values presented in Tables 5.1, 5.2, and 5.3, for discs 2 through 5, it can be seen that the stresses are, for practical purposes the same, as expected.

In addition to the above evaluation, two more wood segments were studied with the objective of verifying the influence of spiral grain and variation of E along the radius. For these segments the following conditions were made:

- a) no spiral grain and E varying (D-2) in each concentric layer (one third of the radius in thickness), and
- b) spiral grain effect and E varying (D-3) in each concentric layer.

The results obtained from the finite element analyses for these two cases are presented in Tables 5.4 and 5.5.

5.3 COMPARISON OF PREVIOUS RESULTS WITH THOSE BASED ON THE STRENGTH OF MATERIALS THEORY

A comparison of the results obtained with the finite element analysis performed with GTSTRUDL program for isotropic and orthotropic materials with those obtained when applying the equations from the elementary mechanics of materials was carried out in order to define the accuracy of the model. Variations on material properties (E) and spiral

Table 5.3. Stresses at Nodal Points, Located on Top Line (of xy Plane) of Tension Side, Using Formulas from Mechanics of Materials.

Joint Number	Stress (PSI)
9	2572
150	2564
203	2556
344	2549
397	2540
538	2533
591	2524
732	2517
785	2509
926	2501
979	2493
1120	2486
1173	2477

Table 5.4. Stresses Parallel to Grain at Joints on xy Plane of a Douglas-fir Segment, With Straight Grain and E varying across the section (D-2)

joint	9	150	203	344	397	538	591	732	785	926	979	1120	1173
stress	2861	2769	2687	2646	2638	2639	2613	2585	2557	2514	2495	2498	2460
joint	37		231		425		619		813		1007		1201
stress	2253		2240		2224		2199		2172		2119		2064
joint	57	166	251	360	445	554	639	748	833	942	1027	1136	1221
stress	1523	1562	1591	1572	1579	1578	1579	1584	1589	1599	1620	1626	1633
joint	85		279		473		667		861		1055		1249
stress	896		1025		1034		1049		1086		1176		1257
joint	105	182	299	376	493	570	687	764	881	958	1075	1152	1269
stress	607	609	618	624	630	641	650	670	689	727	763	782	836
joint	133		327		521		715		909		1103		1297
stress	274		277		285		298		324		384		440
joint	145	194	339	388	533	582	727	776	921	970	1115	1164	1309
stress	5	4	11	10	16	4	0	8	18	30	49	38	22

Table 5.5. Stresses Parallel to Grain at Joints on xy plane of Douglas-fir Segment, With Spiral Grain and E varying across the section (D-3)

joint	9	150	203	344	397	538	591	732	785	928	979	1120	1173
stress	2872	2779	2694	2651	2642	2633	2617	2589	2560	2516	2496	2498	2459
joint	37		231		425		619		813		1007		1201
stress	2254		2241		2225		2200		2173		2120		2063
joint	57	166	251	360	445	554	639	748	833	942	1027	1136	1221
stress	1522	1562	1590	1570	1576	1577	1577	1583	1589	1599	1620	1626	1633
joint	85		279		473		667		861		1055		1249
stress	982		1022		1031		1045		1083		1175		1258
joint	105	182	299	376	493	570	687	764	881	958	1075	1152	1269
stress	605	607	613	621	627	638	646	687	685	724	761	781	835
joint	133		327		521		715		909		1103		1297
stress	272		276		285		299		325		385		439
joint	145	194	339	388	533	582	727	776	921	970	1115	1164	1309
stress	7	6	11	11	10	8	10	15	23	33	52	40	22

grain were introduced to observe their influence on stress distribution.

5.3.1 LONGITUDINAL STRESSES ON THE CROSS SECTION

For better visualization of the results, Figure 5.2 shows the stress distribution on the second disc (see Figure 3.2) of the four segments and that evaluated from elementary mechanics. In this figure, the effect of E variation can be seen on both segments with and without spiral grain. For constant E (steel and D-1) a linear variation was obtained. For the wood pole segments with E variation, as the E decreases toward the pith (D-2, D-3) the stresses follow the same pattern.

Related to the presence of spiral grain, for small angles (in this case 2°), it can be seen that little increase in the stresses (0.3%) grain was observed.

5.3.2 STRESSES ALONG THE TOP LINE OF SEGMENTS

The stresses developed along the segment length for all cases were also verified in order to observe the effect of load applied to the segments, assumed to have linear variation.

Figure 5.3 shows the stress distribution on sections 2 through 6 for the segment of Douglas-fir with grain deviation and E varying in the cross section (D-3). Observing this figure, it can be seen that the farther the section is located from the loading section (section 7) the more accentuated is

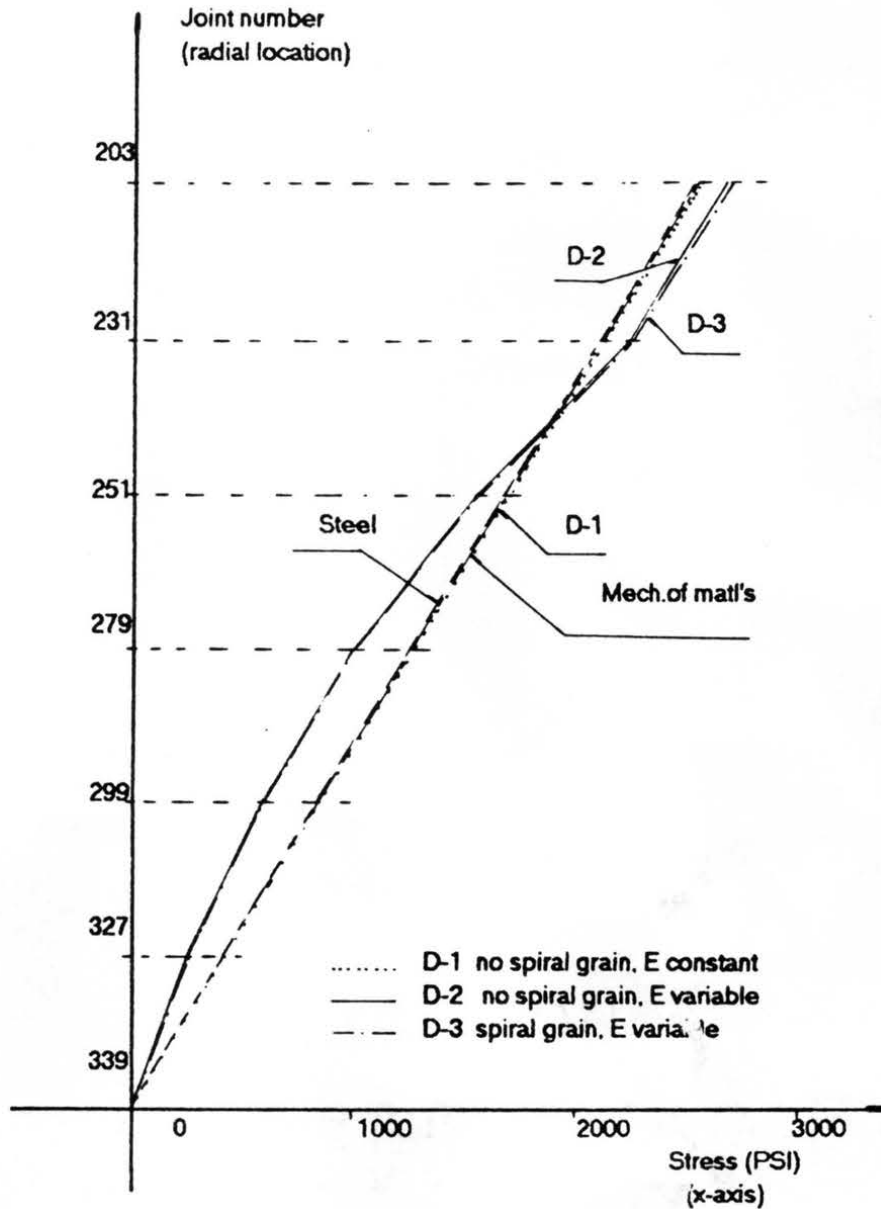


Figure 5.2. Stress Distribution on Second Disc of Segments of Steel and Douglas Fir (D-1, D-2, D-3) at the xy Plane, Using the GTSTRU DL Program.

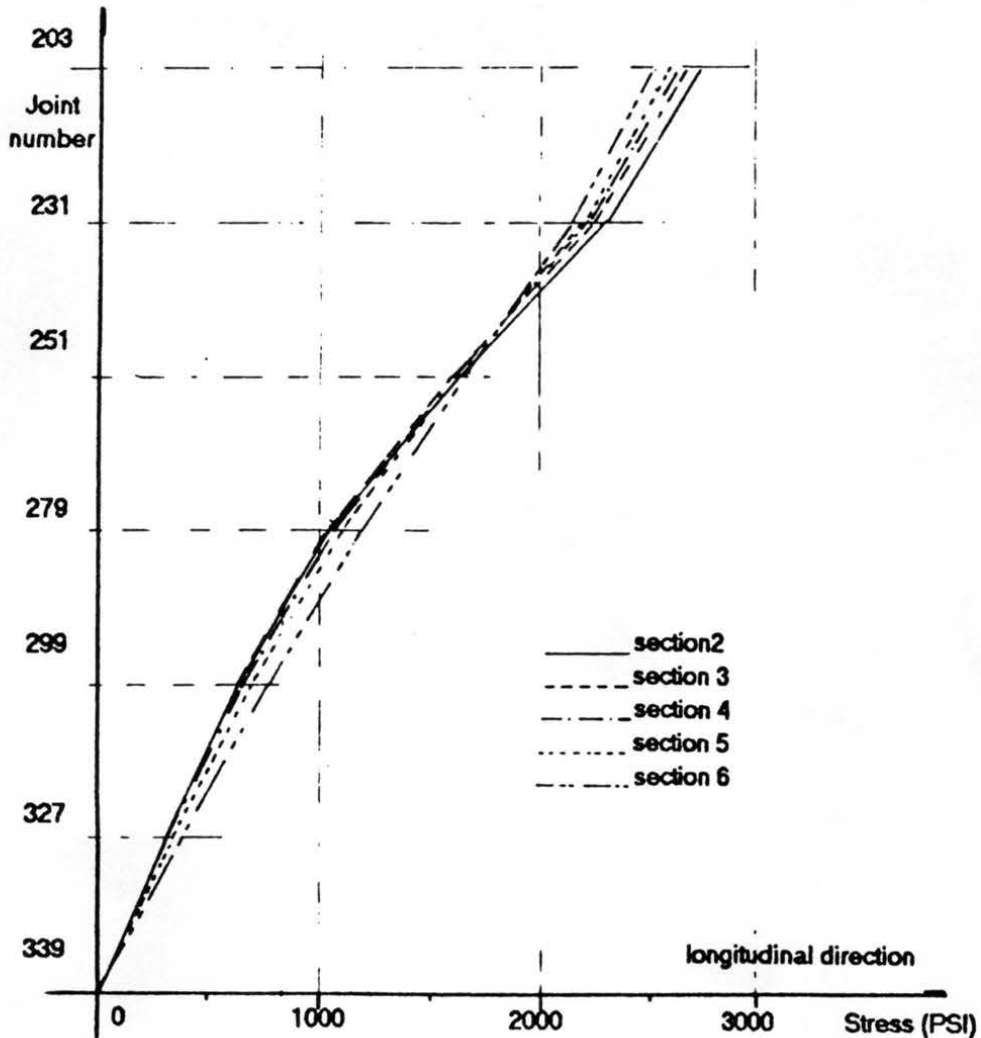


Figure 5.3. Stress Distribution on Sections 2 Through 6 of Douglas-fir Pole Segment with Spiral Grain Angle Presented and E Varying Throughout the Cross Section.

the stress variation. This can be explained by the fact that the applied stresses at the loading section were evaluated according to the strength of materials theory.

Taking the stresses evaluated by the mechanics of materials as basis of comparison, Table 5.6 presents the summary of the stresses developed on steel and wood (D-1) segments, which also includes the results for the segments of Douglas-fir (D-2, D-3). These results can be visualized in Figure 5.4. From this figure it is noted that for section one, in all cases using the finite element analysis, higher values were obtained than those from the elementary theory. The higher values are due to the influence of boundary conditions, adopted to represent the continuity of the near side of the segment of the pole. However for the cases of steel and wood with constant E (D-1), the stresses were the same and 5.8% higher respectively than that from mechanics of materials, which can be considered in reasonable agreement when compared with theoretical values. When the variation in modulus of elasticity is introduced with and without cross grain, the differences in stresses in the first section are even higher, indicating more intensively the boundary conditions effect.

5.4 FINITE ELEMENT ANALYSIS ON SELECTED POLES

The 3-D finite element model was developed with the objective of defining the variations on the stress distribution along a pole which may contain knots and spiral

**Table 5.6. Stresses Along the Top Line of Tension Side of
Finite Element Segments for Steel and Wood**

condition	Joint number						
	9	203	397	591	785	979	1173
D-1	2722	2563	2523	2517	2503	2490	2478
D-2	2861	2687	2638	2613	2557	2495	2460
D-3	2872	2694	2642	2617	2560	2496	2459
STEEL	2575	2537	2521	2506	2490	2475	2462
FSMW	2572	2556	2540	2524	2509	2493	2477

Observations:

- D-1 - Wood with straight grain and MOE constant across the section.
- D-2 - Wood with straight grain and MOE varying across the section.
- D-3 - Wood with spiral grain, MOE varying across the section.
- FMSW - Wood, using formulas from strength of materials.

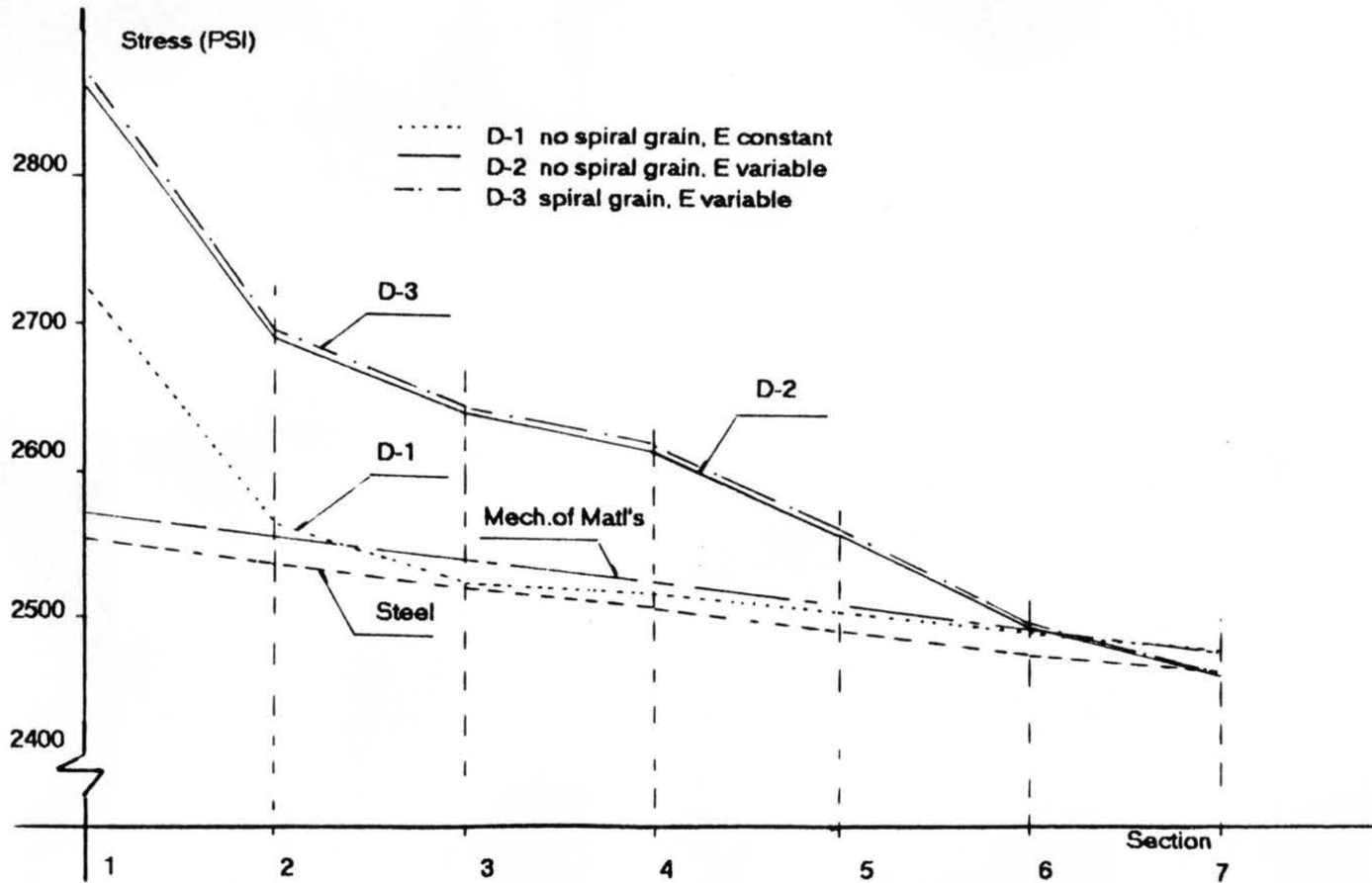


Figure 5.4. Tension Stresses Developed at the Top Line of the Sections of Segments of Steel, Douglas Fir (D-1, D-2, D-3) and the Reference Stresses Evaluated from Elementary Mechanics Theory.

grain. To attain this goal, the first step was to scan the pole using knot mapping to highlight the sections presenting knots or cluster of knots. On each pole in this study, three locations or more, in which the number of knots and their angular position with respect to the neutral plane were considered to have the worst effect over the stress distribution were selected to be analyzed mathematically.

The mesh created for the model was fitted over the segment chosen and was oriented such that the four central discs, 12 inches of the segment, contained the most critical knots. This was done to avoid the effect of boundary conditions on the first disc and loading on the last disc.

Following this procedure, all poles involved in this study were scanned and at least three segments were selected from each to perform the finite element analysis. For each segment selected, the location, the geometric characteristics, the spiral grain and the elastic properties were determined using straight line interpolation as described in Section 4.3.2.2. A data sheet was prepared for each segment to orient the formation of the input file for the GTSTRUDL. Appendix F shows one sample of the data used for Douglas-fir # 162, segment # 2, and the GTSTRUDL data file used to perform the stiffness analysis.

5.4.1 GTSTRUDL ANALYSIS

After the input file was built, the program was executed. Due to the size of the model in terms of unknowns (1309 joints

and more than 3900 degrees of freedom), the time required to perform the stiffness analysis was on average 17000 cpu seconds continuously, which means 8 to 10 hours of normal operation, i.e., including priorities and sharing time. The data and the results of stiffness analysis included in the output for a single segment amounted to more than 280 pages, hence due to the huge volume of output, these data are not presented here but kept in the CSU - Wood Science Laboratory archives.

The results computed during the stiffness analysis were sent to an output file where the average element stresses, node displacements, and principal stresses were presented.

5.4.2 CRITERIA USED TO OBTAIN THE MAXIMUM STRESS AT POLE SEGMENTS

Based on GTSTRUDL output results generated for the load of 1000 pounds, the maximum principal stress, parallel and perpendicular to grain, were searched between discs 2 and 6. The maximum principal stress parallel to grain found in the whole segment was used to compare with the wood strength, determined in small clear specimens, in order to predict the pole strength.

5.5 RESULTS OF FINITE ELEMENT ANALYSIS FOR WESTERN REDCEDAR, DOUGLAS-FIR AND SOUTHERN PINE CHARACTERISTICS

The output for each segment analyzed in the GTSTRUDL Program was scanned and the distribution of the principal

stresses, parallel and perpendicular to grain, in each of the seven discs observed. The maximum stress and corresponding locations were determined in the sections. Twenty nine segments were submitted to the finite element stiffness analysis using the GTSTRUDL program. A table for each segment was assembled which contains for each disc: the maximum principal stress parallel to grain in compression and tension, and the maximum principal stress perpendicular to grain. Appendix G contains these 29 tables (Table G.1 through Table G.29) and the first table of that Appendix is reproduced as Table 5.7.

5.6 PREDICTION OF THE STRENGTH OF THE POLES

Table 5.8 summarizes the results presented in Tables G.1 through G.29 from Appendix G, where only the observed maximum principal stress parallel to grain due to the applied moment and shear in each pole segment (both generated by the 1000 lbs load) is presented. Figures 5.5 through 5.7 present the location of segments and the corresponding maximum stresses.

As the strength of wood varies along the pole, the wood strength at each segment was computed using the test data from the Tables 4.3 through 4.5 and Figures 4.10 through 4.21.

In order to predict the maximum load, i.e. the pole strength, linear behavior was assumed for the stress-strain relationship and a proportional factor between the wood strength and the stress generated by the 1000 lbs load was computed for the segments. These factors applied to the

Table 5.7. Stresses Developed at Joints of Segments of Western redcedar, using GTSTRU DL Finite Element Analysis

Pole # 85 : Segment # 1
 Segment Location: 6" AGL
 Maximum Stress: 1624 PSI

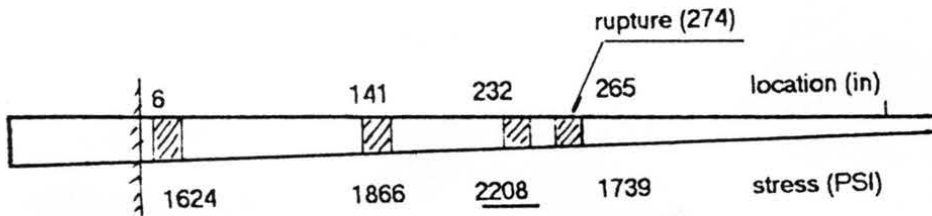
Disc	Stress	Face	Joint	Central	Joint
		Stress	Joint	Stress	Joint
1	Tension par.	1604	9	1496	150
	Stress perp.	88	13	29	150
	Compression	1579	25	1486	158
2	Tension par.	1426	204	1398	345
	Stress perp.	85	219	44	350
	Compression	1382	219	1285	352
3	Tension par.	1384	398	1374	538
	Stress perp.	104	413	80	547
	Compression	1483	415	1624	547
4	Tension par.	1396	591	1394	732
	Stress perp.	97	605	50	741
	Compression	1529	609	1362	741
5	Tension par.	1415	785	1418	926
	Stress perp.	97	803	46	935
	Compression	1371	801	1407	934
6	Tension par.	1380	979	1338	1120
	Stress perp.	27	1111	29	1146
	Compression	1387	995	1333	1128
7	Tension par.	1315	1173	- -	- -
	Stress perp.	44	1257	- -	- -
	Compression	1349	1189	- -	- -

Table 5.8. Summary of Maximum Stresses Developed on Pole Segments by Finite Element Analysis

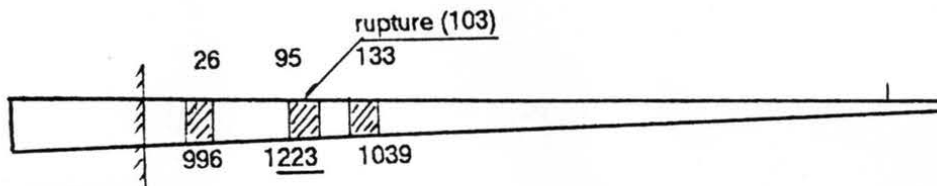
Section No.	Near side (in)	Max. Stress (PSI)	Joint	Near side (in)	Max. Stress (PSI)	Joint	Near side (in)	Max. Stress (PSI)	Joint
WESTERN REDCEDAR									
	POLE # 85			POLE # 88			POLE # 91		
1	6	-1624	547	26	-996	547	26	2521	732
2	141	-1866	414	95	-1223	934	58	-2702	546
3	232	-2208	934	153	-1039	220	95	2459	293
4	265	1739	539						
DOUGLAS-FIR									
	POLE # 162			POLE # 174			POLE # 188		
1	34	2902	732	0	-3006	739	22	-3038	546
2	59	-2748	740	28	-3322	605	119	3113	397
3	88	-2765	740	64	-3151	609	267	-2473	740
4				96	-3039	801			
5				142	-3697	547			
SOUTHERN PINE									
	POLE # 289			POLE # 292			POLE # 297		
1	52	4222	203	10	3186	203	12	2540	203
2	*	*	*	140	3698	538	72	2391	203
3	190	3154	203	213	3718	732	150	2197	203

(*) Data lost due to a processing problem

WRC-85 (l=50')



WRC-88 (l=50')



WRC-91 (l=40')

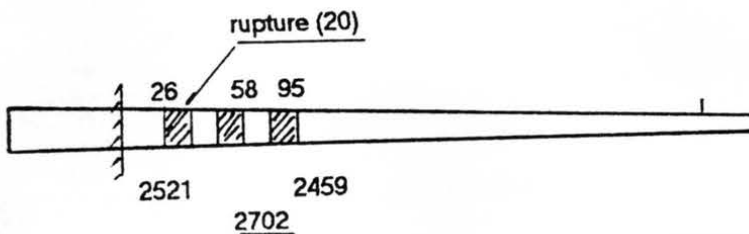
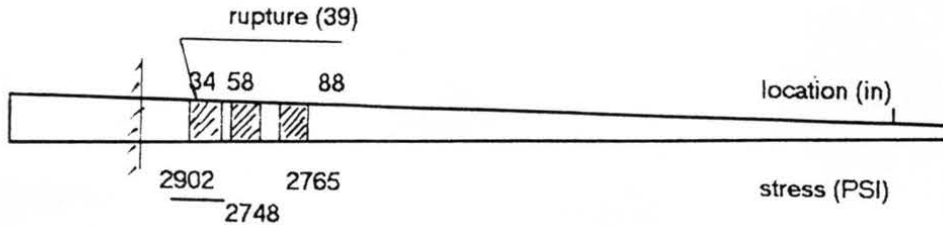
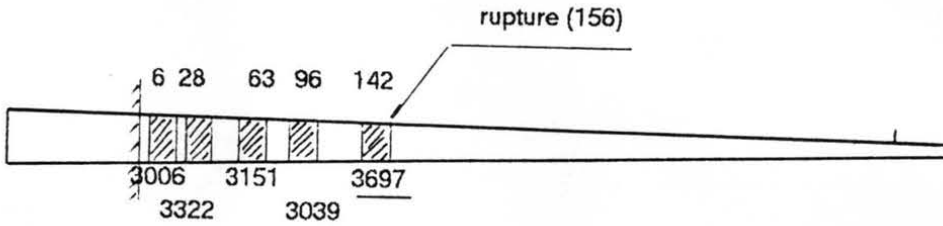


Figure 5.5. Location of the Segments Studied and the Maximum Stresses Generated by the 1000 lbs Load on Western Redcedar Poles. It is Also Indicated the Failure Location on Full Size Test.

DF-162 (l=50')



DF-174 (l=50')



DF-188 (l=60')

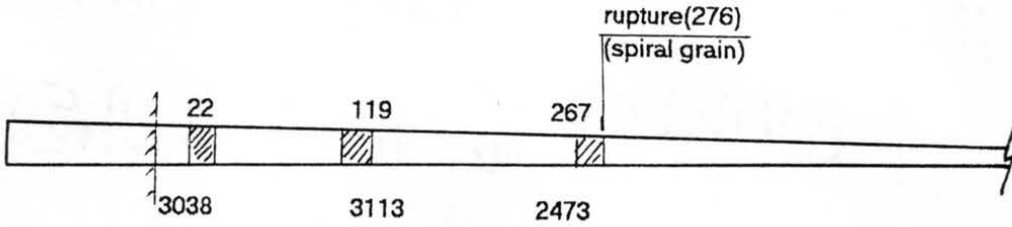
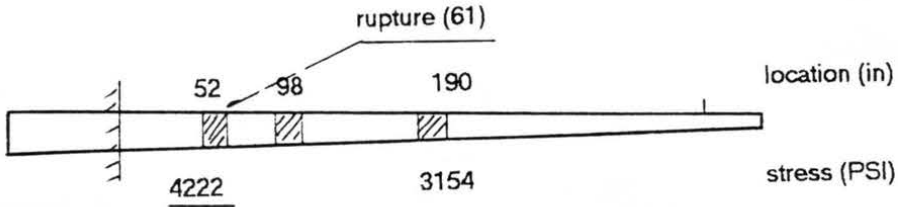
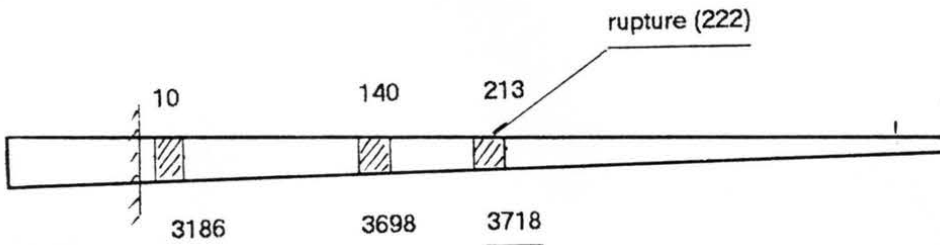


Figure 5.6. Location of the Segments Studied and the Maximum Stresses Generated by the 1000 lbs Load on Douglas Fir Poles. It is Also Indicated the Failure Location on Full Size Test.

SP-289 (l=40')



SP-292 (l=50')



SP-297 (l=50')

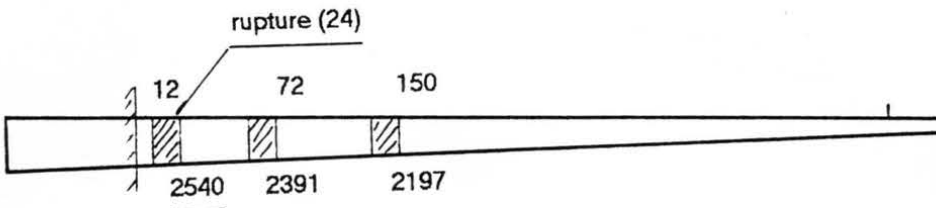


Figure 5.7. Location of the Segments Studied and the Maximum Stresses Generated by the 1000 lbs Load on Southern Pine Poles. It is Also Indicated the Failure Location on Full Size Test.

original load lead to the evaluation of the pole strength. In Table 5.9 the proportional factor is presented for each segment and the maximum load obtained. Using the values from this table, for each pole the least value found was taken as the predicted pole strength.

5.7 ADJUSTMENTS ON PREDICTED LOAD

The pole characteristics in bending were determined from small, clear specimens cut from boles, which were taken from the tested poles. The boles of western redcedar were kept stored at the CSU Wood Science Laboratory for such time until all poles of this species and Douglas-fir had been tested, then the bending samples were cut. The samples of southern pine were cut right after the pole test. During this period some change in the moisture content occurred in some boles of western redcedar.

In order to draw conclusions for the tested poles using the values from the samples tested, adjustments on the strength values of small, clear specimens in Table 5.9, due to the drying were necessary, since the moisture content can affect the results significantly. From Table 4.3 it can be seen that the moisture content for western redcedar specimens averaged 15.7%, 13.6% and 15.2% for poles number 85, 88 and 91 respectively; for Douglas-fir as shown on Table 4.4 the moisture content was not computed due to the oily treatment applied to the poles and for southern pine the moisture

Table 5.9. Evaluation of the Proportional Factor between the Wood Strength and the Stress for 1000 lbs Load.

Pole Segment	Location AGL (1) (in)	Maximum Stress (PSI)	MOR (PSI)	Proportional Factor
Western redcedar				
85-1	6	1624	8224	5.06
85-2	141	1866	8870	4.75
85-3	232	2208	9132	4.14*
85-4	265	1739	9045	5.20
88-1	26	996	8025	8.06
88-2	95	1223	7735	6.32*
88-3	133	1039	7575	7.29
91-1	26	2521	11330	4.49
91-2	58	2702	10763	3.98*
91-3	95	2459	10254	4.17
Douglas-Fir				
162-1	34	2902	10097	3.48*
162-2	59	2748	10114	3.68
162-3	88	2765	10134	3.67
174-1	6	3006	9723	3.24
174-2	28	3322	9847	2.96
174-3	63	3151	10044	3.19
174-4	96	3039	10230	3.37
174-5	142	3697	10288	2.78*
188-1	22	3038	13011	4.28
188-2	119	3113	11253	3.62*
188-3	267	2473	10445	4.23
Southern pine				
289-1	52	4222	7641	1.80*
289-2	**	**	**	**
289-3	190	3154	7763	2.46
292-1	10	3186	6071	1.91
292-2	140	3698	6913	1.87
292-3	213	3718	6703	1.80*
297-1	12	2540	7980	3.14
297-2	72	2391	7176	3.00*
297-3	150	2197	6690	3.06

(1) - AGL - Above Ground Line

* - Controlling ratio

** - Data lost due to processing problem

content averaged 64.5%, 96.8% and 85.6% for the poles number 289, 292 and 297 respectively.

According to Bodig and Jayne (1982) the fiber saturation point for the wood species under this study are 22.0% for western redcedar, 26.0% for Douglas-fir and 27.0% for southern pine. This reference also states that the ratio of dry to green for modulus of rupture for these species as 1.50; 1.64 and 1.70, respectively.

On the other hand, according to the data presented on Table 4.1, the moisture content of the poles measured with a moisture meter at 6 and 16 feet from the butt at 2.5 inches deep, the poles of western redcedar and Douglas-fir were tested at moisture content very close to the fiber saturation point and the poles of southern pine well above this limit. It is assumed that all poles were tested in the green condition in the full scale test.

However as seen above, adjustments are only necessary for poles of western redcedar for which the moisture content during the bending test in small specimens presented values below the fiber saturation point. Using the data presented here, the correction factors evaluated for this species had the values of 1.32 for pole 85, 1.42 for pole 88 and 1.34 for pole 91. The predicted values, adjusted for moisture content, for the pole strength were consequently evaluated and presented in Table 5.10.

Table 5.10. Predicted Values for Pole Strength and Failure Location

Pole Number	Pole Strength (pounds)	Adjusted Pole Strength (pounds)	Failure (inches)	Location (feet)
Western redcedar				
85	4140	3140	245.5	20.5
88	6320	4450	108.5	9.0
91	3980	2970	65.5	5.5
Douglas-Fir				
162	3480	3480	44.5	3.7
174	2780	2780	149.5	12.5
188	3620	3620	125	10.9
Southern pine				
289	1800	1800	55.0	4.6
292	1800	1800	223.5	18.6
297	3000	3000	7.5	6.3

5.8 PREDICTION OF FAILURE LOCATION

The criteria to predict the failure location was based on the combined stress parallel to grain due to the applied load and the wood strength determined in small clear specimens, as indicated in Section 5.6. The sketches presented in Figures 5.5 through 5.7 show the locations where the maximum stresses occurred on each pole, and underlined the segment where the combined stress and wood strength was found to be critical (lowest ratio). By this criteria, failures were predicted to occur at these locations (underlined sections). Table 5.10 includes the distance from groundline where the predicted failure occurred on each pole.

5.9 RESULTS FROM FULL SCALE TESTS

The actual pole strength were determined in the full scale bending test described in Section 4.3.1. The ultimate load observed in each test is tabulated on Table 5.11, along with the indication of the failure location. These data were taken from the pole data form and load deflection curve used by the EDM during the pole test (see Appendix D-4).

Table 5.11. Results of Pole Test on Full Scale Basis

Pole Number	Pole Strength (pounds)	Failure (Inches)	Location (feet)
WESTERN REDCEDAR			
85	2834	274	22.9
88	4471	103	8.6
91	3196	20	1.6
DOUGLAS FIR			
162	3579	40	3.3
174	2778	156	13.0
188	3820	276	23.0
SOUTHERN PINE			
289	2164	61	5.1
292	2072	222	18.5
297	3495	24	2.0

CHAPTER 6

DISCUSSION

6.1 GENERAL

In the prior chapters, the results of the finite element analysis performed with the GTSTRU DL program, along with the results observed on actual tests on wood poles were presented. The experimental tests were conducted to verify the pole strength prediction model.

Although some discussions have already been made in the presentation of the results, the following paragraphs are concerned about discussions of tests, findings, and analyses from the completed study.

6.2 BASIC MATERIAL PROPERTIES

The mechanical properties of the poles studied were determined to provide data for the analytical study conducted on the poles.

To built the curves to represent the variation of wood bending strength and MOE in bending along each pole, four samples located between the groundline and the point of load application were evaluated. The strength and MOE in bending for points located in any interval were assumed to lie on a line linking the properties evaluated in the two adjacent segments (Figures 4.10 through 4.21). In spite of the care

dispensed on these tests, some inherent variations were observed with respect to the general pattern of properties. For instance, some segments presented atypically low values of properties for western redcedar, pole # 91 (Figure 4.19) and southern pine, poles # 292 and 297 (Figure 4.21). Although it is difficult to determine the source to which the variation may be attributed, internal defects, or mechanical damage realized during the bending test are possible. For this study, one sample was taken to determine the bending properties of poles (MOE and MOR), hence there was no ability to determine the variability of material. In future studies, it is advised that several samples be taken in order to increase the accuracy on bending strength and MOE determination.

6.3 GRAIN DEVIATION

Grain deviation that is due to spiral grain or local deviation associated to knots reduces pole strength. In the model, the grain deviation was taken into account by rotating the material orientation reference axes accordingly during assembling of the element stiffness matrices. As a result, in the elements containing knots and grain deviation, the principal stresses generated by the 1000 pound load applied to the pole tip increased, indicating some stress concentration in those elements. These stress concentrations affect pole strength by decreasing the capacity to carry external loads.

The spiral grain strength reducing effect was observed on the examples presented in Chapter 5, where a segment with 2° spiral grain resulted in a stress 0.3% higher than that of a similar segment with straight grain (Figure 5.2).

6.4 PREDICTION OF POLE STRENGTH AND FAILURE LOCATION

Related to strength prediction of poles, the basic parameters used were the stress parallel to grain generated by the finite element model and the bending strength of wood parallel to grain determined in small, clear specimens for the same segment. As the bending strength was evaluated in discrete points using small, clear specimens, it was assumed that this property varies linearly between two adjacent points, therefore straight line equations were used to evaluate strength at the segments.

In order to evaluate the proportional factor to evaluate the predicted pole strength, for each segment the bending strength was divided by the maximum stress originated by the unitary load (1 kips) in the segment, using the finite element analysis. This factor applied to the 1000 lbs load led to the predicted ultimate pole tip load.

The following comments concerning the pole strength and failure location of each species can be made:

a) Western redcedar poles: The Figure 5.5 shows a picture of each pole scanned with the finite element model. It can be seen that the actual and predicted failure locations as shown in Table 6.1 were very close, the error being less than 3.0

Table 6.1. Predicted vs Actual Values for Pole Strength and Failure Location

Pole Number	Predicted Pole Strength (pounds)	Actual Pole Strength (pounds)	Difference (%)	Predicted Failure Location* (feet)	Actual Failure Location (feet)
Western redcedar					
85	3140	2834	10.8	20.5	22.9
88	4450	4471	-0.5	9.0	8.6
91	2970	3196	-7.1	5.5	1.6
Douglas-Fir					
162	3480	3579	-2.8	3.7	3.3
174	2780	2778	0	12.5	13.0
188	3620	3820	-5.2	10.9	23.0
Southern pine					
289	1800	2164	-16.8	4.6	5.1
292	1800	2072	-13.1	18.6	18.5
297 **	3240	3495	-7.3	1.3	2.0

* The predicted failure location was located where the lowest stress/strength ratio occurred

** Values adjusted using the revised values for bending strength of small, clear specimens

feet on these three poles. For actual and predicted strengths also shown in Table 6.1, good agreement between the model and the experimental results was seen, with the maximum difference being 10.8%;

b) Douglas-fir poles: The best results were obtained for this species for which the strength predicted from the model differed from the actual values in less than 6%. As far as failure locations are concerned, only in one pole of this species the predicted one differed from the actual. The actual failure occurred at 23 feet above groundline, while the predicted one was observed at 10.9' feet above groundline in the segment 9.9-11.3 feet above groundline. For this pole, although the visual inspection by scanning the knot map indicated that the most critical sections were those analyzed, it could be possible that some material flaw or undetectable defect was also present that triggered the failure in a different location;

c) Southern pine poles: Two facts are noticed for this species. First, for pole # 289, the results for one of the three segments was lost due to a computer processing problem. The GTSTRUDL program was later deactivated by the CSU computer center and the file could not be reprocessed. Nevertheless, results were obtained for the two remaining segments showing the predicted pole strength and failure location. The second issue for this species relates to the low strength value obtained for pole # 292 as shown in Figure 4.21. This is probably due to some damage, or material variation, in the

bending test specimen since in this case the small, clear specimen was cut close to the actual failure location. If the bending strength for the second segment is taken in the line joining the strength of specimens 1 and 3, this value would be 7910 instead of 6452 psi. Making the appropriate corrections for the segments studied, the values of 8235, 8064 and 7842 psi result for the segments 1, 2 and 3 respectively. Therefore, the new proportional factor can be evaluated as 3.24, 3.37 and 3.56, respectively. Applying this modification, Table 6.1 shows the revised values predicted for poles of southern pine. For this adjustment in the bending strength of wood, the actual failure locations for the three poles fell in the segment where they were predicted.

The summary of pole strength and failure location predicted with the model is therefore presented in Table 6.1 for the three species. The difference between the predicted and the actual strength is presented in percentage, having the actual value as basis of comparison. Also part of this table is the predicted and the actual location of the failure.

From these results, it is clear that the process has limitations. Growth characteristics on poles were observed by visual inspections of pole surface and the modeled segments were located where occurrence of such growth characteristics was judged to be the most critical. However poles may present flaws or mechanical damages which are not possible to detect by visual inspection that may have influence on failure mechanism.

CHAPTER 7

SUMMARY AND CONCLUSION

7.1 SUMMARY

Prediction of pole strength has been studied with the aim of attempting to define the influence of defects and variation of wood characteristics on pole tip lateral load capacity (Wood and Markwardt 1965; Dashiell 1985; Phillips et al. 1985; Bodig 1986; Bodig et al. 1986, Vol. 1 and 2; Wang 1987). In some of the past studies, variability in wood bending strength, knot effect, and spiral grain have been included using empirical relationships and/or experimental data from full size pole tests. However, a general prediction model has not been previously defined.

The studies including the effects of knots have considered the knot diameter and the sum of the knots per foot (cluster of knots) as variables, but did not include the associated grain deviation surrounding the knots.

The effect of knots and their associated grain deviations, as well as any overall spiral grain, had been studied only in boards, where a 2-D finite element method has been used in the analysis (Dabholkar 1980; Cramer 1981, 1984; Zandbergs 1985; Stahl and Cramer 1990). In these studies, the

prediction of the tension behavior of members loaded in uniaxial tension has been made.

The true 3-D behavior of wood leads to the inference that planar (2-D) analysis for round structural members is not suitable, rather is incomplete and too approximate. The problem is even more complicated when defects with a significant 3-D character are represented in two dimensions. Because of these restrictions a 3-D analysis was attempted here, using the finite element method as the mathematical tool for modeling.

The objective of the study presented here was to develop a strength prediction model using the 3-D finite element method to evaluate the stresses along the pole at segments containing described knots and other defects. These stresses were the basis for the prediction of pole strength and failure location. Due to the large dimensions of poles, only a small length segment of the pole, rather than the entire pole, was chosen as the basic item to be analyzed. Only the more critical segments need to be considered. In this way the information for the model, including the number of joints and elements, and presence of defects, is reduced and the finite element analysis becomes practical. Taking small segments, the entire pole can be studied by moving the segment along its length, in order to scan the pole to search for the maximum stress. The process of scanning the pole consists of a visual selection of segments for the finite element analysis. These segments are chosen to contain the most severe defects, such

as cluster of knots and spiral grain, in the more highly stressed regions. The information included in the knot map, prepared for the poles later destructively tested, was used to identify the worst knot clusters in any 18 inch long segment. These worst clusters were chosen based on the number of knots, knot diameter and their angular position relative to the neutral plane. Use of the model indicated that consideration of only a few locations on the lower third of the pole height is, in general, sufficient to detect the critical stress location; these critical locations can be found by identifying spots, located in the lower third, where defects are present.

The finite element model developed has six discs or slices along the segment length, each one containing 48 3-D elements. This results in a total of 288 elements and 1309 joints. Mesh generation and a methodology for assigning the element properties, spiral grain and modeling the knots including the knot itself and associated grain deviation were developed and have been described. The strength prediction model was tested by its use to predict the strength and failure location of nine poles, three each of western redcedar, Douglas-fir and southern pine. The results were compared with those obtained in full size tests performed on the same nine poles.

7.2 CONCLUSIONS

The new approach developed to model the growth characteristics, including knots, spiral grain and variation

of basic wood properties (MOE and bending strength), through the use of the 3-D finite element method applied to the more critical segments identified along the pole length proved to be very successful and showed a good improvement over the 2-D approaches. Favorable results were obtained using data from poles of the three different species of wood used to validate the model.

Although somewhat cumbersome and time consuming, the 3-D finite element analysis presented reliable and accurate results for pole strength and failure location prediction. For the nine poles studied, the predicted values for strength differ from the test results of full size members in the range of 10.8% and -16.8%, with an average deviation of 7% (average predicted values 7% below the actual). Concerning the failure location, in 2/3 of the cases, 6 poles, the actual failures were verified in the same places as those predicted in the model. In these cases knots were observed to be present in the segments. In the remaining 1/3 of the cases, 3 poles, the failure mechanisms were missed and the failures occurred in the adjacent segments with the maximum error (length deviation from the actual failure) of 3 feet, except for one pole for which the result from the finite element analysis for the predicted location was inconclusive where the deviation observed was 12 feet. The failure mechanism in these cases, may have been influenced by some phenomena, or internal problem, not recognizable from visual inspection of the pole surface.

Based on the trial runs and on data collected from the poles, the following general conclusions can be drawn:

1. The knot effect and associated grain deviation was found to be the most important factor related to strength reduction;

2. As the finite element analysis and the pole strength prediction criteria use data collected from tests on clear wood, in general, the variation in the MOE and bending strength in the cross section and along the length was verified to be an important factor affecting the location of maximum stress and poles failure;

3. Due to the importance of the modulus of elasticity and bending strength of wood to compute the pole strength, it was observed that more samples, not just one, need to be obtained per segment taken along the length of the pole tested, in order to have less variability and more accurate values for the wood properties on a single segment.

7.3 FUTURE RESEARCH NEEDS

The problem involving the determination of the stress field in a 3-D segment containing knots and spiral grain is very complex. Although good results were obtained with the model presented here, some improvement may be introduced in order to obtain better performance as far as reducing computer time and consequently cost is concerned. The model developed to include the growth characteristics and wood properties can now be used in specific research projects, designed to better

understand the influence of defects in individual wood members. In this way, studies concerning the overall effect of variation of spiral grain along a pole, effect of changing in direction of spiral grain across the cross section (inside a pole), effect of knot size in a pole segment, and verification of the critical effect - knot hole or associated grain deviation - on the stress distribution, can be verified with the proposed model. Although the model treats a pole as individual member, it might be able to be used with average strength data and variation data from small-clear specimens of an unknown or different wood species in order to study the pole behavior and simulate the strength distribution of poles.

7.4 LIMITATIONS OF THE MODEL

The 3-D finite element model developed for prediction of pole strength was verified with data collected from three different softwood species western redcedar, Douglas-fir and southern pine. Hardwood species or even different species of softwoods other than those used in this studied, may present different patterns of surface knots and spiral grain which should be known in order to provide the required data for the model.

Because of the restricted data used in the study as far as species of wood is concerned, the model presents some limitations, and possibly some adjustment or modifications may be required in order to apply it for hardwood species.

REFERENCES

1. Al Dabbagh, A.M.A. 1970. "Finite Element Stress Analysis for Anisotropic Solids." Ph.D. Dissertation. Dept. of Civil Engineering. Colorado State University. Fort Collins, CO.
2. American National Standard Institute-ANSI. 1987. "Standard for Wood Poles - Specification and Dimensions for Wood Poles." ANSI 05.1-1987. NY.
3. American Society for Testing and Materials. 1990. "Testing Small Clear Specimens of Timber." ASTM Designation: ASTM D 143-83. Annual Book of ASTM Standards. Sec 4-Construction. Vol 04.09-Wood.
4. Anthony, R.W. 1986. "Experimental Data for the Tension Behavior of Douglas Fir with Defects." M.S. Thesis. Dept. of Forest and Wood Sciences. Colorado State University. Fort Collins, CO.
5. Associacao Brasileira de Normas Tecnicas-ABNT. 1953. "Physical and Mechanical Tests for Wood (Ensaio Fisicos e Mecanicos de Madeira)." Original in Portuguese. Standard NBR-6230. Rio de Janeiro. Brazil.
6. Associacao Brasileira de Normas Tecnicas-ABNT. 1973. "Eucalypti Poles Treated under Pressure. (Postes de Eucalipto Tratados sob Pressao)." Original in Portuguese. Standard NBR-6229. Rio de Janeiro. Brazil.
7. Associacao Brasileira de Normas Tecnicas-ABNT. 1980. "Wood Poles - Bending Strength. (Postes de Madeira Resistencia a flexao)." Original in Portuguese. Standard NBR-6231. Rio de Janeiro. Brazil.
8. Associacao Brasileira de Normas Tecnicas-ABNT. 1984. "Preserved Eucalypti Poles for Distribution Lines (Postes de Eucalipto Preservado para Redes de Distribuicao de Energia Eletrica)." Original in Portuguese. Standard NBR-8456. Rio de Janeiro. Brazil.

9. Bendtsen, B.A., Freese, F. and Ethington, R.L. 1970. "A Forest Sampling Method for Wood Strength." Forest Products Journal. Vol. 20(11).
10. Biblis, E.J. 1965. "Shear Deflection of Wood Beams." Forest Products Journal. Vol 15(11), pp. 492-498.
11. Bodig, J. 1986. "Effect of Knots on Pole Strength." Final Report submitted to the Western Wood Preservers Institute. WLS-5. Fort Collins, CO.
12. Bodig, J. and Goodman, J.R. 1973. "Prediction of Elastic Parameters for Wood." Wood Science 5(4), pp. 249-264.
13. Bodig, J. and Jayne, B.A. 1982. "Mechanics of Wood and Wood Composites." Van Nostrand-Reinhold Company, Inc. New York, NY.
14. Bodig, J. and Phillips, G.E. 1983. "Strength and Stiffness of Wood Utility Poles." Paper prepared for the American Wood Preservers Association's 1984 meeting.
15. Bodig, J., Goodman J.R., Phillips G.E. and Fagan G.B. 1986. "Wood Pole Properties. Vol. 2: Douglas Fir Data." Electric Power Research Institute-EPRI. EL-4109. Palo Alto, CA.
16. Bodig, J., and Goodman J.R. 1986. "Wood Pole Properties. Vol. 3: Western Red Cedar Data and Size Effect." Electric Power Research Institute-EPRI. EL-4109. Palo Alto, CA.
17. Bohannon, B. 1971. "Height-Strength Relationship for Round Timber." Paper.
18. Boresi, A.P. and Sidebottom, O.M. 1985. "Advanced Mechanics of Materials." 4th ed. John Willey & Sons, Inc. New York, NY.
19. Brotero, F.A. 1956. "Testing Methods Adopted by IPT for the Study of National Woods (Metodos de Ensaio adotados no IPT para Estudo de Madeiras Nacionais)." Original in Portuguese. Instituto de Pesquisas Tecnologicas. Sao Paulo. Brasil. Bulletin No. 31. pp. 7-25.
20. Coates, R.C., Coutie, M.G. and Kong, F.K. 1988. "Structural Analysis." Van Nostrand Reinhold Co. Ltd. England.

21. Cook, R.D., Malkus D.S. and Plesha M.E. 1989. "Concepts and Application of Finite Element Analysis." 3rd edition. John Wiley and Sons. New York. NY.
22. Cramer, S.M. 1981. "A Stress Analysis Model for Wood Structural Members." M.S. Thesis. Dept of Civil Engineering. Colorado State University. Fort Collins, CO.
23. Cramer, S.M. 1984. "Failure Modeling of Wood Structural Members." Ph.D. Dissertation. Dept. of Civil Engineering. Colorado State University. Fort Collins, Co.
24. Cramer, S.M. and McDonald K.A. 1989. "Predicting Lumber Tensile Stiffness and Strength with Local Grain Angle Measurements and Failure Analysis." Wood and Fiber Science 21(4). pp. 393-410.
25. Criswell M.E. 1988. Class Notes of "Advanced Mechanics of Materials". Dept. of Civil Engineering. Colorado State University. Fort Collins. CO.
26. Dabholkar, A. 1980. "Finite Element Analysis of Wood with Knots and Cross Grain." Ph.D. Dissertation. Dept. of Civil Engineering. Colorado State University. Fort Collins, Co.
27. Dashiell, J.A. 1985. "Effect of Growth Characteristics on the Bending Strength of Wood Poles." M.S. Thesis. Dept. of Forest and Wood Sciences. Colorado State University. Fort Collins, CO.
28. de Freitas, A.R. 1973. "Dimensioning Wood Poles (Dimensionamento de Postes de Madeira)." Associacao Brasileira de Presevadores de Madeira. Preservacao de Madeiras 3-4(1). pp. 41-50. Sao Paulo. Brazil.
29. de Freitas, A.R. 1978. "Probabilistic Approach in the Design of Wood Structures in Brazil, Based on the Variability of 23 Species." Ph.D. Dissertation. Virginia Polytechnic Institute and State University. Blacksburg, VA.
30. Faherty, K.E. and Williamson, T.G. 1988. "Wood Engineering and construction Handbook." McGraw Hill Book Publishing Inc. New York, NY.
31. Fan, C. 1991. Ancient Chinese Timber Structure. Proceeding of the International Timber Engineering Conference. TRADA. London U.K. Vol. 3: 563-570.

32. Gojkovic, M. 1991. Bridges over the Danube, Between Belgrade and the Mouth of the Black Sea, Built in the Beginning of Our Era. Proceedings of the International Timber Engineering Conference. TRADA. London. U.K. Vol. 3: 557-562.
33. Goodman, J.R. and Bodig, J. 1970. "Orthotropic Elastic Properties of Wood." Journal of Structural Division. ASCE 96(ST11), pp. 2301-2319.
34. Goodman, J.R. and Bodig, J. 1971. "Orthotropic Strength of Wood in Compression." Wood Science 4(2), pp. 83-94.
35. Goodman, J.R., Vanderbilt, M.D., Criswell, M.E. and Bodig, J. 1981. "Probability-Based Design of Wood Transmission Structures." Vol. 1: Strength and Stiffness of Wood Utility Poles. Electric Power Research Institute-EPRI. EL-2040. Palo Alto, CA.
36. Goodman, J.R., Vanderbilt, M.D., Criswell, M.E. and Bodig, J. 1981. "Probability-Based Design of Wood Transmission Structures." Vol. 2: Analysis and Probability-Based Design of Wood Utility Structures. Electric Power Research Institute-EPRI. EL-2040. Palo Alto, CA.
37. GTSTRU DL User's Manual. 1985. Georgia Institute of Technology. Atlanta. Georgia.
38. Gunnerson R.A., Goodman J.R. and Bodig J. 1973. Plate Test for Determination of Elastic Parameters of Wood. Wood Science 5(4), pp. 241-248.
39. Gutkowski, R.M. 1981. "Structures - Fundamental Theory and Behavior." Van Nostrand Reinhold Co. New York. NY.
40. Harris J.M. 1989. "Spiral Grain and Wave Phenomena in Wood Formation". Springer-Verlag. Berlin.
41. Jayne, B.A. and Suddarth, S.K. 1966. "Matrix-Tensor Mathematics in Orthotropic Elasticity." Orientation effects in the Mechanical Behavior of Anisotropic Structural Materials. ASTM STP 405, pp. 39-58.
42. Jayne B.A. 1972. "Theory and Design of Wood and Fiber Composite Materials." Benjamin A. Jayne Editor. Syracuse University Press. Syracuse. NY.
43. Kauman, W.G. and Kloot, N.H. 1968. "Technological Appraisal of Little Known or Unused Timber Species." Division of Forest Products Commonwealth Scientific and Industrial Research Organization. Australia.

44. Koch, P. 1972. "Utilization of Southern Pine, Vol. 1: The Raw Material." U. S. Department of Agriculture. Forest Service. Agriculture Handbook No. 420.
45. Koch, P. 1985. "Utilization of Hardwoods Growing on Southern Pine Sites, Vol. 1: The Raw Material." U. S. Department of Agriculture. Forest Service. Agriculture Handbook No. 605.
46. Kollmann, F.F.P. and Cote Jr., W.A. 1968. "Principles of Wood Science and Technology." Vol 1. Springer Verlag. New York, NY.
47. Lowery D.P. and Erickson E.C.O. 1967. Effect of Spiral Grain on Pole Twist and Bending Strength. USDA. Forest Service Research Society Paper INT-35. Intermountain Forest and Range Experiment Station. Ogden, UT.
48. Milne-Thompson L.M. 1950. "Theoretical Hydrodynamics". The MacMillan Company. New York. NY.
49. Noack, D. 1971. "Evaluation of Properties of Tropical Timbers." Journal of the Institute of Wood Science. No. 29.
50. Panshin, A.J., deZeeuw, C., and Brown, H.P., 1968. "Textbook of Wood and Wood Technology." McGraw Hill Book Co. New York, NY.
51. Pearson, R.G. and Williams, E.J. 1958. "A Review of Methods for Sampling of Timber." Forest Products Journal. Sept. 1958, pp. 263-268.
52. Pellicane, P.J. 1980. "Ultimate Tensile Strength Analysis of Wood." Ph.D. Dissertation. Dept. of Forest and Wood Sciences. Colorado State University. Fort Collins, CO.
53. Pellicane, P.J. 1984. Application of the S_b Distribution to the Simulation of Correlated Lumber Properties Data. Wood Science and Technology. No. 18: 147-156.
54. Pellicane, P.J. 1985. Goodness-of-Fit Analysis for Lumber Data. Wood and Science Technology. No. 19: 117-129.
55. Pellicane, P.J., Bodig, J. and Goodman J.R. 1982. Simulation of the Tensile Strength Fracture Toughness Relationship. Wood Science. Vol. 14. No.4.

56. Phillips, G.E. 1980. "Grain Deviation Around Knots in Conifers." M.S. Thesis. Dept. of Forest and Wood Sciences. Colorado State University. Fort Collins. Colorado.
57. Phillips, G.E., Bodig, J. and Goodman, J.R. 1981. "Flow grain analogy." Wood Science, Vol. 14(2), pp. 55-64.
58. Phillips, G.E., Bodig, J., and Goodman J.R. 1985. "Wood Pole Properties." Vol. 1: Background and Southern Pine Data. Electric Power Research Institute-EPRI. EL-4109. Palo Alto, CA.
59. Przemieniecki, J.S. 1985. "Theory of Matrix Structural Analysis." Dover Publications, Inc. New York, NY.
60. Pugel, A.D. 1980. Evaluation of Selected Mechanical Properties of Conifers Knotty Wood. M.S. Thesis. Dept. of Forest and Wood Sciences. Colorado State University. Fort Collins. Co.
61. Stahl, D.C., Cramer S.M. and McDonald K.A. 1990. "Modeling the effect of Out-of-Plane Fiber Orientation in Lumber Specimens. Wood and Fiber Science 22(2), pp. 173-192.
62. Timoshenko, S. and Young D.H. 1962. "Elements of Strength of Materials." Van Nostrand Reinhold. New York, NY.
63. U.S. Forest Products Laboratory. 1974. "Wood Handbook: Wood as Engineering Material." U.S. Department of Agriculture. Agriculture Handbook No 72.
64. Wang, Y. 1987. "Stress Grading of Utility Poles." Ph.D. Dissertation. Colorado State University. Fort Collins, CO.
65. Wangaard, F.F. 1950. "Mechanical Properties of Wood." John Willey and Sons, Inc. New York, NY.
66. Wangaard, F.F. 1981. "Wood: Its Structure and Properties." Vol 1. Clark C. Heritage Memorial Series. University Park, Pa.
67. Weaver, W. and Gere J. 1965. "Analysis of Framed Structures." 2nd ed. Van Nostrand Reinhold Co. New York, NY.
68. Weaver, W. and Johnson, P.R. 1984. "Finite Elements for Structural Analysis". Prentice Hall. Englewood Cliff. NJ.

69. Weibull, W. 1939. A Statistical Theory of the Strength of Materials. The Royal Swedish Institute for Engineering Research. No. 151.
70. Wood, L.W. and Markwardt, L.J. 1965. "Derivation of Fiber Stress Values of Wood Poles." U.S.D.A. Forest Service. Forest Products Laboratory Research Paper No. 39. Madison, WIS.
71. Zahn, J.J. 1977. Reliability-Based Design Procedures for Wood Structures. Forest Products Journal. Vol. 27 (3): 21-28.
72. Zandbergs, J.G. 1985. "Finite Element Fracture Prediction for Orthotropic, Inhomogeneous Materials." M.S. Thesis. Colorado State University. Fort Collins, CO
73. Zobel, B. 1988. Eucalyptus in the Forest Industry. Tappi Journal. Vol 74(12), pp 42-46.

APPENDICES

APPENDIX A

TRANSFORMATION MATRIX FOR 3-D ELEMENTS

The rigidity specifications used to specify the material stress-strain relationship for orthotropic materials is:

$$\{\sigma\} = [D] * \{\epsilon\}$$

where: σ is the vector containing the stresses;

D is the rigidity matrix, and;

ϵ is the vector containing the strains.

For the 3-D case, the rigidity matrix is a 6 x 6 matrix

$$\begin{Bmatrix} \sigma_x \\ \sigma_y \\ \sigma_z \\ \tau_{xy} \\ \tau_{xz} \\ \tau_{yz} \end{Bmatrix} = [D_{6 \times 6}] \begin{Bmatrix} \epsilon_x \\ \epsilon_y \\ \epsilon_z \\ \gamma_{xy} \\ \gamma_{xz} \\ \gamma_{yz} \end{Bmatrix}$$

if the principal material axes are with respect to a coordinate system other than the global reference system, the orthotropic matrix must be transformed to the global system.

Let xyz and XYZ be two orthogonal systems as shown in Figure B-1, the rotational (direction cosines) matrix is defined as (Criswell 1988):

$$[T] = \begin{bmatrix} l_1 & m_1 & n_1 \\ l_2 & m_2 & n_2 \\ l_3 & m_3 & n_3 \end{bmatrix} = \begin{bmatrix} c\alpha*c\beta & s\beta & s\alpha*c\beta \\ -c\alpha*s\beta*c\gamma - s\alpha*s\gamma & c\beta*c\gamma & -s\alpha*s\beta*c\gamma + c\alpha*s\gamma \\ c\alpha*s\beta*s\gamma - s\alpha*c\gamma & -c\beta*s\gamma & s\alpha*s\beta*s\gamma + c\alpha*c\gamma \end{bmatrix}$$

where s and c are the sine and cosine of the angles α , β and γ , (Figure B-1).

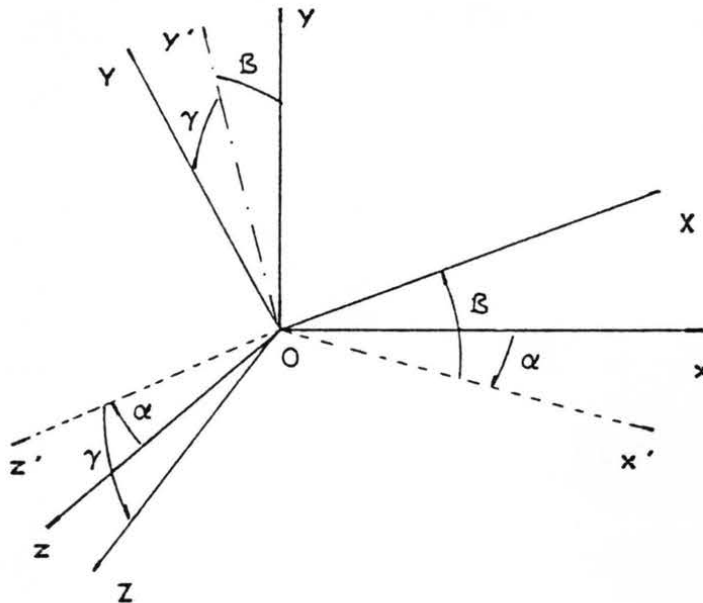


Figure B-1. Coordinate systems for the material axes xyz and global reference system used in the finite element analysis XYZ .

For tensor transformation of a second order tensor, the transformation matrices form are given by (Cook et al. 1989):

$$\{\sigma'\} = [T] * \{\sigma\} * [T]^T$$

$$\{\epsilon'\} = [T] * \{\epsilon\} * [T]^T$$

Using symmetry, each of the 3×3 matrices σ' , σ , and ϵ' ,

ϵ can be represented by a 6x1 matrix. The transformation matrices T_o , and T_e can be arranged in the final form of 6x6 matrices, as:

$$[T_o] * \{\sigma\}$$

$$[T_e] * \{\epsilon\}$$

where:

$$[T_o] = \begin{bmatrix} l_1^2 & m_1^2 & n_1^2 & 2(l_1m_1) & 2(l_1n_1) & 2(m_1n_1) \\ l_2^2 & m_2^2 & n_2^2 & 2(l_2m_2) & 2(l_2n_2) & 2(m_2n_2) \\ l_3^2 & m_3^2 & n_3^2 & 2(l_3m_3) & 2(l_3n_3) & 2(m_3n_3) \\ l_1l_2 & m_1m_2 & n_1n_2 & (l_1m_2+l_2m_1) & (l_1n_2+l_2n_1) & (m_1n_2+m_2n_1) \\ l_1l_3 & m_1m_3 & n_1n_3 & (l_1m_3+l_3m_1) & (l_1n_3+l_3n_1) & (m_1n_3+m_3n_1) \\ l_2l_3 & m_2m_3 & n_2n_3 & (l_2m_3+l_3m_2) & (l_2n_3+l_3n_2) & (m_2n_3+m_3n_2) \end{bmatrix}$$

and

$$[T_o] = \begin{bmatrix} T_{11} & T_{12} \\ T_{21} & T_{22} \end{bmatrix}, \quad [T_e] = \begin{bmatrix} T_{11} & 0.5 * T_{12} \\ 2.0 * T_{21} & T_{22} \end{bmatrix}$$

For either of the systems, the constitutive law is written as:

$$\{\sigma\} = [D] * \{\epsilon\}$$

$$\{\sigma'\} = [D'] * \{\epsilon'\}$$

The stiffness matrix D can be expressed in terms of matrix D' , using the virtual work for any virtual displacement

in the system. The resulting increase in the strain energy U_0 must be the same in regardless of the coordinate system adopted. therefore:

$$\delta * U_0 = \{\delta \epsilon\}^T * [\sigma] = \{\delta \epsilon'\}^T * [\sigma']$$

and using the equations above,

$$\{\delta \epsilon\}^T * \{\sigma\} = \{\delta \epsilon\}^T * [T_\epsilon]^T * [D'] * \{\epsilon'\}$$

$$\{\sigma\} = [T_\epsilon]^T * [D'] * [T_\epsilon] * \{\epsilon\}$$

$$[D] * \{\epsilon\} = [T_\epsilon]^T * [D'] * [T_\epsilon] * \{\epsilon\}$$

therefore:

$$[D] = [T_\epsilon]^T * [D'] * [T_\epsilon]$$

The stiffness matrix transformation presented earlier for orthotropic material is then defined by:

$$[D] = [T_\epsilon]^T * [D_{\text{prin}}] * [T_\epsilon]$$

where: D is the orthotropic rigidity matrix to be input in the finite element program;

D_{prin} is the orthotropic rigidity matrix with respect to the principal axes, and;

T_ϵ is the strain transformation tensor.


```

          BETA=((I-1)*ALFA)*TR
          NL(IA,1)=ERD*SIN(BETA)
700      CONTINUE
600      CONTINUE
      ELSE
          ALFA=11.25
          DO 800 K=1,3
              DO 900 I=1,32
                  IA=I+(K-1)*48
                  ERD=(RD/3.)*(4-K)
                  BETA=((I-1)*ALFA)*TR
                  NL(IA,1)=ERD*SIN(BETA)
900      CONTINUE
800      CONTINUE
      ENDIF
500 CONTINUE
      NL(145,1)=0.0
C
CCCCCCCCCCCCCCCCCCCCCCCCCCCCCCCCCCCCCCCCCCCCCCCCCCCCCCCCCCCC
C
C          EVALUATION OF THE NODAL HORIZONTAL LOAD DUE TO
C          APPLIED MOMENT
C
CCCCCCCCCCCCCCCCCCCCCCCCCCCCCCCCCCCCCCCCCCCCCCCCCCCCCCCCCCCC
C
C          CALCULATE THE LEVER ARM FOR THE FAR SECTION OF THE
C          GIVEN SEGMENT (IN INCHES)
C
          XLA=(0.9*LH-5.5-XL)*12.
C
C          CALCULATE THE MOMENT OF INERTIA, (IN**4), FOR THE
C          CROSS SECTION
C
          XIN=(PI*RD**4)/4.
C
C          CALCULATE THE ACTUAL MOMENT DUE TO A LOAD OF 1000 LB
C          APPLIED AT THE TIP OF THE POLE, IN (LB*IN).
C
          XMOM=1000.*XLA
C
C          EVALUATE THE STRESSES AT THE JOINT LOCATION
C          (SECOND COLUMN OF MATRIX NL), (IN PSI).
C
          DO 1000 I=1,145
              NL(I,2)=(XMOM/XIN)*NL(I,1)
C
1000 CONTINUE
C
C          PRINT THE RESULTS
C
          WRITE(6,2) HED
1  FORMAT(10A8)
2  FORMAT('1',10A8)
          WRITE(6,50) LH,XL*12.,XL*12.+18.,2.*RD

```

```

50 FORMAT(' ',//,25X,'HORIZONTAL JOINT STRESS FOR THE
  *GIVEN SECTION, IN
  * POUNDS',//,36X,'POLE LENGTH (FEET):      ',F15.1,/
  *,36X,'NEAR SIDE LOCATION (IN): ',F15.3,/
  *,36X,'FAR SIDE LOCATION (IN): ',F15.3,/
  *,36X,'SEGMENT DIAMETER (IN): ',F15.3)
  WRITE(6,51)
51 FORMAT(/,11X,'JOINT      LOAD      JOINT      LOAD
  *      JOINT      LOAD      JOINT      LOAD',//)
  DO 1100 I=0,35
    WRITE(6,52) (4*I+J+1164,NL(4*I+J,2),J=1,4)
52 FORMAT(11X,4(I4,F10.0,5X),/)
1100 CONTINUE
    I=145
    WRITE (6,52) I+1164,NL(I,2)
CCCCCCCCCCCCCCCCCCCCCCCCCCCCCCCCCCCCCCCCCCCCCCCCCCCCCCCC
C      EVALUATION OF THE VERTICAL STRESSES DUE TO
C      SHEAR FORCES
CCCCCCCCCCCCCCCCCCCCCCCCCCCCCCCCCCCCCCCCCCCCCCCCCCCCCCCC
C
C      EVALUATE THE AREA MOMENT "Q" AT THE ORDINATE OF
C      ELEMENT NODES
C
    DO 2000 IS=1,145
      A=SQRT(RD**2-(NL(IS,1))**2)
      B=A*2.
      NL(IS,3)=A**3/1.5
C
C      CALCULATE THE SHEAR STRESSES AT EACH NODE
C
      NL(IS,4)=(1000.*NL(IS,3))/(B*XIN)
C
2000 CONTINUE
C
C      OUTPUT OF CALCULATIONS
C
    WRITE(6,57)
57  FORMAT('1',//,25X,'VERTICAL STRESSES AT ELEMENTS DUE
  *TO SHEAR, IN "PSI"',//)
    WRITE(6,51)
    DO 1010 IT=0,35
C
      WRITE(6,59) (4*IT+1164+J,NL(4*IT+J,4),J=1,4)
59  FORMAT(12X,4(I4,3X,F6.1,6X),/)
1010 CONTINUE
    IT=145
    WRITE (6,59) IT+1164,NL(I,4)
C
    STOP
    END

```

APPENDIX C.

EXAMPLE OF INPUT FILE FOR THE GTSTRU DL PROGRAM

```

STRU DL 'DFPOLE' 'DOUGLAS-FIR POLE CIRCULAR SECTION-CONSTANT TAPER'
$ SECTION WITH 16 DIVISIONS, 20 NODE ELEMENTS.
$ DOUGLAS FIR POLE # 162 "SECTION 2"
UNITS LBS INCHES DEGREE
TYPE TRIDIMENSIONAL
JOINT COORDINATES
JOINT 'OG' COORDINATES X 59.000 Y 0.00 Z 0.00
NODE COORDINATES
GENERATE 32 JOINTS CYL ID 1,1 R 6.133 0. TH -90.0 11.25 LX 0. 0. -
      OFFSET 'OG'
REPEAT 2 TIMES ID 48 R INC -2.044
REPEAT 6 TIMES ID 194 LX INC 3.
GENERATE 16 JOINTS CYL ID 33,1 R 5.111 0. TH -90.0 22.5 LX 0.00 0. -
      OFFSET 'OG'
REPEAT 2 TIMES ID 48 R INC -2.044
REPEAT 6 TIMES ID 194 LX INC 3.
GENERATE 16 JOINTS CYL ID 146,1 R 6.133 0. TH -90.0 22.5 LX 1.5 0. -
      OFFSET 'OG'
REPEAT 2 TIMES ID 16 R INC -2.044
REPEAT 5 TIMES ID 194 LX INC 3.
GENERATE 7 NODES ID 145,194 X 0. 3. Y 0. 0. Z 0. 0. -
      OFFSET 'OG'
GENERATE 6 NODES ID 194,194 X 1.5 3.0 Y 0. 0. Z 0. 0. -
      OFFSET 'OG'
STATUS SUPPORT 1 TO 145
INACTIVE JOINT 'OG'
JOINT RELEASES
$ SPRINGS ON Y AND Z DIRECTIONS WITH SPRG-CTE = (ET+ER)/2
1 TO 145 KFZ 120000.
1 TO 145 KFY 120000.
ELEMENT INCIDENCES
GENERATE 15 ELEMENTS ID 'F1',1 F 1 I 2 T 49 I 2 T 51 I 2 T 3 I 2 T 33 -
I 1 T 50 I 2 T 34 I 1 T 2 I 2 T 146 I 1 T 162 I 1 T 163 I 1 T 147 I 1 -
T 195 I 2 T 243 I 2 T 245 I 2 T 197 I 2 T 227 I 1 T 244 I 2 T 228 -
I 1 T 196 I 2
REPEAT 1 ID 16 F 48 T 16 T 16 T 16 -
T 16 T 48 T 48
REPEAT 5 TIMES ID 48 F 194
GENERATE 2 ELEMENTS ID 'F16',16 F 31 I 48 T 79 I 48 T 49 I 48 T 1 -
I 48 T 48 I 48 T 80 I 48 T 33 I 48 T 32 I 48 T 161 I 16 T 177 -
I 16 T 162 I 16 T 146 I 16 T 225 I 48 T 273 I 48 T 243 I 48 -
T 195 I 48 T 242 I 48 T 274 I 48 T 227 I 48 T 226 I 48
REPEAT 5 TIMES ID 48 F 194
GENERATE 15 ELEMENTS ID 'F33',1 F 97 I 2 T 145 I 0 T 99 I 2 T 291 -
I 2 T 339 I 0 T 293 I 2 T 129 I 1 T 130 I 1 T 98 I 2 T 178 -
I 1 T 194 I 0 T 179 I 1 T 323 I 1 T 324 I 1 T 292 I 2
REPEAT 5 TIMES ID 48 F 194

```

GENERATE 6 ELEMENTS ID 'F48',48 F 127 I 194 T 145 I 194 T 97 I 194 -
T 321 I 194 T 339 I 194 T 291 I 194 T 144 I 194 T 129 I 194 -
T 128 I 194 T 193 I 194 T 194 I 194 T 178 I 194 T 338 I 194 -
T 323 I 194 T 322 I 194

ELEMENT PROPERTIES

'F1' TO 'F32' 'F49' TO 'F80' 'F97' TO 'F128' 'F145' TO 'F176' -
'F193' TO 'F224' 'F241' TO 'F272' TYPE 'IPQS'
'F33' TO 'F48' 'F81' TO 'F96' 'F129' TO 'F144' 'F177' TO 'F192' -
'F225' TO 'F240' 'F273' TO 'F288' TYPE 'WEDGE15'

LOADING 1 'BENDING AND SHEAR AT FAR SIDE'

PLOT DEVICE PRINTER

PRINT DATA ALL JOINTS AND ELEMENTS

STIFFNESS ANALYSIS

CALCULATE AVERAGE STRESSES ALL

LIST DISPLACEMENTS

CALCULATE AVERAGE PRINCIPAL STRESSES

FINISH

APPENDIX D.

EXAMPLES RECORDS ON POLE DATA

- D-1. Example of pole profile data file.
- D-2. Example of pole spiral grain data file.
- D-3. Example of pole knot map data file.
- D-4. Example of pole data form and deflection curves from pole test.
- D-5. Example of load-deflection curves from bending test on small-clear specimens.

APPENDIX D-1.

EXAMPLE OF POLE PROFILE DATA FILE

DOUGLAS-FIR POLE # 188
 LENGTH = 60'

Location in (*)	Circumfer. in	Diameter in	Radius in	Decrem. in/in
-96	44.76	14.2	7.1	
-60	44.28	14.1	7.0	-0.0042
-24	42.48	13.5	6.8	-0.0159
0	41.16	13.1	6.6	-0.0117
12	41.04	13.1	6.5	-0.0011
48	40.32	12.8	6.4	-0.0064
84	39.24	12.5	6.2	-0.0095
120	38.64	12.3	6.1	-0.0053
156	38.28	12.2	6.1	-0.0032
192	37.20	11.8	5.9	-0.0095
228	36.48	11.6	5.8	-0.0064
264	36.00	11.5	5.7	-0.0042
300	34.80	11.1	5.5	-0.0106
336	34.80	11.1	5.5	0.0000
372	34.44	11.0	5.5	-0.0032
408	33.48	10.7	5.3	-0.0085
444	32.40	10.3	5.2	-0.0095
480	31.80	10.1	5.1	-0.0053
516	30.84	9.8	4.9	-0.0085
552	29.88	9.5	4.8	-0.0085
588	28.56	9.1	4.5	-0.0117
600	28.20	9.0	4.5	-0.0032
624	27.36	8.7	4.4	-0.0074

(*) Start (zero at Grounline

APPENDIX D-2.

EXAMPLE OF SPIRAL GRAIN DATA FILE

DOUGLAS -FIR ** POLE # 188 **

Interval	Deviation*,in (to left)	ngle of dev- iation,dg
0 - 3	1.9	3.0
3 - 6	1.9	3.0
6 - 9	2.1	3.3
9 - 12	2.4	3.8
12 - 15	2.7	4.3
15 - 18	3.5	5.6
18 - 21	4.5	7.2
21 - 24	3.8	6.0
24 - 27	3.6	5.7
27 - 30	3.5	5.6
30 - 33	3.5	5.6
33 - 36	3.1	4.9
36 - 39	3.2	5.1
39 - 42	3.1	4.9
42 - 45	3.5	5.6
45 - 48	3.9	6.2
48 - 51	3.7	5.9
51 - 54	3.4	5.4
54 - 57	2.8	4.5
57 - 60	2.8	4.5

(*) See Figure 4.3

APPENDIX D-3.

EXAMPLE OF POLE KNOT MAP* DATA FILE

SPECIES: WESTERN RED CEDAR

POLE # 85

LENGTH: 50'

Abscissa in (**)	Sec. Dia in	LTL in	LTR in	LCL in	LCR in	Knot Dia in.	Theta deg.
0	15.5			7.5		1.7	215
9	15.3		6.5			0.9	139
14	15.1			1.5		1.6	259
18	15.0	3.5				0.5	63
22	14.8		9.0			9.0	159
27	14.7			2.5		1.0	251
32	14.7	9.0				0.5	20
37	14.6		8.5			0.7	157
41	14.6				0.5	1.2	274
47	14.5	5.0				0.5	50
51	14.4		7.5			0.9	150
56	14.4				3.0	1.1	294
66	14.2			4.5		1.3	234
76	14.1		8.0			1.3	155
79	14.1				6.5	1.1	323
84	14.0		2.5			0.6	110
88	14.0			5.0		1.4	229
93	13.9	8.5				0.6	20
97	13.9		9.5			0.9	169
102	13.8				1.0	0.9	278
107	13.8	0.5				0.5	86
111	13.7			4.5		1.4	232
114	13.7				3.0	1.1	295
121	13.6		8.5			1.4	161
125	13.6				5.5	1.2	316
130	13.5		4.0			0.5	124
136	13.4			3.5		1.9	240
143	13.3			9.0		0.9	193
145	13.3		6.5			1.0	146
149	13.2				0.2	1.6	272
155	13.1	3.0				0.5	64

163	12.9		8.0		1.9	198
165	12.9			1.0	0.8	279
167	12.9			6.0	1.0	323
170	12.8		5.5		0.8	139
174	12.7			1.5	1.1	257
178	12.7	8.0			0.8	18
182	12.6		7.0		1.0	154
186	12.5			5.0	1.2	316
192	12.5		2.0		0.5	108
196	12.4			6.5	0.9	210
198	12.4		6.5		1.3	150
200	12.3			3.0	0.5	242
206	12.3		1.5		0.8	104
207	12.2			3.0	0.6	298
210	12.2			1.0	1.2	279
213	12.1	2.0			0.5	71
218	12.1			5.0	1.4	223
222	12.0		4.5		1.1	133
228	11.9	9.0			0.9	4
232	11.9			6.0	1.5	212
236	11.8			3.0	0.9	299
237	11.8			5.0	1.1	319
237	11.8		4.5		0.8	134
240	11.8		1.0		1.0	100
241	11.8			7.5	1.1	197
244	11.7			4.0	1.6	231
248	11.7			5.0	0.8	319
257	11.5			2.0	1.5	250
259	11.5	1.5			0.5	75
261	11.5	6.0			0.9	30
264	11.4			9.0	1.9	180
272	11.3		6.0		1.2	151
278	11.2			6.5	1.0	337
281	11.1			5.0	1.1	219
282	11.1		7.0		1.4	162
285	11.1			3.5	1.2	306
288	11.0	1.5			0.5	74
295	10.9			2.0	1.6	291
295	10.9	7.0			0.5	16
302	10.7			5.5	1.5	211
307	10.6			5.5	1.1	329
312	10.5		2.0		1.2	112
314	10.5			1.0	1.4	281
314	10.5			7.0	0.8	194
316	10.5			2.5	1.6	297
323	10.3			8.0	1.7	181
327	10.2		0.2		0.9	92
329	10.2	2.5			0.9	62
334	10.1			5.0	1.2	213
339	10.0			1.0	1.0	281
340	10.0			5.5	1.2	333
345	9.9			5.5	1.1	334

346	9.8			8.0		1.4	177
348	9.8				3.0	0.7	305
352	9.8			3.0		1.5	235
356	9.7				1.5	0.8	288
361	9.6		5.0			0.7	150
362	9.6		0.5			0.9	96
364	9.6			2.5		1.8	240
368	9.5	6.0				0.9	18
371	9.5			6.5		1.4	191
375	9.4		6.0			1.1	163
382	9.3	5.0				0.5	28
386	9.2		2.0			0.6	115
388	9.2		5.0			1.4	152
392	9.1				0.5	1.2	276
394	9.1	4.5				0.9	33
398	9.0			1.5		0.9	251
398	9.0		3.0			0.6	128
400	9.0			4.5		1.2	213
402	9.0				5.5	0.6	340
412	8.8				1.0	0.8	283
414	8.8			2.0		0.7	244
415	8.8				5.0	0.7	335
417	8.7	6.0				0.9	11
421	8.7		2.0			0.9	116
421	8.7		5.0			0.5	156
421	8.7			5.0		1.1	204
426	8.6				3.0	1.1	310
428	8.6		3.0			0.5	130
429	8.5	0.2				0.6	87
433	8.5			6.0		0.8	189
434	8.5			2.5		1.3	236
436	8.5				0.5	1.0	277
439	8.4	3.0				0.5	49
439	8.4		1.0			0.9	104
439	8.4		3.5			0.7	138
444	8.3			1.0		0.5	256
447	8.3	5.5				0.6	14
451	8.2		4.5			0.9	153
451	8.2			2.0		1.1	242
452	8.2			5.0		0.8	200
464	8.1			2.0		1.2	242
466	8.1				5.0	0.7	341
466	8.1	2.5				0.5	55
467	8.1	3.5				0.8	41
472	8.1		4.0			1.1	147

* See Figure 4.4

** Start (zero) at Groundline

APPENDIX D-4.

Example of Pole Data Form and Observed
Deflection Curves from Pole Test.

POLE DATA FORM

Pole ID 292
 Supplier 56
 Species 20
 Treatment 7
 Class 5

Date 5-10-91
 Recorder NS

Total pole length (ft, to nearest inch) 50.0
 Circumference @ groundline (ft, nearest 0.01 ft) 3.10
 Circumference @ 6' from butt (ft, nearest 0.01 ft) 3.18
 Circumference @ original tip (ft, nearest 0.01 ft) 1.84
 Circumference @ cut tip (ft, nearest 0.01 ft) —
 Length removed from cut pole (ft, to nearest inch) —

Measurements to be taken in the lower half of the lever arm:

Growth rate Rings per inch for outer one inch 7
 Rings per inch for next inch 5
 Rings per inch for next inch 4

Maximum knot diameter (0.1") 1.9
 Maximum sum of knot diameters in a 1' section (0.1") 5.1

Maximum spiral grain (0.1 in of deviation over a 5' length) 1.7

Description of any pole damage prior to test:

Distance from groundline to breakpoint (ft, nearest in) 18.5
 Longitudinal deflection of loadpoint (in, to nearest in) 22

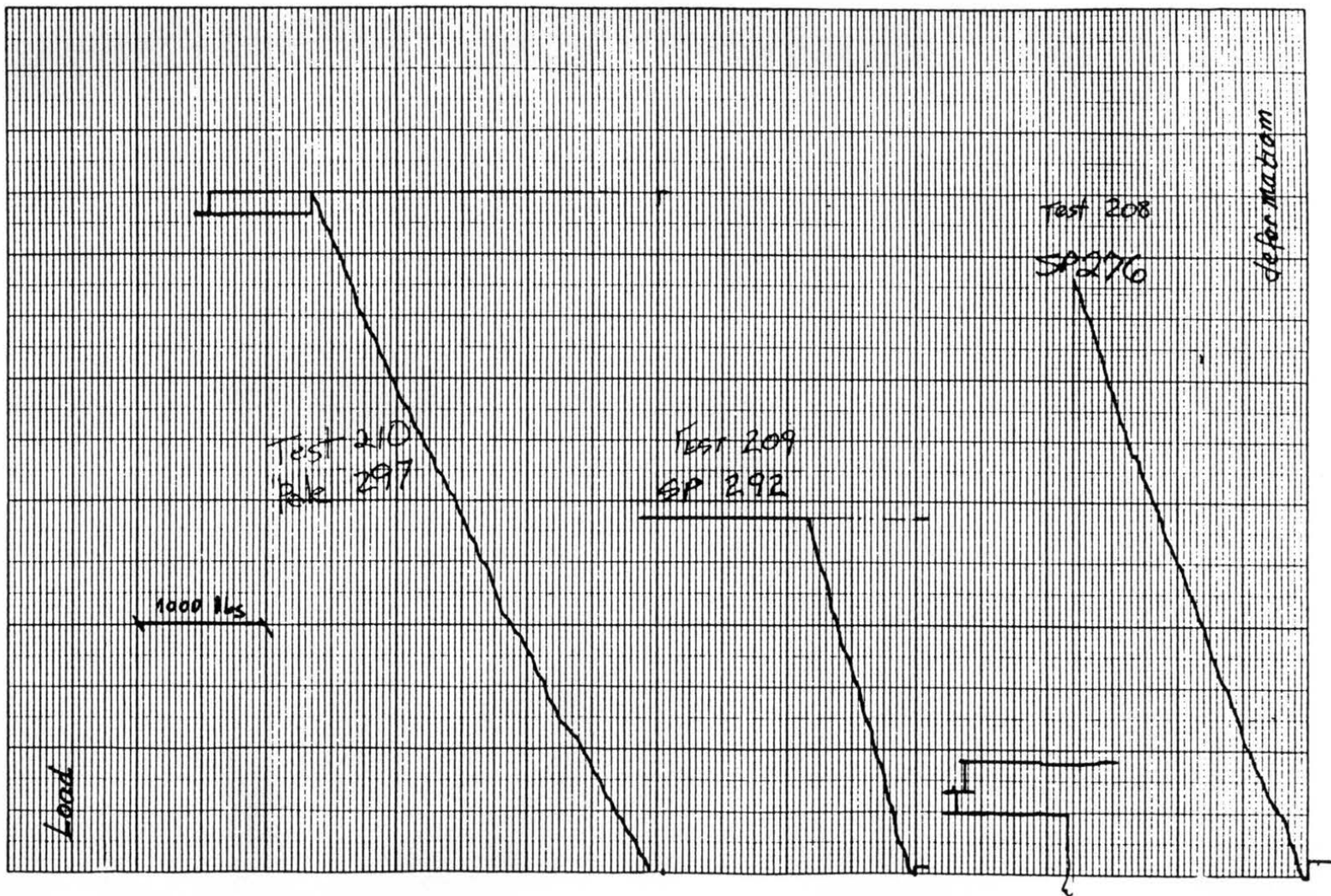
Description of failure:

Tension Compression Butt shear
 Multiple failure Failure @ maximum knot NO
 Failure @ maximum sum of knot diameters NO Other

Comments:

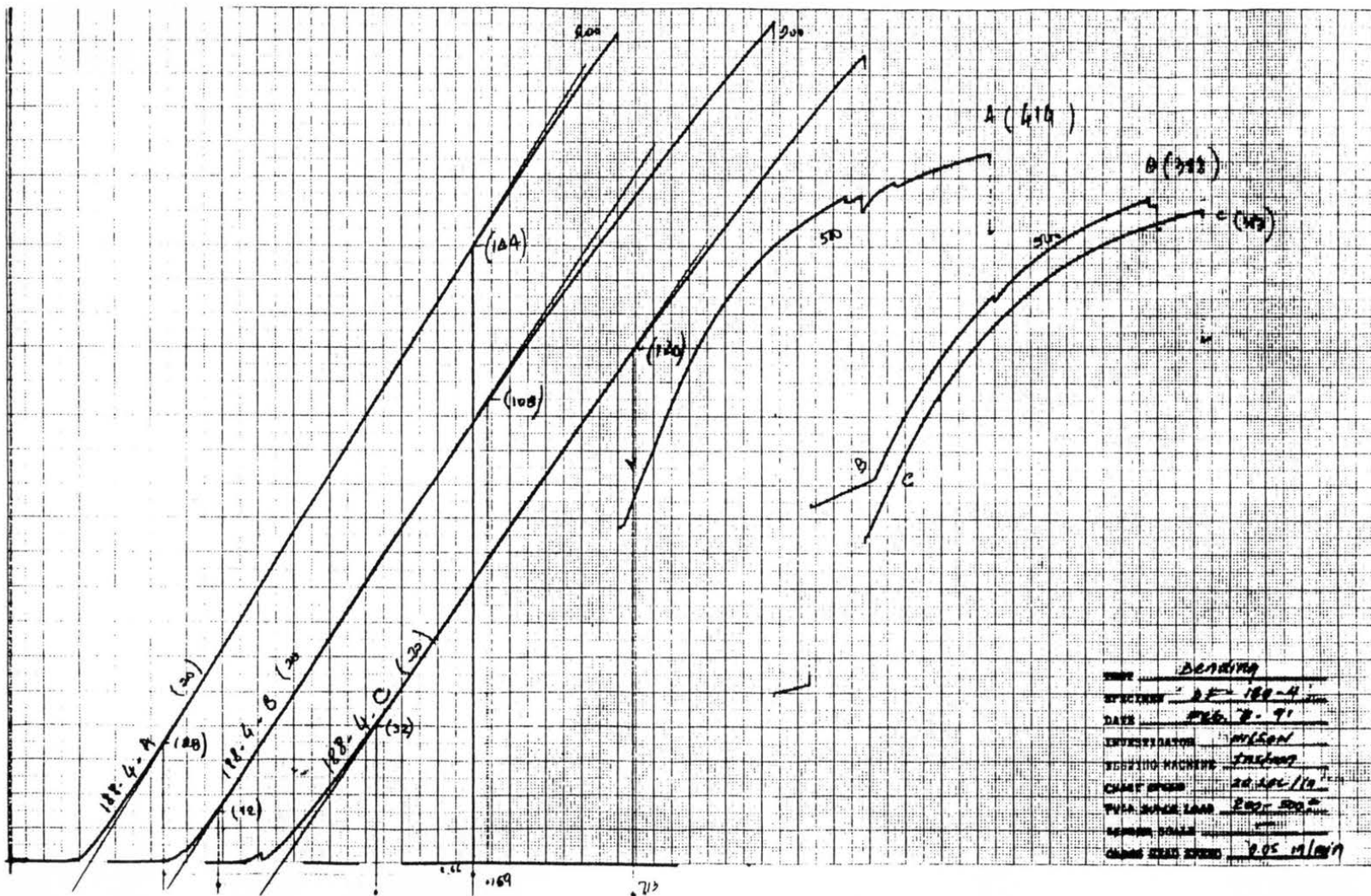
Failed at knot whorl

Max load - graph - 2150°
 cut pt - 2072±
 (load cell)



APPENDIX D-5.

Example of Pole Load-Deflection Curves from
Bending Test on Small-Clear Specimens.




```

2  FORMAT('1',10A8)
C
C  EVALUATE THE TRUE LONGITUDINAL MODULUS OF ELASTICITY
C    *** CORRECTION FOR SHEAR EFFECT ONLY ***
C
    EL=MOE*KSH
C
C  EVALUATE THE RADIAL AND TANGENTIAL MOD. OF ELASTICITY
C
    ER=393.17*EL**0.40598
    ET=5.2140*EL**0.67490
C
C  EVALUATE THE MODULI OF RIGIDITY
C
    GLR=77924+0.019865*EL
    GTL=74005+0.018047*EL
    GTR=2.7424*EL**0.57879
    EL=EL*KE
C
C  EVALUATION OF THE COMPLIANCE MATRIX
C
    DO 100 I=1,6
      DO 100 J=1,6
        CPC(I,J)=0.0
        STF(I,J)=0.0
100 CONTINUE
    CPC(1,1)=1.0/EL
    CPC(1,2)=- (NLR/EL)
    CPC(2,1)=CPC(1,2)
    CPC(1,3)=- (NLT/EL)
    CPC(3,1)=CPC(1,3)
    CPC(2,2)=1.0/ER
    CPC(2,3)=- ( (NTR/ET) + (NRT/ER) ) / 2.0
    CPC(3,2)=CPC(2,3)
    CPC(3,3)=1.0/ET
    CPC(4,4)=1.0/GLR
    CPC(5,5)=1.0/GTL
    CPC(6,6)=1.0/GTR
C
C  INVERSION OF THE COMPLIANCE MATRIX TO OBTAIN THE
C  STIFFNESS MATRIX, USING THE GAUSS METHOD.
C
    DO 250 I=1,3
      DO 250 J=1,3
        INV(I,J)=CPC(I,J)
250 CONTINUE
    DO 200 I=1,3
      DO 200 J=4,6
        INV(I,J)=0.0
200 CONTINUE
    INV(1,4)=1.0
    INV(2,5)=1.0
    INV(3,6)=1.0
C

```

```

C      GET THE UPPER TRIANGULAR MATRIX
C
      DO 300 K1=1,2
        DO 400 I1=K1+1,3
          F=INV(I1,K1)/INV(K1,K1)
          DO 500 J1=K1,6
            INV(I1,J1)=INV(I1,J1)-F*INV(K1,J1)
500      CONTINUE
400      CONTINUE
300      CONTINUE

C
C      GET THE IDENTITY MATRIX
C
      DO 600 K2=2,1,-1
        DO 700 I2=K2,1,-1
          TMP=INV(I2,K2+1)/INV(K2+1,K2+1)
          DO 800 J2=K2+1,6
            INV(I2,J2)=INV(I2,J2)-INV(K2+1,J2)*TMP
800      CONTINUE
700      CONTINUE
600      CONTINUE
      DO 850 I=1,3
        DO 950 J=4,6
          INV(I,J)=INV(I,J)/INV(I,I)
950      CONTINUE
850      CONTINUE

C
C      ASSEMBLING THE STIFFNESS MATRIX (ON THE ORIGINAL
C      REFERENCE AXES)
C
      DO 900 I=1,3
        DO 1000 J=1,3
          STF(I,J)=INV(I,J+3)
1000     CONTINUE
900     CONTINUE
      STF(4,4)=GLR
      STF(5,5)=GTL
      STF(6,6)=GTR

C
C
C      PRINT OUT THE ORIGINAL STIFFNESS MATRIX ** STF **
C
      WRITE(6,3) LH
      3  FORMAT(' ',//,21X,'POLE LENGTH = ',F10.2,' FEET')
      WRITE(6,51) MOE
      51 FORMAT(' ',///,21X,'LONGITUDINAL MODULUS OF ELASTICITY
* GIVEN= ',F10.0,' PSI')
      WRITE(6,151) EL
      151 FORMAT(21X,'TRUE MODULUS OF ELASTICITY EL=
* ',F10.0,' PSI')
      WRITE(6,152) ER
      152 FORMAT(21X,'RADIAL MODULUS OF ELASTICITY ER=
* ',F10.0,' PSI')
      WRITE(6,153) ET

```

```

153 FORMAT(21X,'TANGENTIAL MODULUS OF ELASTICITY ET=
* ',F10.0,' PSI')
WRITE(6,154) GLR
154 FORMAT(21X,'MODULUS OF RIGIDITY GLR= ',17X,F10.0,'
* PSI')
WRITE(6,155) GTL
155 FORMAT(21X,'MODULUS OF RIGIDITY GTL= ',17X,F10.0,'
* PSI')
WRITE(6,156) GTR
156 FORMAT(21X,'MODULUS OF RIGIDITY GTR= ',17X,F10.0,'
*PSI',/)
WRITE(6,52) XL+1.5,XL
52 FORMAT(21X,'SEGMENT LOCATION',/,26X,'FAR SIDE SECTION:
*',F5.2,' FEET',/26X,'NEAR SIDE SECTION: ',F5.2,'
*FEET AGL')
WRITE(6,53)
53 FORMAT(21X,'ELEMENT POSITION ACROSS THE CROSS
*SECTION')
IF(NCOND.EQ.1) THEN
WRITE(6,54)
54 FORMAT(26X,'POSITION: OUTERMOST THIRD',/)
ELSEIF(NCOND.EQ.2) THEN
WRITE(6,55)
55 FORMAT(26X,'POSITION: INTERMEDIATE THIRD',/)
ELSE
WRITE(6,56)
56 FORMAT(26X,'POSITION: INNERMOST THIRD',/)
ENDIF
WRITE(6,57)
57 FORMAT(/,21X,'STIFFNESS MATRIX FOR THE SECTION GIVEN
* ABOVE',///)
DO 1100 I=1,6
WRITE(6,58) (STF(I,J),J=1,6)
58 FORMAT(21X,6(F10.1,3X),/)
1100 CONTINUE
C
C EVALUATION OF THE ORIGINAL MATRIX WHEN SPIRAL GRAIN
C PRESENTED
C INDICATE THE FIBER DEVIATION ANGLE OR 0.0 IF NONE
C
C THIS PART EVALUATES THE STIFFNESS MATRICES FOR THE
C ELEMENTS (20 OR 15 NODES) WHICH ARE ROTATED IN THE
C CROSS SECTION ABOUT THE X-AXIS . THE LOCAL
C COORDINATE SYSTEM IS ROTATED OF AN ANGLE "GAMA" IN
C RELATION TO THE GLOBAL COORDINATE SYSTEM.
C IT ALSO INCLUDES THE ROTATION OF THE RADIAL AXIS TO
C ACCOUNT FOR THE SPIRAL GRAIN EFFECT.
C **** TYPE OF LOAD == NODAL == ****
C
DO 1200 NI=1,3
DO 1300 NJ=1,3
FIBER(NI,NJ)=0.0
CROSS(NI,NJ)=0.0
1300 CONTINUE

```

```

1200    CONTINUE
C
C
      RT=(PI/180.0)
      FIBER(1,1)=COS(DELTA*RT)
      FIBER(2,2)=1.0
      FIBER(3,3)=FIBER(1,1)
      FIBER(1,3)=SIN(DELTA*RT)
      FIBER(3,1)=-FIBER(1,3)
C
C
      FOR EACH ELEMENT IN THE CROSS SECTION, EVALUATE:
      THE ANGLE "FI" BETWEEN THE VERTICAL (LINE)
      AXIS "Y" AND THE CENTER OF THE ELEMENT.
      *** FI STARTS AT 90 DEG FOR NODAL LOAD ***
C
C
      DO 1400 NG=1,16
      FI=438.75-((NG-1)*22.50)
      IF(FI.GE.360.) FI=FI-360
C
C
      EVALUATE THE ELEMENTS OF CROSS MATRIX
C
      CROSS(1,1)=1.0
      CROSS(2,2)=COS(FI*RT)
      CROSS(3,3)=CROSS(2,2)
      CROSS(2,3)=SIN(FI*RT)
      CROSS(3,2)=-CROSS(2,3)
C
C
      EVALUATION OF THE MATRIX OF TRANSFORMATION
      *** TF = CROSS*FIBER ***
C
      DO 1500 NJ=1,3
      DO 1600 NK=1,3
      TF(NJ,NK)=0.0
      DO 1700 NL=1,3
      TF(NJ,NK)=TF(NJ,NK)+CROSS(NJ,NL)
      *FIBER(NL,NK)
      *
1700      CONTINUE
1600      CONTINUE
1500      CONTINUE
C
C
      CALCULATION OF THE STRESS TRANSFORMATION MATRIX IN
      THE FORM OF 6 X 6
      SIGMA2 = TF * SIGMA1 * TFT
      SIGMA2 = TS * SIGMA1
      TS = STRESS TRANSFORMATION MATRIX
      TF = ROTATION MATRIX
      TFT= TRANSPOSE OF ROTATION MATRIX
C
C
      DO 1800 IJ=1,6
      DO 1900 JI=1,6
      TS(IJ,JI)=0.0
1900      CONTINUE

```



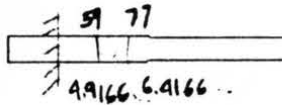
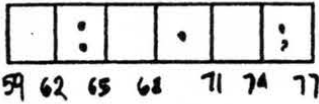
```

C          MATRICES ** STFEL **
C
C          PRODUCT OF MATRICES STF AND TSS
C
      DO 3200 KP= 1,6
        DO 3300 LP=1,6
          TEMP(KP,LP)=0.0
          DO 3400 IP=1,6
            TEMP(KP,LP)=TEMP(KP,LP)+STF(KP,IP)
            *TSS(IP,LP)
          *
3400          CONTINUE
3300          CONTINUE
3200          CONTINUE
C
C          PRODUCT OF THE MATRICES TST AND TEMP
C          STIFFNESS MATRIX OF POSITIONED ELEMENT.
C          *** STFEL ***
C
      DO 3500 KP=1,6
        DO 3600 LP=1,6
          STFEL(KP,LP)=0.0
          DO 3700 IP=1,6
            STFEL(KP,LP)=STFEL(KP,LP)+TST(KP,IP)
            *TEMP(IP,LP)
          *
3700          CONTINUE
3600          CONTINUE
3500          CONTINUE
C
C          PRINT OUT THE STIFFNESS MATRICES
C          FOR THE ELEMENTS
C
      WRITE(6,59) ((NG+((NCOND-1)*16)+48*J),J=0,5),DELTA,
      *KE,FI
59      FORMAT('1',////////,30X,'STIFFNESS MATRIX FOR THE
      *ELEMENTS',*I5,I5,I5,I5,I5,I5,/,41X,'WITH:      FIBER
      *DEVIATION ANGLE: ',F10.3,' DEGREES (KE=',F8.4,')',/
      *,50X,'CROSS SECTION ANGLE: ',F12.3,' DEGREES',////////,)
C
      DO 3800 I=1,6
        WRITE(6,60) I,(STFEL(I,J),J=1,6)
        60      FORMAT(' ', 'ROW', 1X, I1, 2X, 6F10.0)
3800      CONTINUE
1400      CONTINUE
3900      CONTINUE
      STOP
      END

```

APPENDIX F.

EXAMPLE OF A POLE SEGMENT CHARACTERISTICS
DATA SHEET.



DF 1.2
#162

Diameter • 59, in: 12.266
 radius : 6.133
 5/6 radius : 5.111
 1/3 radius : 2.0444
 circumference: 38.536"

Spiral Grain (dg): 2.069 ✓

Modulus of Elasticity (psi):

outermost: 1775 310
 intermediate: 13 67 620
 innermost: 1237 370 ✓

Knot Map:

x=	<u>63</u>	fi=	<u>0.7</u>	o	alfa=	<u>281.25</u>	<u>280.46</u>
	<u>63</u>		<u>0.6</u>	t		<u>11.25</u>	<u>9.36</u>
	<u>70</u>		<u>0.7</u>	c		<u>236.25</u>	<u>236.32</u>
	<u>75</u>		<u>1.0</u>	t		<u>160.75</u>	<u>161.19</u>
	<u>76</u>		<u>0.7</u>	t		<u>101.25</u>	<u>100.00</u>
	_____		_____			_____	_____
	_____		_____			_____	_____

3
7.225 2.4085

IDENTIFICATION OF THE ELEMENTS CONTAINING
KNOTS AND ELEMENTS WITH ASSOCIATED GRAIN
DEVIATION.

ELEMENT CONTAINING KNOTS			DF 1.2.
#	61	77 93	0.7094
	49	65 81	0.7509
	155	171 187	0.7094
	248	264 280	0.5848
	245	261 277	0.7094

$$\epsilon \left(1 - \frac{\phi_k}{\epsilon}\right) \quad (\alpha = 2.069)$$

#	12	28	44	110	126	142	$\alpha = 10.951$
	16	32	48	98	114	130	7.119
	106	122	138	204	220	236	10.951
	199	215	231				15.863
	196	212	228				10.951

#	14	30	46	108	124	140	- 6.813
	2	18	34	112	128	144	- 2.981
	108	124	140	202	218	234	- 6.813
	201	217	233				- 11.725
	198	214	230				- 6.813

areas	0.6	5.050
	0.7	8.882
	1.0	13.794



APPENDIX G.

TABLES WITH THE RESULTS OF THE GTSTRU DL
FINITE ELEMENT FOR EACH SEGMENT.

- Tables G-1. through G-10. Stresses at nodal points of segments of Western red cedar, using GTSTRU DL finite element analysis.
- Tables G-11. through G-21. Stresses at nodal points of segments of Douglas-fir, using GTSTRU DL finite element analysis.
- Tables G-22. through G-29. Stresses at nodal points of segments of Southern pine, using GTSTRU DL finite element analysis.

Table G-1. Stresses Developed at Nodal Points of Segments of Western red cedar, using GTSTRU DL Finite Element Analysis

Pole # 85 : Segment # 1
 Segment Location: 6" AGL
 Maximum Stress: 1624 PSI

Disc	Stress	Face Joint		Central Joint	
		Stress	Joint	Stress	Joint
1	Tension par.	1604	9	1496	150
	Stress perp.	88	13	29	150
	Compression	1579	25	1486	158
2	Tension par.	1426	204	1398	345
	Stress perp.	85	219	44	350
	Compression	1382	219	1285	352
3	Tension par.	1384	398	1374	538
	Stress perp.	104	413	80	547
	Compression	1483	415	1624	547
4	Tension par.	1396	591	1394	732
	Stress perp.	97	605	50	741
	Compression	1529	609	1382	741
5	Tension par.	1415	785	1418	926
	Stress perp.	97	803	46	935
	Compression	1371	801	1407	934
6	Tension par.	1380	979	1338	1120
	Stress perp.	27	1111	29	1146
	Compression	1387	995	1333	1128
7	Tension par.	1315	1173	--	--
	Stress perp.	44	1257	--	--
	Compression	1349	1189	--	--

Table G-2. Stresses Developed at Nodal Points of Segments of Western red cedar, using GTSTRU DL Finite Element Analysis

Pole # 85 : Segment # 2
 Segment Location: 141" AGL
 Maximum Stress: 1866 PSI

Disc	Stress	Face Joint		Central Joint	
		Stress	Joint	Stress	Joint
1	Tension par.	1909	9	1769	150
	Stress perp.	118	13	56	158
	Compression	1956	26	1716	158
2	Tension par.	1694	204	1652	344
	Stress perp.	82	219	38	352
	Compression	1805	220	1430	352
3	Tension par.	1627	397	1700	538
	Stress perp.	92	433	68	546
	Compression	1866	414	1771	545
4	Tension par.	1672	591	1532	732
	Stress perp.	94	627	44	755
	Compression	1852	608	1481	739
5	Tension par.	1533	786	1448	926
	Stress perp.	100	799	46	933
	Compression	1692	802	1579	934
6	Tension par.	1436	980	1427	1120
	Stress perp.	23	1003	17	1152
	Compression	1548	996	1463	1128
7	Tension par.	1409	1173	--	--
	Stress perp.	39	1269	--	--
	Compression	1438	1189	--	--

Table G-3. Stresses Developed at Nodal Points of Segments of Western red cedar, using GTSTRU DL Finite Element Analysis

Pole # 85 : Segment # 3
 Segment Location: 232" AGL
 Maximum Stress: 2208 PSI

Disc	Stress	Face Joint		Central Joint	
		Stress	Joint	Stress	Joint
1	Tension par.	1830	11	1759	150
	Stress perp.	177	29	49	150
	Compression	2082	23	1871	157
2	Tension par.	1835	203	1645	344
	Stress perp.	123	203	81	354
	Compression	1877	218	1869	352
3	Tension par.	1800	395	1838	537
	Stress perp.	82	413	62	537
	Compression	1840	413	1632	546
4	Tension par.	1752	589	1514	731
	Stress perp.	179	607	79	756
	Compression	1788	608	1690	740
5	Tension par.	1589	785	1589	926
	Stress perp.	120	799	87	933
	Compression	2004	801	2208	934
6	Tension par.	1551	979	1497	1120
	Stress perp.	128	989	166	1128
	Compression	2110	995	1860	1128
7	Tension par.	1470	1173	--	--
	Stress perp.	230	1190	--	--
	Compression	2041	1189	--	--

Table G-4. Stresses Developed at Nodal Points of Segments of Western red cedar, using GTSTRU DL Finite Element Analysis

Pole # 85 : Segment # 4
 Segment Location: 265" AGL
 Maximum Stress: 1739 PSI

Disc	Stress	Face Joint		Central Joint	
		Stress	Joint	Stress	Joint
1	Tension par.	1776	9	1729	150
	Stress perp.	65	8	38	152
	Compression	1719	25	1645	156
2	Tension par.	1721	203	1644	344
	Stress perp.	64	207	11	344
	Compression	1581	219	1574	352
3	Tension par.	1659	398	1739	539
	Stress perp.	62	401	47	539
	Compression	1572	413	1596	546
4	Tension par.	1673	592	1605	732
	Stress perp.	56	595	34	734
	Compression	1625	607	1561	740
5	Tension par.	1626	785	1531	926
	Stress perp.	80	791	37	936
	Compression	1612	803	1671	935
6	Tension par.	1488	979	1466	1120
	Stress perp.	63	985	25	1127
	Compression	1608	997	1439	1129
7	Tension par.	1416	1173	--	--
	Stress perp.	67	1190	--	--
	Compression	1458	1189	--	--

Table G-5. Stresses Developed at Nodal Points of Segments of Western red cedar, using GTSTRU DL Finite Element Analysis

Pole # 88 : Segment # 1
 Segment Location: 26" AGL
 Maximum Stress: 996 PSI

Disc	Stress	Face Joint		Central Joint	
		Stress	Joint	Stress	Joint
1	Tension par.	975	9	940	150
	Stress perp.	37	24	35	158
	Compression	1019	25	970	158
2	Tension par.	909	203	885	344
	Stress perp.	52	219	17	344
	Compression	893	219	822	352
3	Tension par.	861	397	826	538
	Stress perp.	56	413	44	546
	Compression	910	412	996	547
4	Tension par.	878	593	899	733
	Stress perp.	53	607	27	733
	Compression	901	606	834	739
5	Tension par.	871	787	808	927
	Stress perp.	56	803	34	932
	Compression	909	799	974	933
6	Tension par.	826	979	834	1120
	Stress perp.	52	993	21	1127
	Compression	924	993	874	1128
7	Tension par.	836	1173	- -	- -
	Stress perp.	78	1187	- -	- -
	Compression	898	1189	- -	- -

Table G-6. Stresses Developed at Nodal Points of Segments of Western red cedar, using GTSTRU DL Finite Element Analysis

Pole # 88 : Segment # 2
 Segment Location: 95" AGL
 Maximum Stress: 1223 PSI

Disc	Stress	Face Joint		Central Joint	
		Stress	Joint	Stress	Joint
1	Tension par.	1082	7	949	149
	Stress perp.	108	11	31	151
	Compression	991	25	936	158
2	Tension par.	978	202	975	344
	Stress perp.	61	203	51	344
	Compression	852	219	797	353
3	Tension par.	937	397	864	537
	Stress perp.	52	397	40	546
	Compression	873	412	856	547
4	Tension par.	899	590	793	731
	Stress perp.	62	607	44	740
	Compression	852	606	911	740
5	Tension par.	864	784	783	925
	Stress perp.	63	803	47	935
	Compression	1085	801	1223	934
6	Tension par.	790	978	776	1120
	Stress perp.	91	997	90	1128
	Compression	1148	995	960	1128
7	Tension par.	780	1173	- -	- -
	Stress perp.	124	1189	- -	- -
	Compression	939	1189	- -	- -

Table G-7. Stresses Developed at Nodal Points of Segments of Western red cedar, using GTSTRUDL Finite Element Analysis

Pole # 88 : Segment # 3
 Segment Location: 133" AGL
 Maximum Stress: 1039 PSI

Disc	Stress	Face Joint		Central Joint	
		Stress	Joint	Stress	Joint
1	Tension par.	1054	9	992	150
	Stress perp.	50	24	38	150
	Compression	1113	26	954	158
2	Tension par.	903	203	820	344
	Stress perp.	54	203	34	350
	Compression	1039	220	922	352
3	Tension par.	941	399	1004	539
	Stress perp.	60	397	52	539
	Compression	922	414	834	547
4	Tension par.	947	593	838	733
	Stress perp.	43	593	20	733
	Compression	850	608	821	740
5	Tension par.	834	785	850	926
	Stress perp.	51	787	27	926
	Compression	810	801	795	934
6	Tension par.	830	979	791	1120
	Stress perp.	12	978	10	1134
	Compression	783	995	783	1128
7	Tension par.	780	1173	--	--
	Stress perp.	23	1223	--	--
	Compression	770	1189	--	--

Table G-8. Stresses Developed at Nodal Points of Segments of Western red cedar, using GTSTRUDL Finite Element Analysis

Pole # 91 : Segment # 1
 Segment Location: 26" AGL
 Maximum Stress: 2521 PSI

Disc	Stress	Face Joint		Central Joint	
		Stress	Joint	Stress	Joint
1	Tension par.	2568	9	2474	150
	Stress perp.	79	25	30	150
	Compression	2603	25	2513	158
2	Tension par.	2399	202	2340	344
	Stress perp.	17	231	16	345
	Compression	2434	219	2398	352
3	Tension par.	2380	396	2418	538
	Stress perp.	33	398	6	537
	Compression	2393	413	2388	546
4	Tension par.	2510	591	2521	732
	Stress perp.	29	593	24	734
	Compression	2395	607	2355	740
5	Tension par.	2476	785	2346	926
	Stress perp.	31	787	13	930
	Compression	2332	801	2299	934
6	Tension par.	2260	979	2250	1120
	Stress perp.	29	979	18	1116
	Compression	2277	995	2267	1128
7	Tension par.	2220	1173	--	--
	Stress perp.	43	1249	--	--
	Compression	2237	1189	--	--

Table G-9. Stresses Developed at Nodal Points of Segments of Western red cedar, using GTSTRU DL Finite Element Analysis

Pole # 91 : Segment # 2
 Segment Location: 58" AGL
 Maximum Stress: 2702 PSI

Disc	Stress	Face Joint		Central Joint	
		Stress	Joint	Stress	Joint
1	Tension par.	2715	9	2618	150
	Stress perp.	86	9	29	149
	Compression	2623	23	2489	157
2	Tension par.	2557	203	2533	344
	Stress perp.	44	216	22	344
	Compression	2472	220	2506	352
3	Tension par.	2503	397	2415	538
	Stress perp.	48	398	31	545
	Compression	2670	413	2702	546
4	Tension par.	2471	589	2492	731
	Stress perp.	45	591	36	732
	Compression	2639	607	2459	740
5	Tension par.	2435	783	2291	926
	Stress perp.	42	799	15	934
	Compression	2395	802	2294	934
6	Tension par.	2334	979	2334	1120
	Stress perp.	44	979	26	1116
	Compression	2312	996	2293	1128
7	Tension par.	2318	1173	- -	- -
	Stress perp.	50	1258	- -	- -
	Compression	2270	1189	- -	- -

Table G-10. Stresses Developed at Nodal Points of Segments of Western red cedar, using GTSTRU DL Finite Element Analysis

Pole # 91 : Segment # 3
 Segment Location: 95" AGL
 Maximum Stress: 2459 PSI

Disc	Stress	Face Joint		Central Joint	
		Stress	Joint	Stress	Joint
1	Tension par.	2625	9	2540	150
	Stress perp.	80	25	28	151
	Compression	2631	25	2534	158
2	Tension par.	2459	203	2432	344
	Stress perp.	16	232	16	346
	Compression	2451	217	2414	352
3	Tension par.	2453	397	2411	538
	Stress perp.	35	401	18	550
	Compression	2407	413	2399	546
4	Tension par.	2377	592	2392	733
	Stress perp.	34	595	27	734
	Compression	2384	607	2359	740
5	Tension par.	2337	787	2298	926
	Stress perp.	37	789	15	937
	Compression	2334	801	2294	934
6	Tension par.	2302	979	2252	1120
	Stress perp.	38	981	22	1116
	Compression	2265	995	2248	1128
7	Tension par.	2198	1174	- -	- -
	Stress perp.	52	1249	- -	- -
	Compression	2210	1189	- -	- -

Table G-11. Stresses Developed at Nodal Points of Segments of Douglas-fir, using GTSTRU DL Finite Element Analysis

Pole # 182 : Segment # 1
 Segment Location: 34" AGL
 Maximum Stress: 2902 PSI

Disc	Stress	Face Joint		Central Joint	
		Stress	Joint	Stress	Joint
1	Tension par.	2702	8	2533	150
	Stress perp.	83	8	34	150
	Compression	2710	25	2631	158
2	Tension par.	2570	202	2437	345
	Stress perp.	47	209	42	345
	Compression	2555	219	2534	352
3	Tension par.	2532	396	2549	538
	Stress perp.	94	399	38	541
	Compression	2525	413	2524	546
4	Tension par.	2812	591	2902	732
	Stress perp.	73	599	60	732
	Compression	2554	607	2451	740
5	Tension par.	2807	785	2527	927
	Stress perp.	102	789	41	932
	Compression	2565	799	2619	933
6	Tension par.	2404	978	2334	1120
	Stress perp.	82	979	18	1116
	Compression	2507	993	2365	1128
7	Tension par.	2385	1172	--	--
	Stress perp.	134	1185	--	--
	Compression	2381	1189	--	--

Table G-12. Stresses Developed at Nodal Points of Segments of Douglas-fir, using GTSTRU DL Finite Element Analysis

Pole # 162 : Segment # 2
 Segment Location: 59" AGL
 Maximum Stress: 2748 PSI

Disc	Stress	Face Joint		Central Joint	
		Stress	Joint	Stress	Joint
1	Tension par.		9	2654	150
	Stress perp.	169	25	33	150
	Compression	2937	25	2717	158
2	Tension par.	2573	203	2534	344
	Stress perp.	89	217	70	352
	Compression	2510	217	2519	351
3	Tension par.	2556	397	2576	538
	Stress perp.	83	413	13	537
	Compression	2438	411	2437	546
4	Tension par.	2622	591	2646	732
	Stress perp.	80	605	61	739
	Compression	2645	607	2748	740
5	Tension par.	2573	785	2454	926
	Stress perp.	123	789	12	924
	Compression	2683	801	2422	934
6	Tension par.	2367	979	2291	1120
	Stress perp.	116	983	29	1119
	Compression	2335	995	2298	1128
7	Tension par.	2415	1173	--	--
	Stress perp.	84	1177	--	--
	Compression	2300	1189	--	--

Table G-13. Stresses Developed at Nodal Points of Segments of Douglas-fir, using GTSTRUDL Finite Element Analysis

Pole # 162 : Segment # 3
 Segment Location: 88" AGL
 Maximum Stress: 2765 PSI

Disc	Stress	Face Joint		Central Joint	
		Stress	Joint	Stress	Joint
1	Tension par.	2632	9	2546	150
	Stress perp.	204	16	28	150
	Compression	2553	24	2395	158
2	Tension par.	2484	203	2451	344
	Stress perp.	16	204	18	344
	Compression	2445	218	2300	353
3	Tension par.	2420	397	2348	538
	Stress perp.	76	415	14	576
	Compression	2422	412	2443	546
4	Tension par.	2355	590	2349	731
	Stress perp.	79	609	63	741
	Compression	2693	607	2765	740
5	Tension par.	2297	785	2217	927
	Stress perp.	81	803	19	937
	Compression	2664	801	2376	934
6	Tension par.	2236	979	2245	1120
	Stress perp.	76	995	39	1116
	Compression	2262	994	2192	1128
7	Tension par.	2219	1173	--	--
	Stress perp.	67	1270	--	--
	Compression	2220	1188	--	--

Table G-14. Stresses Developed at Nodal Points of Segments of Douglas-fir, using GTSTRUDL Finite Element Analysis

Pole # 174 : Segment # 1
 Segment Location: 6" AGL
 Maximum Stress: 3006 PSI

Disc	Stress	Face Joint		Central Joint	
		Stress	Joint	Stress	Joint
1	Tension par.	2869	8	2734	150
	Stress perp.	86	9	37	149
	Compression	2980	25	2877	158
2	Tension par.	2736	202	2762	344
	Stress perp.	39	230	28	351
	Compression	2836	219	2812	352
3	Tension par.	2905	397	2875	538
	Stress perp.	109	413	39	538
	Compression	2717	413	2567	545
4	Tension par.	2752	591	2745	733
	Stress perp.	192	627	92	740
	Compression	2899	605	3006	739
5	Tension par.	2690	787	2467	926
	Stress perp.	116	821	36	936
	Compression	2880	799	2515	933
6	Tension par.	2526	980	2478	1120
	Stress perp.	102	993	34	1117
	Compression	2555	995	2586	1128
7	Tension par.	2485	1174	--	--
	Stress perp.	92	1209	--	--
	Compression	2573	1189	--	--

Table G-15. Stresses Developed at Nodal Points of Segments of Douglas-fir, using GTSTRUDL Finite Element Analysis

Pole # 174 : Segment # 2
 Segment Location: 28" AGL
 Maximum Stress: 3322 PSI

Disc	Stress	Face Joint		Central Joint	
		Stress	Joint	Stress	Joint
1	Tension par.	3115	9	2981	150
	Stress perp.	115	7	48	152
	Compression	3115	25	3045	158
2	Tension par.	2837	204	2724	345
	Stress perp.	95	199	49	351
	Compression	3068	219	2979	352
3	Tension par.	2920	399	2853	539
	Stress perp.	158	413	55	537
	Compression	2810	413	2965	545
4	Tension par.	2735	589	2767	732
	Stress perp.	187	605	105	740
	Compression	3322	605	3165	739
5	Tension par.	2823	785	2654	926
	Stress perp.	151	801	51	933
	Compression	2831	799	2519	934
6	Tension par.	2588	979	2567	1120
	Stress perp.	120	995	44	1131
	Compression	2644	995	2679	1128
7	Tension par.	2479	1173	--	--
	Stress perp.	97	1269	--	--
	Compression	2630	1189	--	--

Table G-16. Stresses Developed at Nodal Points of Segments of Douglas-fir, using GTSTRUDL Finite Element Analysis

Pole # 174 : Segment # 3
 Segment Location: 63" AGL
 Maximum Stress: 3151 PSI

Disc	Stress	Face Joint		Central Joint	
		Stress	Joint	Stress	Joint
1	Tension par.	2891	9	2698	151
	Stress perp.	88	11	50	151
	Compression	3036	25	2939	158
2	Tension par.	2729	202	2716	344
	Stress perp.	73	205	47	353
	Compression	2953	219	2829	352
3	Tension par.	2877	397	2949	538
	Stress perp.	143	413	62	538
	Compression	2649	413	2834	547
4	Tension par.	2847	591	2651	732
	Stress perp.	167	609	80	740
	Compression	3151	609	2941	741
5	Tension par.	2590	784	2352	926
	Stress perp.	152	797	63	935
	Compression	2569	803	2391	934
6	Tension par.	2459	978	2379	1120
	Stress perp.	152	991	28	1116
	Compression	2463	995	2535	1128
7	Tension par.	2331	1173	--	--
	Stress perp.	93	1270	--	--
	Compression	2508	1189	--	--

Table G-17. Stresses Developed at Nodal Points of Segments of Douglas-fir, using GTSTRUDL Finite Element Analysis

Pole # 174 : Segment # 4
 Segment Location: 96" AGL
 Maximum Stress: 3039 PSI

Disc	Stress	Face Joint		Central Joint	
		Stress	Joint	Stress	Joint
1	Tension par.	2706	8	2540	150
	Stress perp.	81	8	33	150
	Compression	3095	25	2939	158
2	Tension par.	2556	205	2449	345
	Stress perp.	128	221	36	343
	Compression	2718	219	2440	352
3	Tension par.	2570	398	2586	538
	Stress perp.	168	417	71	562
	Compression	2844	412	2943	545
4	Tension par.	2874	591	2923	732
	Stress perp.	142	607	57	732
	Compression	2848	607	2751	740
5	Tension par.	2792	785	2478	926
	Stress perp.	229	801	39	933
	Compression	3039	801	2704	934
6	Tension par.	2355	980	2306	1120
	Stress perp.	138	997	35	1119
	Compression	2393	995	2323	1128
7	Tension par.	2286	1174	--	--
	Stress perp.	103	1270	--	--
	Compression	2338	1188	--	--

Table G-18. Stresses Developed at Nodal Points of Segments of Douglas-fir, using GTSTRUDL Finite Element Analysis

Pole # 174 : Segment # 5
 Segment Location: 142" AGL
 Maximum Stress: 3697 PSI

Disc	Stress	Face Joint		Central Joint	
		Stress	Joint	Stress	Joint
1	Tension par.	2860	9	2843	150
	Stress perp.	90	11	53	159
	Compression	3168	25	3036	158
2	Tension par.	2823	205	2718	344
	Stress perp.	213	221	35	369
	Compression	2893	219	2441	352
3	Tension par.	2708	397	2638	538
	Stress perp.	238	415	93	546
	Compression	3301	415	3697	547
4	Tension par.	2830	589	2883	731
	Stress perp.	225	609	68	731
	Compression	3277	609	2610	739
5	Tension par.	2544	786	2473	926
	Stress perp.	217	803	82	935
	Compression	2631	799	2570	934
6	Tension par.	2457	980	2308	1120
	Stress perp.	162	991	42	1117
	Compression	2465	995	2256	1128
7	Tension par.	2391	1173	--	--
	Stress perp.	109	1268	--	--
	Compression	2195	1188	--	--

Table G-19. Stresses Developed at Nodal Points of Segments of Douglas-fir, using GTSTRUDL Finite Element Analysis

Pole # 188 : Segment # 1
 Segment Location: 22" AGL
 Maximum Stress: 3038 PSI

Disc	Stress	Face Joint		Central Joint	
		Stress	Joint	Stress	Joint
1	Tension par.	3008	9	2923	150
	Stress perp.	98	9	54	157
	Compression	2987	23	2844	157
2	Tension par.	2829	203	2784	344
	Stress perp.	70	217	19	345
	Compression	2777	218	2817	352
3	Tension par.	2779	397	2799	538
	Stress perp.	51	411	47	546
	Compression	2996	413	3038	546
4	Tension par.	2810	591	2743	732
	Stress perp.	47	607	44	729
	Compression	2958	607	2760	740
5	Tension par.	2743	784	2649	926
	Stress perp.	59	799	37	922
	Compression	2679	802	2593	934
6	Tension par.	2598	978	2607	1120
	Stress perp.	65	975	44	1116
	Compression	2610	996	2594	1128
7	Tension par.	2587	1173	- -	- -
	Stress perp.	74	1167	- -	- -
	Compression	2572	1189	- -	- -

Table G-20. Stresses Developed at Nodal Points of Segments of Douglas-fir, using GTSTRUDL Finite Element Analysis

Pole # 188 : Segment # 2
 Segment Location: 119" AGL
 Maximum Stress: 3113 PSI

Disc	Stress	Face Joint		Central Joint	
		Stress	Joint	Stress	Joint
1	Tension par.	3092	7	2899	149
	Stress perp.	132	25	62	149
	Compression	3229	25	3053	157
2	Tension par.	2755	202	2824	344
	Stress perp.	85	219	32	353
	Compression	2884	219	2745	352
3	Tension par.	3113	397	3055	538
	Stress perp.	184	415	63	538
	Compression	2681	415	2633	546
4	Tension par.	2826	591	2706	731
	Stress perp.	72	609	47	731
	Compression	2721	607	2665	739
5	Tension par.	2811	784	2577	925
	Stress perp.	131	799	49	922
	Compression	2725	799	2569	934
6	Tension par.	2513	979	2522	1120
	Stress perp.	88	995	85	1116
	Compression	2564	995	2535	1128
7	Tension par.	2525	1173	- -	- -
	Stress perp.	126	1180	- -	- -
	Compression	2535	1189	- -	- -

Table G-21. Stresses Developed at Nodal Points of Segments of Douglas-fir, using GTSTRUDL Finite Element Analysis

Pole # 188 : Segment # 3
 Segment Location: 267" AGL
 Maximum Stress: 2473 PSI

Disc	Stress	Face Joint		Central Joint	
		Stress	Joint	Stress	Joint
1	Tension par.	2583	9	2492	150
	Stress perp.	98	9	36	150
	Compression	2579	25	2444	157
2	Tension par.	2405	203	2365	344
	Stress perp.	50	219	28	295
	Compression	2305	219	2220	353
3	Tension par.	2401	397	2429	538
	Stress perp.	79	404	25	539
	Compression	2321	415	2255	547
4	Tension par.	2379	591	2269	732
	Stress perp.	68	602	40	741
	Compression	2381	607	2473	740
5	Tension par.	2257	783	2265	925
	Stress perp.	74	803	50	925
	Compression	2466	801	2307	934
6	Tension par.	2211	977	2183	1120
	Stress perp.	66	977	56	1117
	Compression	2166	995	2137	1128
7	Tension par.	2153	1974	- -	- -
	Stress perp.	133	1177	- -	- -
	Compression	2133	1189	- -	- -

Table G-22. Stresses Developed at Nodal Points of Segments of Southern pine, using GTSTRU DL Finite Element Analysis

Pole # 289 : Segment # 1
 Segment Location: 52" AGL
 Maximum Stress: 4222 PSI

Disc	Stress	Face Joint		Central Joint	
		Stress	Joint	Stress	Joint
1	Tension par.	4568	9	4382	150
	Stress perp.	176	25	56	158
	Compression	4558	25	4376	158
2	Tension par.	4222	203	4164	344
	Stress perp.	95	243	77	364
	Compression	4219	219	4161	352
3	Tension par.	4166	397	4167	538
	Stress perp.	101	519	80	572
	Compression	4163	413	4164	546
4	Tension par.	4149	591	4120	732
	Stress perp.	106	725	68	770
	Compression	4145	607	4116	740
5	Tension par.	4093	785	4049	926
	Stress perp.	104	907	62	964
	Compression	4087	801	4042	934
6	Tension par.	4003	979	3961	1120
	Stress perp.	53	989	83	1116
	Compression	3997	995	3957	1128
7	Tension par.	3920	1173	--	--
	Stress perp.	125	1165	--	--
	Compression	3974	1189	--	--

Table G-23. Stresses Developed at Nodal Points of Segments of Southern pine, using GTSTRU DL Finite Element Analysis

Pole # 289 : Segment # 3
 Segment Location: 190" AGL
 Maximum Stress: 3154 PSI

Disc	Stress	Face Joint		Central Joint	
		Stress	Joint	Stress	Joint
1	Tension par.	3420	9	3255	150
	Stress perp.	137	9	43	157
	Compression	3325	25	3185	158
2	Tension par.	3154	203	3072	344
	Stress perp.	77	243	67	356
	Compression	3062	219	3076	352
3	Tension par.	3015	397	2828	539
	Stress perp.	83	397	44	576
	Compression	3148	413	3085	546
4	Tension par.	3110	593	3095	733
	Stress perp.	73	724	44	739
	Compression	3062	605	3036	739
5	Tension par.	3003	787	2913	926
	Stress perp.	79	911	49	964
	Compression	3006	800	2946	934
6	Tension par.	2946	979	2898	1120
	Stress perp.	82	977	58	1116
	Compression	2931	995	2836	1128
7	Tension par.	2886	1173	--	--
	Stress perp.	81	1169	--	--
	Compression	2802	1188	--	--

Table G-24. Stresses Developed at Nodal Points of Segments of Southern pine, using GTSTRUDL Finite Element Analysis

Pole # 292 : Segment # 1
 Segment Location: 10" AGL
 Maximum Stress: 3186 PSI

Disc	Stress	Face	Joint	Central	Joint
		Stress	Joint	Stress	Joint
1	Tension par.	3417	9	3285	150
	Stress perp.	121	25	40	159
	Compression	3382	25	3253	158
2	Tension par.	3186	203	3131	344
	Stress perp.	26	233	36	347
	Compression	3143	219	3099	352
3	Tension par.	3117	398	3086	538
	Stress perp.	85	401	34	540
	Compression	3096	413	3087	546
4	Tension par.	3053	591	3000	732
	Stress perp.	62	595	69	734
	Compression	3067	607	3034	740
5	Tension par.	2969	785	2915	926
	Stress perp.	87	791	54	930
	Compression	2999	801	2942	934
6	Tension par.	2878	980	2892	1120
	Stress perp.	117	983	29	1152
	Compression	2909	995	2897	1128
7	Tension par.	2874	1173	- -	- -
	Stress perp.	120	1269	- -	- -
	Compression	2845	1189	- -	- -

Table G-25. Stresses Developed at Nodal Points of Segments of Southern pine, using GTSTRUDL Finite Element Analysis

Pole # 292 : Segment # 2
 Segment Location: 140" AGL
 Maximum Stress: 3698 PSI

Disc	Stress	Face	Joint	Central	Joint
		Stress	Joint	Stress	Joint
1	Tension par.	3396	10	3096	149
	Stress perp.	114	6	92	149
	Compression	3360	25	3305	158
2	Tension par.	3273	204	2961	344
	Stress perp.	191	201	54	340
	Compression	3348	219	3212	352
3	Tension par.	3666	398	3698	538
	Stress perp.	198	395	158	538
	Compression	3271	414	3309	547
4	Tension par.	3678	592	3067	732
	Stress perp.	184	589	72	728
	Compression	3225	608	3067	740
5	Tension par.	3261	785	2635	934
	Stress perp.	188	785	86	926
	Compression	3123	801	2870	934
6	Tension par.	2960	980	2619	1120
	Stress perp.	30	1015	27	1117
	Compression	2762	996	2705	1128
7	Tension par.	2645	1173	- -	- -
	Stress perp.	60	1250	- -	- -
	Compression	2592	1190	- -	- -

Table G-26. Stresses Developed at Nodal Points of Segments of Southern pine, using GTSTRU DL Finite Element Analysis

Pole # 292 : Segment # 3
 Segment Location: 213" AGL
 Maximum Stress: 3718 PSI

Disc	Stress	Face Joint		Central Joint	
		Stress	Joint	Stress	Joint
1	Tension par.	3316	9	2380	150
	Stress perp.	247	9	48	150
	Compression	3114	25	2953	158
2	Tension par.	3098	201	3373	343
	Stress perp.	157	205	155	345
	Compression	2942	219	2810	353
3	Tension par.	3566	397	2801	537
	Stress perp.	301	397	118	534
	Compression	2946	413	2926	546
4	Tension par.	3352	591	3718	732
	Stress perp.	328	591	177	732
	Compression	3248	607	3315	740
5	Tension par.	3514	785	2790	926
	Stress perp.	167	787	104	922
	Compression	3196	801	2745	934
6	Tension par.	2791	979	2642	1120
	Stress perp.	186	979	45	1121
	Compression	2647	995	2491	1128
7	Tension par.	2730	1173	--	--
	Stress perp.	122	1201	--	--
	Compression	2569	1188	--	--

Table G-27. Stresses Developed at Nodal Points of Segments of Southern pine, using GTSTRU DL Finite Element Analysis

Pole # 297 : Segment # 1
 Segment Location: 12" AGL
 Maximum Stress: 2540 PSI

Disc	Stress	Face Joint		Central Joint	
		Stress	Joint	Stress	Joint
1	Tension par.	704	9	2618	150
	Stress perp.	32	25	30	150
	Compression	2704	25	2618	158
2	Tension par.	2540	203	2504	344
	Stress perp.	15	231	11	340
	Compression	2540	219	2504	352
3	Tension par.	2501	397	2502	538
	Stress perp.	9	396	4	538
	Compression	2501	413	2502	546
4	Tension par.	2494	591	2486	732
	Stress perp.	5	590	3	772
	Compression	2494	607	2486	740
5	Tension par.	2475	785	2466	926
	Stress perp.	4	784	9	965
	Compression	2475	801	2466	934
6	Tension par.	2457	979	2453	1120
	Stress perp.	4	978	11	1116
	Compression	2457	995	2453	1128
7	Tension par.	2447	1173	--	--
	Stress perp.	28	1297	--	--
	Compression	2447	1189	--	--

Table G-28. Stresses Developed at Nodal Points of Segments of Southern pine, using GTSTRU DL Finite Element Analysis

Pole # 297 : Segment # 2
 Segment Location: 72" AGL
 Maximum Stress: 2391 PSI

Disc	Stress	Face Joint		Central Joint	
		Stress	Joint	Stress	Joint
1	Tension par.	2559	9	2471	150
	Stress perp.	85	25	30	150
	Compression	2559	25	2470	158
2	Tension par.	2391	203	2358	344
	Stress perp.	15	231	6	344
	Compression	2391	219	2358	352
3	Tension par.	2357	397	2362	538
	Stress perp.	9	396	4	538
	Compression	2357	413	2362	546
4	Tension par.	2357	591	2357	732
	Stress perp.	6	590	8	762
	Compression	2357	607	2357	740
5	Tension par.	2356	785	2364	926
	Stress perp.	6	782	17	938
	Compression	2355	801	2364	934
6	Tension par.	2362	979	2359	1120
	Stress perp.	10	971	15	1116
	Compression	2362	995	2359	1128
7	Tension par.	2372	1173	--	--
	Stress perp.	40	1257	--	--
	Compression	2372	1189	--	--

Table G-29. Stresses Developed at Nodal Points of Segments of Southern pine, using GTSTRU DL Finite Element Analysis

Pole # 297 : Segment # 3
 Segment Location: 150" AGL
 Maximum Stress: 2197 PSI

Disc	Stress	Face Joint		Central Joint	
		Stress	Joint	Stress	Joint
1	Tension par.	2361	9	2273	150
	Stress perp.	80	25	27	150
	Compression	2361	25	2273	158
2	Tension par.	2197	203	2166	344
	Stress perp.	14	231	7	352
	Compression	2197	219	2166	352
3	Tension par.	2165	397	2169	538
	Stress perp.	8	396	4	538
	Compression	2165	413	2169	546
4	Tension par.	2163	591	2164	732
	Stress perp.	5	590	5	762
	Compression	2163	607	2164	740
5	Tension par.	2165	785	2180	926
	Stress perp.	6	878	8	956
	Compression	2165	801	2180	934
6	Tension par.	2182	979	2183	1120
	Stress perp.	5	972	12	1158
	Compression	2182	995	2183	1128
7	Tension par.	2205	1173	--	--
	Stress perp.	57	1257	--	--
	Compression	2205	1189	--	--